

LOCKHEED MARTIN ENERGY RESEARCH LIBRARIES



3 4456 0513462 7

CENTRAL RESEARCH LIBRARY
DOCUMENT COLLECTION

1

OAK RIDGE NATIONAL LABORATORY

operated by

UNION CARBIDE CORPORATION
NUCLEAR DIVISION

for the

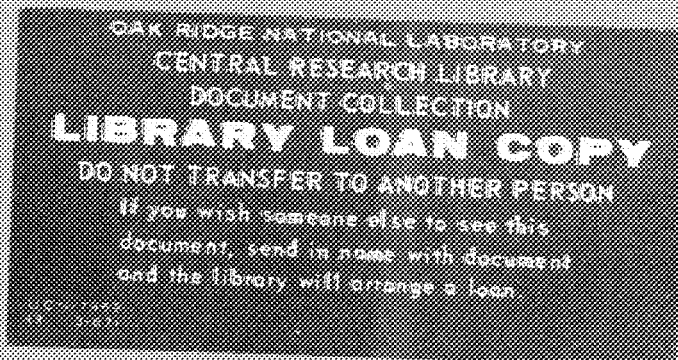
U.S. ATOMIC ENERGY COMMISSION



ORNL - TM - 2016

HELIUM GAS BUBBLE MIGRATION IN URANIUM
MONONITRIDE IN A TEMPERATURE GRADIENT
(Thesis)

Samuel Cavin Weaver



Submitted as a thesis to the Graduate Council of the University of Tennessee in partial fulfillment of the requirements for the degree of Master of Science.

LEGAL NOTICE

This report was prepared as an account of Government sponsored work. Neither the United States, nor the Commission, nor any person acting on behalf of the Commission:

- A. Makes any warranty or representation, expressed or implied, with respect to the accuracy, completeness, or usefulness of the information contained in this report, or that the use of any information, apparatus, method, or process disclosed in this report may not infringe privately owned rights; or
- B. Assumes any liabilities with respect to the use of, or for damages resulting from the use of any information, apparatus, method, or process disclosed in this report.

As used in the above, "person acting on behalf of the Commission" includes any employee or contractor of the Commission, or employee of such contractor, to the extent that such employee or contractor of the Commission, or employee of such contractor prepares, disseminates, or provides access to, any information pursuant to his employment or contract with the Commission, or his employment with such contractor.

Contract No. W-7405-eng-26

METALS AND CERAMICS DIVISION

HELIUM GAS BUBBLE MIGRATION IN URANIUM
MONONITRIDE IN A TEMPERATURE GRADIENT

Samuel Cavin Weaver

Submitted as a thesis to the Graduate Council of the
University of Tennessee in partial fulfillment of the
requirements for the degree of Master of Science.

DECEMBER 1967

OAK RIDGE NATIONAL LABORATORY
Oak Ridge, Tennessee
operated by
UNION CARBIDE CORPORATION
for the
U.S. ATOMIC ENERGY COMMISSION



ACKNOWLEDGMENTS

The author wishes to express his appreciation to his thesis advisor, Dr. J. E. Spruiell, for his advice and encouragement throughout the course of this investigation and for his contributions to the preparation of this manuscript.

Special thanks are extended to Earl Rosson whose mechanical ingenuity and tireless cooperation were an invaluable aid throughout this investigation.

Special thanks are also extended to Richard Perkins, a summer employee, who helped with the experimental work.

Thanks are extended to R. A. Potter for his help in fabricating the UN samples used in these experiments.

The author is grateful to W. C. Colwell of the Graphic Arts Department for preparation of the drawings. The light microscope photomicrographs were produced in the Metallography group of the Metals and Ceramics Division.

The author thanks the members of the Electron Microscopy Group of the Metals and Ceramics Division for their continuous assistance and for developing the electron photomicrographs.

Special thanks are extended to the Metals and Ceramics Division Reports Office, especially Frances Scarboro, for the typing and preparation of this manuscript.

Thanks are extended to the Union Carbide Corporation for allowing the author to participate in its educational assistance program. The research was sponsored by the Oak Ridge National Laboratory, operated by Union Carbide Corporation for the United States Atomic Energy Commission.

ABSTRACT

Helium bubble migration in uranium mononitride was studied in the temperature range of 985 to 1585°C. with temperature gradients ranging from 75 to 880°C. per centimeter. The UN specimens were inoculated with 250-kilo-electron volt helium ions from a Cockcroft-Walter accelerator. Both the temperature and temperature gradients were known accurately and could be controlled. The migration distances and bubble sizes were examined by replication electron microscopy applied to longitudinal sections (parallel to the temperature gradient) through the UN specimens. Thin-film transmission and replicas of fractured surfaces were used to support the results obtained from the longitudinal sections. The bubbles were observed to migrate by surface diffusion up the temperature gradient at velocities ranging from 300 angstroms per second at 985°C. to greater than 11,000 angstroms per second at 1585°C.

From measurements of the migration distances, an approximate surface diffusion coefficient, D_s , for UN was calculated to be:

$$D_s = 1.92 \times 10^3 \exp(-42,200/RT) \text{ square centimeters per second .}$$

Although the bubbles migrated large distances, they were not observed to coalesce during the heat treatments. It is suggested that this behavior was caused by the existence of large stress fields in the UN matrix surrounding the bubbles which caused the bubbles to repel each other. These stress fields were presumably caused by high nonequilibrium internal pressures in the gas bubbles.

TABLE OF CONTENTS

CHAPTER	PAGE
I. INTRODUCTION	1
I. Objective of the Study	1
II. Importance of the Study	1
II. LITERATURE SURVEY	5
I. Description of the Uranium-Nitrogen System and the Properties of Uranium Mononitride	5
II. Gas Bubble Migration	12
III. MATERIALS AND EQUIPMENT	21
I. Preparation of Uranium Nitride Samples	21
II. Sample Holder for Cockcroft-Walton Accelerator	27
III. Temperature Gradient Furnace	30
IV. EXPERIMENTAL PROCEDURE	33
I. Injection of Helium Gas	33
II. Heat Treatment	37
III. Sample Preparation and Examination	38
V. RESULTS AND DISCUSSION	40
I. Control Samples	40
II. Effects of Helium Ion Bombardment	46
III. Results of Bubble Migration in a Temperature Gradient	52
IV. Further Discussion and Comparison of the Results with Those for Previous Investigations	81
VI. CONCLUSIONS AND RECOMMENDATIONS	86

REFERENCES	88
APPENDIXES	92

LIST OF TABLES

TABLE	PAGE
I. Characteristics of Uranium Nitride Specimens Used for Helium Inoculation	26
II. Heat Treatments and Conditions of Helium Ion Injection for Specimens Examined	41
III. Results of Calculations of Diffusion Coefficients	79
IV. Comparison of Migration Rates of Helium Bubbles Subjected to a Temperature Gradient in UN, UC, and Copper	82
V. Comparison of Surface Diffusion Coefficients of UN, UC, and Copper	83
VI. Sight Glass Calibration for Temperature Gradient Furnace	93

LIST OF FIGURES

FIGURE	PAGE
1. Uranium-nitrogen phase diagrams according to J. Bugl and D. L. Keller	6
2. Thermal conductivity of reactor fuel materials	7
3. Thermal conductivity of uranium mononitride	8
4. Thermal expansion of uranium nitride, uranium carbide, and uranium dioxide	10
5. Compressive creep of uranium mononitride. Legend: □, ○, △ 6000 pounds per square; ● 8000 pounds per square inch	11
6. Diffusion coefficient of nitrogen in uranium nitride versus reciprocal absolute temperature	13
7. Pressure of nitrogen in equilibrium with uranium nitride plus uranium (l, sat. N ₂) from 1450 to 2850°C.	14
8. Pressure of nitrogen in equilibrium with uranium nitride plus uranium (l, sat. N ₂) from 1300°C. to 2225°C.	15
9. Helium bubble migration distance in uranium carbide as a function of average reciprocal bubble radius. The specimen was held at temperature for one minute	20
10. Synthesis of uranium nitride powder	22
11. Fabrication of uranium nitride pellets	23
12. Sintering cycle for uranium nitride pellets	24

FIGURE	PAGE
13. Typical microstructure of as-sintered uranium mononitride	25
14. Schematic drawing of sample holder for Cockcroft-Walton accelerator	28
15. As-bombarded surface of Type 304 stainless steel sample showing impressions where helium bubbles have migrated out of the bombarded surface. 12,500X. Reduced 16.5 per cent of the original	29
16. Temperature gradient furnace	31
17. Heating unit for temperature gradient furnace	32
18. Illustration of ion bombardment step	34
19. Representative photomicrographs from unbombarded control samples. (a) Replica of as-sintered uranium nitride showing a smooth matrix and associated sintering porosity. 25,000X. (b) Sintering porosity showing definite crystallographic surfaces. 58,000X. (c) Fractured surface of as-sintered uranium nitride showing sintering porosity in a grain boundary. 33,750X. (d) Fractured surface of as-sintered uranium nitride showing a three-grain intersection. 50,000X. Reduced 16 per cent of the original . . .	42
20. Transmission photomicrographs of unbombarded control sample. (a) As-sintered uranium nitride. 50,000X. (b) Arc-cast uranium nitride containing precipitates of free uranium. 25,000X. Reduced 15 per cent of the original	47

FIGURE	PAGE
21. Replicas of as-bombarded surface prior to heat treatment.	
(a) A low magnification photograph illustrating the general features of the surface. 5,500X. (b) A region in the bombarded surface in which bubbles appear to have migrated preferentially down grain boundaries back out of the surface during bombardment; the matrix appears relatively clean compared with the grain boundaries. 37,500X.	
(c) Impressions where bubbles have burst through the surface associated with defects which suggest preferential migration down defects in the structure. 60,000X. Reduced 16 per cent of the original	49
22. Disturbed region of the matrix observed to be two microns from the bombarded surface of specimen 353-12 after heat treatment. 57,500X	53
23. Examples of helium bubbles which have migrated into the uranium nitride samples. (a) Specimen 353-E heat treated at 1585°C. in a temperature gradient of 560°C. per centimeter. 16,250X. (b) Specimen 336-6 heat treated at 1075°C. in a temperature gradient of 400°C. per centimeter. 17,000X. (c) Fractured surface of specimen 353-10 heat treated at 1190°C. in a temperature gradient of 170°C. per centimeter. 60,000X. (d) Low magnification photomicrograph of specimen 353-A heat treated at 1445°C. in a temperature gradient of	

FIGURE	PAGE
23 (continued). 250°C. per centimeter. 5,000X. Reduced 16.5 per cent of the original	54
24. Transmission electron photomicrographs of the single crystal specimen. (a) Helium bubbles with peripheral dark areas indicating strain fields. 100,000X. (b) Very thin region of sample with large light areas which may have resulted from bubbles bursting through the surface of the film or from preferential etching of the region near the bubble. 100,000X Reduced 18 per cent of the original	60
25. Bubble distribution in specimen 336-6 heat treated at 1075°C. for one hour with a temperature gradient of 400°C. per centimeter. The bombarded surface was to the right of the photograph and the bubbles appear to pile up in the left hand region probably at a grain boundary	64
26. Bubble size as function of distance from boundary	65
27. Bubble density as function of distance from boundary	66
28. Surface of specimen 353-10 intergranular fractured with associated helium bubbles. The line showing a preponderance of gas bubbles is a three-grain intersection which appears to be an unusually stable trapping site for the bubbles. 15,000X Reduced 17 per cent of the original	68
29. Bubbles in specimen 353-E which have apparently been trapped at a grain boundary. This specimen was heat treated at	

FIGURE	PAGE
29 (continued). 1585°C. in a temperature gradient of 560°C. per centimeter. 35,000X. Reduced 17 per cent of the original	69
30. Bubbles lined up at grain boundaries both parallel and perpendicular to the temperature gradient. The bubbles were shadowed in the direction parallel to the temperature gradient. 42,000X. Reduced 17 per cent of the original	71
31. Illustration of how bubbles may form projections on the surface after polishing	73
32. Photomicrographs of specimen 353-12 after multiple heat treatments. Large bubbles (1000 angstroms in diameter) which exhibit planar interfaces are surrounded by smaller satellite bubbles (200 angstroms in diameter) which are nearly spherical. 115,000X. Reduced 16 per cent of the original	74
33. Illustration of multiple heat treatments of specimen 353-12	76
34. Surface diffusion coefficient as a function of reciprocal temperature	80
35. A graph of true temperature versus observed temperature to correct for the lack of blackbody conditions	94
36. Temperatures recorded during heat treatment of specimen 353-1 as a function of time	95

FIGURE	PAGE
37. Temperature of bombarded end of specimen 16-353 as a function of time	96
38. Temperature of bombarded end of specimen 353-19 as a function of time	97
39. Temperature recorded during heat treatment of specimen 353-A as a function of time	98
40. Temperature of bombarded end of specimen 353E as a function of time	99
41. Temperature of bombarded end of specimen 353-FAS as a function of time	100
42. Temperature of bombarded end of specimen 353G as a function of time	101
43. Temperature of bombarded end of single-crystal specimen as a function of time	102

CHAPTER I

INTRODUCTION

I. OBJECTIVE OF THE STUDY

The purpose of this study was to examine the migration and coalescence of inert helium-gas bubbles in uranium mononitride in a temperature gradient. The primary objective was to determine the mode and velocity of bubble movement. We hoped the results would closely relate to the migration of the inert fission-product gases, krypton and xenon, which are known to have very detrimental effects on irradiation stability of nuclear fuels. Uranium mononitride was chosen as the nuclear fuel in which to conduct this study because it is considered to be an attractive fuel candidate for both central power station fast breeder and space electric power reactors.

II. IMPORTANCE OF THE STUDY

The interest in inert gas-bubble migration in nuclear fuels is derived from the performance limitations imposed by the formation of fission-gas atoms during irradiation. Approximately 0.25 inert-gas atoms of krypton and xenon are produced for every uranium atom fissioned. Johnson and Shuttleworth (1)* have shown that these gas atoms exhibit a very low atomic solubility of 10^{-4} to less than 10^{-11} in some metals in

*Denotes reference. See page 88.

the liquid state. In addition, Ruffe (2) reports helium solubilities in UO_2 at 100 atmospheres pressure of 1.0×10^{-8} and 4.8×10^{-9} (atom fraction) at 1200 and 1300°C., respectively. It is likely that the larger atoms of krypton and xenon have solubilities even less than that observed for helium.

It is postulated that the fission-gas atoms (3,4,5), initially trapped within the lattice, initiate movement by combining with one or two vacancies which render the gas atoms mobile. The gas atom-vacancy combinations further react with other gas atoms or gas atom-vacancy combinations until two or three gas atoms have formed a nucleus (4). These nuclei, essentially stable, then grow by the addition of gas atoms and vacancies until the gas-vacancy combination can be called a bubble (a bubble is arbitrarily designated as a gas-vacancy configuration containing sufficient vacancies so that the gas may be described by the van der Waals' equation).

The bubbles, once formed, are probably free to migrate, by mechanisms to be described in a later section, until they reach an internal surface such as a grain boundary. These grain-boundary trapping sites enhance coalescence with other gas bubbles, resulting in a volume increase which severely limits the use of nuclear fuels in most reactor applications. As these fission-gas bubbles become interconnected at grain boundaries, fission-gas release is increased.

Solid fission products also contribute to fuel swelling. This type of swelling probably cannot be prevented although it can be accommodated by design. Swelling caused by gaseous fission products

may be of much larger magnitude and must be controlled. It is with this prospect in mind that the present study of helium-gas diffusion was undertaken.

In addition to the fundamental interest and the possible application of the results to existing irradiation data, there is a third reason for studying this system. There presently exists no established out-of-reactor experimental or theoretical technique for predicting the irradiation behavior of nuclear fuels. Scientific and engineering estimates are all that can be used to predict the outcome of experiments whose cost is on the order of \$100,000 each. The successful development of a technique by which inert gases in materials may be studied could eliminate much of this guesswork. Since accelerator costs are low (about one to ten dollars per specimen), it may be possible to study existing and potential fuels for the cost of the material plus the manpower spent in examining a specimen of interest.

For example, it has been shown that additions of stable precipitates enhance the irradiation stability of some fuels (6). This experimental technique should allow us to predict which precipitates would be effective in pinning bubbles and thereby improving the irradiation behavior.

Uranium mononitride was chosen as the nuclear fuel in which to conduct this study because it is considered to be an attractive fuel candidate for both fast breeder and space reactors. Uranium mononitride is face-centered cubic (rock salt crystal structure) with a lattice

parameter of 4.8889 angstroms and has the following desirable properties:

(1) high thermal conductivity, (2) high uranium density, (3) high melting point, (4) good compatibility with most cladding materials, and (5) good compatibility with most liquid metals.

CHAPTER II

LITERATURE SURVEY

I. DESCRIPTION OF THE URANIUM-NITROGEN SYSTEM AND THE PROPERTIES OF URANIUM MONONITRIDE

Three phase diagrams of the uranium-nitrogen system at varying overpressures of nitrogen are shown in Figure 1. These phase diagrams indicate a very narrow solubility region at the UN phase boundary. Inouye has used pressure measurements to study this region (7) and has concluded that there exists a composition width of 0.5 to 1.0 atomic per cent nitrogen. The relatively narrow width of this region plus a difference of 10^{10} in vapor pressure between UN and U_2N_3 makes stoichiometric UN fairly easy to fabricate. Uranium mononitride melts congruently at $2850 \pm 30^\circ C.$, at 2.5 atmospheres (8).

Two properties of UN which make it interesting as a fuel are high thermal conductivity and high uranium density. The thermal conductivity of UN (8) is shown in Figure 2 along with that of UC, UO_2 , and uranium metal for comparison. It is interesting that the thermal conductivity of UN, as shown in Figure 3 (ref. 9), increases with temperature from 0.16 watts per centimeter per degree Centigrade at $200^\circ C.$ to 0.26 watts per centimeter per degree Centigrade at $1500^\circ C.$ where it appears to remain relatively constant as temperature increases.

The x-ray density of UN is 14.32 grams per cubic centimeter at room temperature compared to 13.63 grams per cubic centimeter for UC,

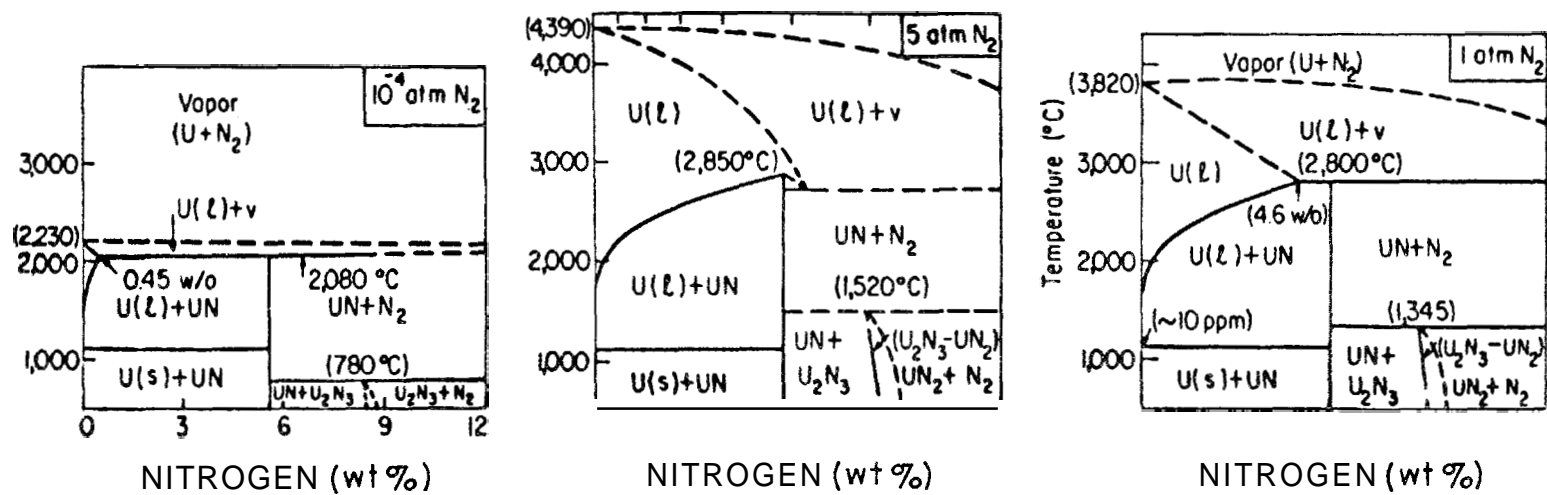


Figure 1. Uranium-nitrogen phase diagrams according to J. Bugl and D. L. Keller.*

* J. Bugl and D. L. Keller, "Uranium Mononitride - A New Reactor Fuel," *Nucleonics* 22(9), 66 (1964).

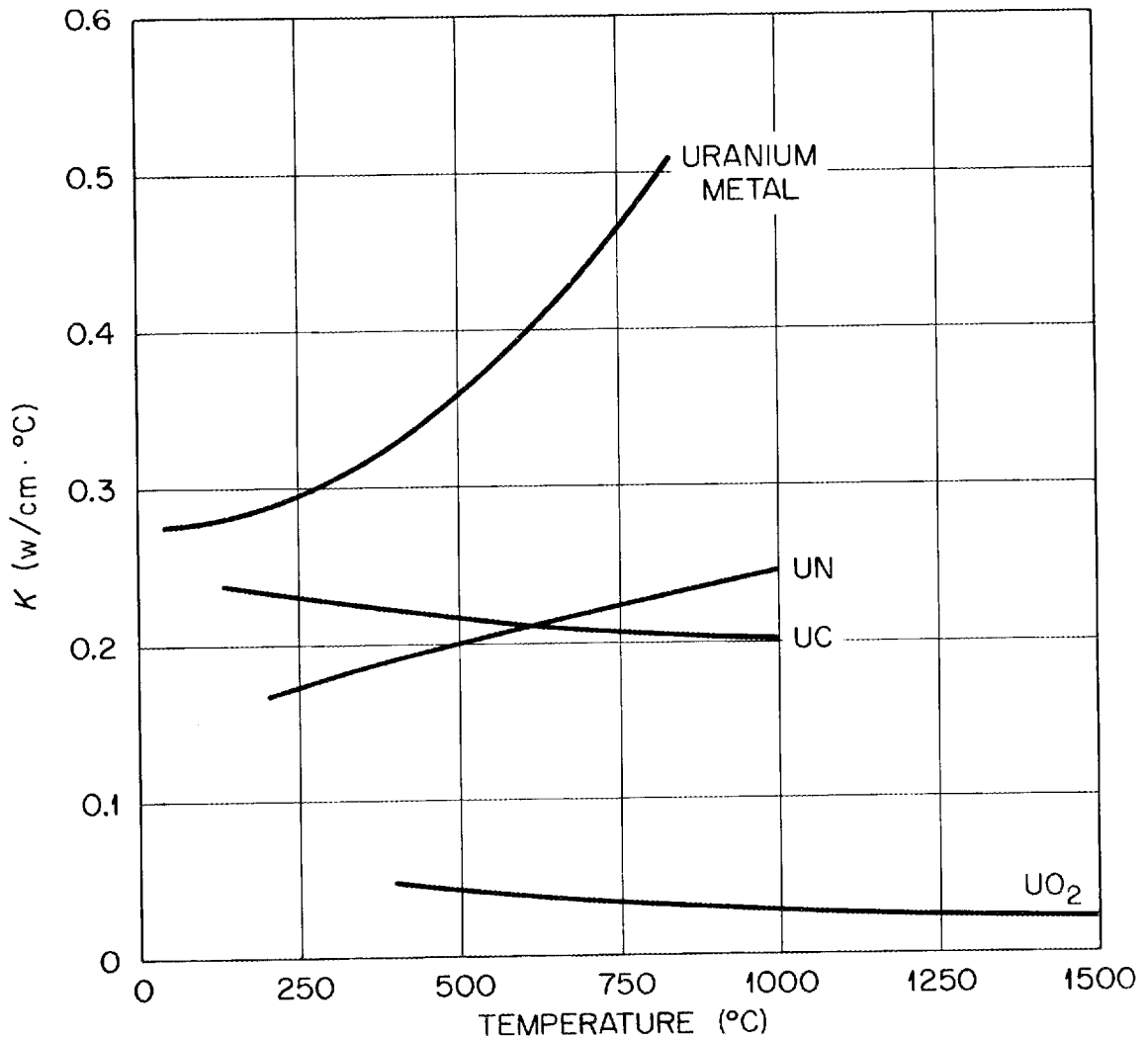


Figure 2. Thermal conductivity of reactor fuel materials.*

*J. Bugl and D. L. Keller, "Uranium Mononitride - A New Reactor Fuel," *Nucleonics* 22(9), 66 (1964).

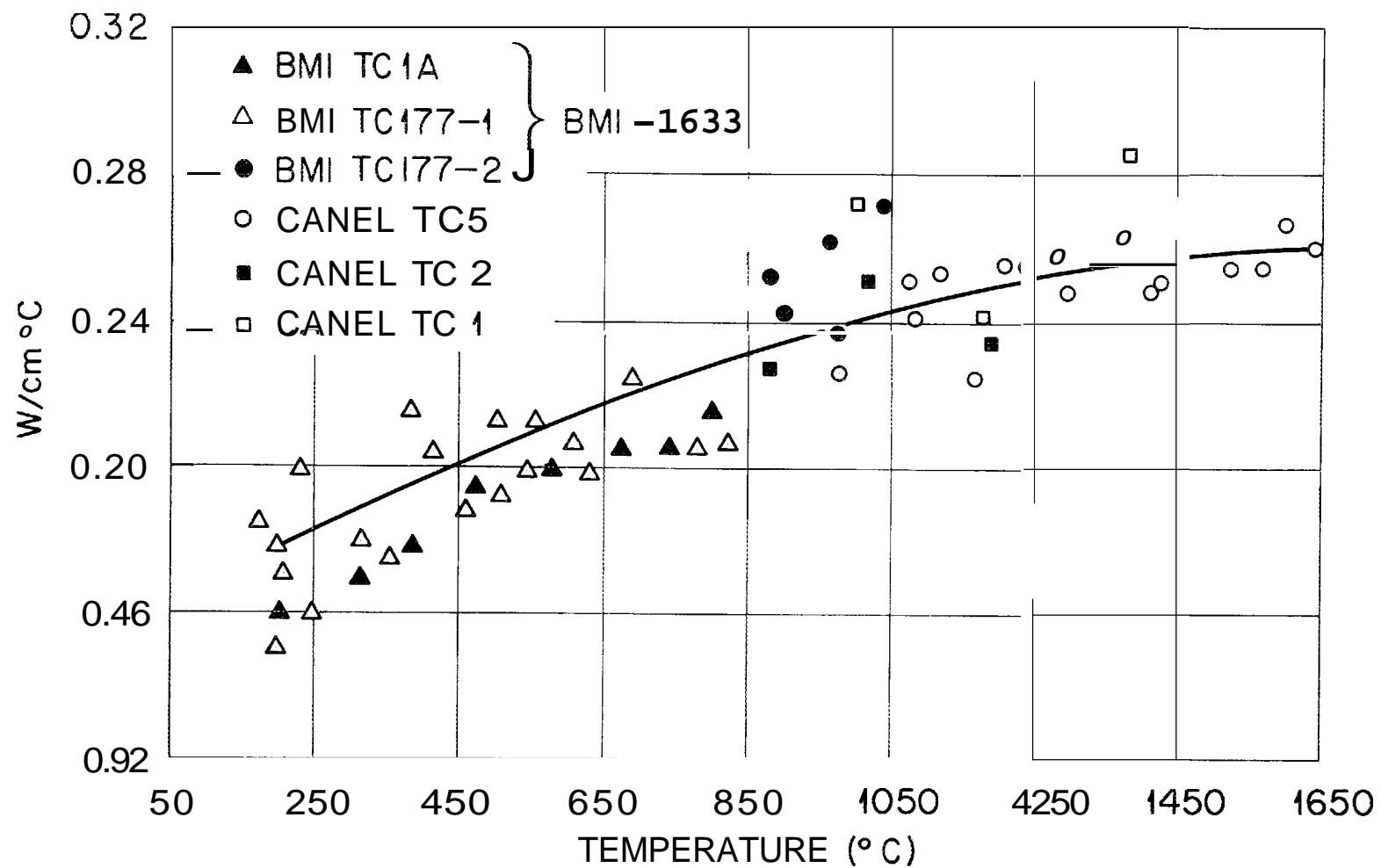


Figure 3. Thermal conductivity of uranium mononitride.*

*
 B. A. Hayes and M. A. DeCrescente, "Thermal Conductivity and Electrical Resistivity of Uranium Mononitride," PWAC-481, Middletown, Connecticut, Pratt and Whitney-CANEL, Division of United Aircraft Corporation (October 1965).

10.97 grams per cubic centimeter for UO_2 , and 19.12 grams per cubic centimeter for uranium metal (8). Upon heating, the UN lattice expands at a rate of about 1 per cent per 1000°C . as shown in Figure 4 (ref. 8). X-ray diffraction data show that the crystal structure of UN_2 is face-centered cubic lattice with a room-temperature lattice constant of $a = 4.8889$ angstroms (10). Also formed in the uranium-nitrogen system are uranium sesquinitride, U_2N_3 , and uranium dinitride, UN_2 . Uranium sesquinitride is body-centered cubic with a lattice parameter of $a = 10.68$ and an x-ray density of 11.25 grams per cubic centimeter (11). The UN_2 forms a face-centered cubic lattice with a parameter $a = 5.339$ angstroms. The dinitride phase is formed only at very high pressures and is never seen in the routine fabrication process. The U_2N_3 , however, is often seen associated with second-phase UO_2 in specimens containing a high oxygen content (2000 parts per million or greater).

Some mechanical properties, tested on 96 per cent theoretically dense material by Bugl and Keller of Battelle Memorial Institute (8), are shown below:

Modulus of elasticity:	31×10^6 pounds per square inch
Shearing modulus of elasticity:	14×10^6 pounds per square inch
Poisson's ratio:	0.1
Knoop hardness:	600 to 700

The compressive creep rate was measured by Fassler, Huegel, and DeCrescente (12), and the results are illustrated graphically in Figure 5.

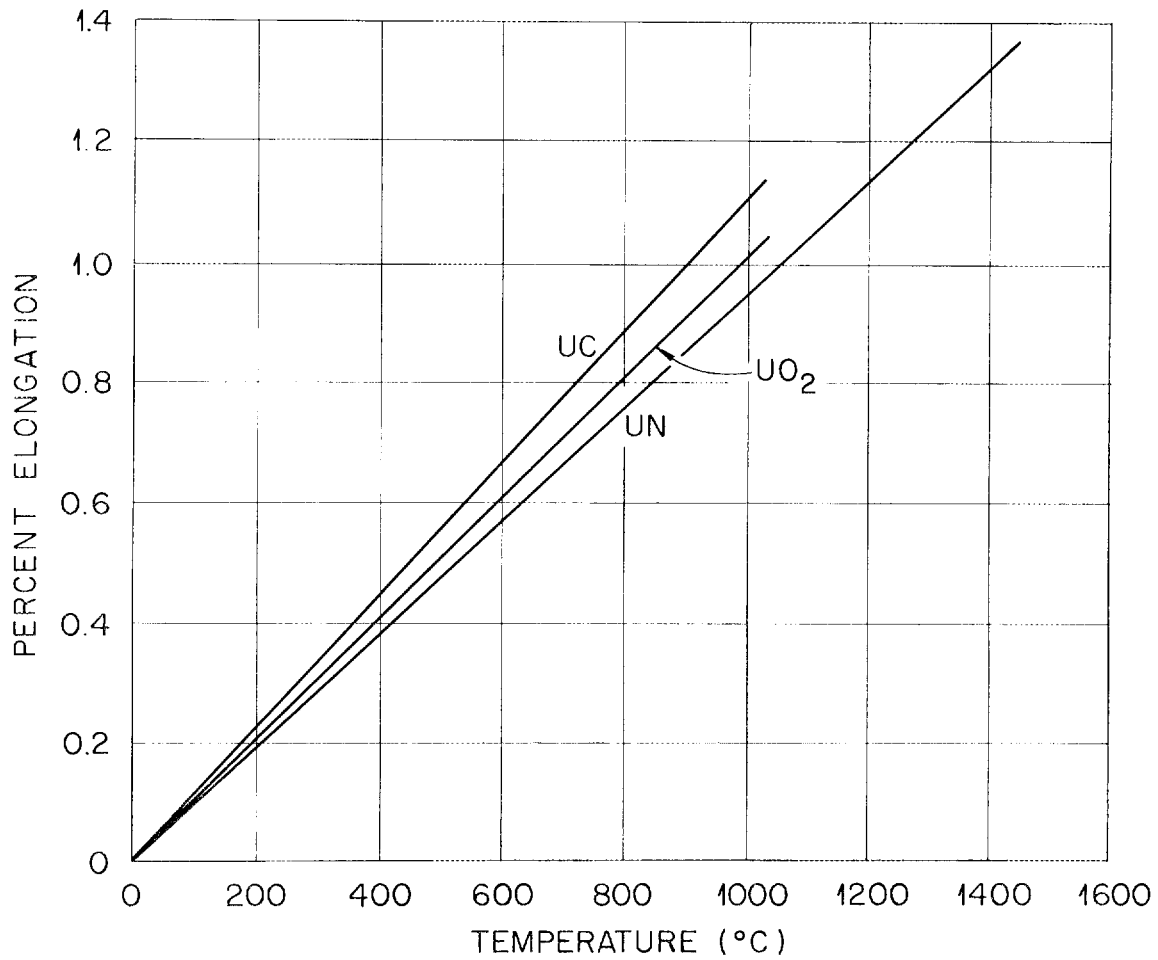


Figure 4. Thermal expansion of uranium nitride, uranium carbide, and uranium dioxide.*

*J. Bugl and D. L. Keller, "Uranium Mononitride - A New Reactor Fuel," *Nucleonics* 22(9), 66 (1964).

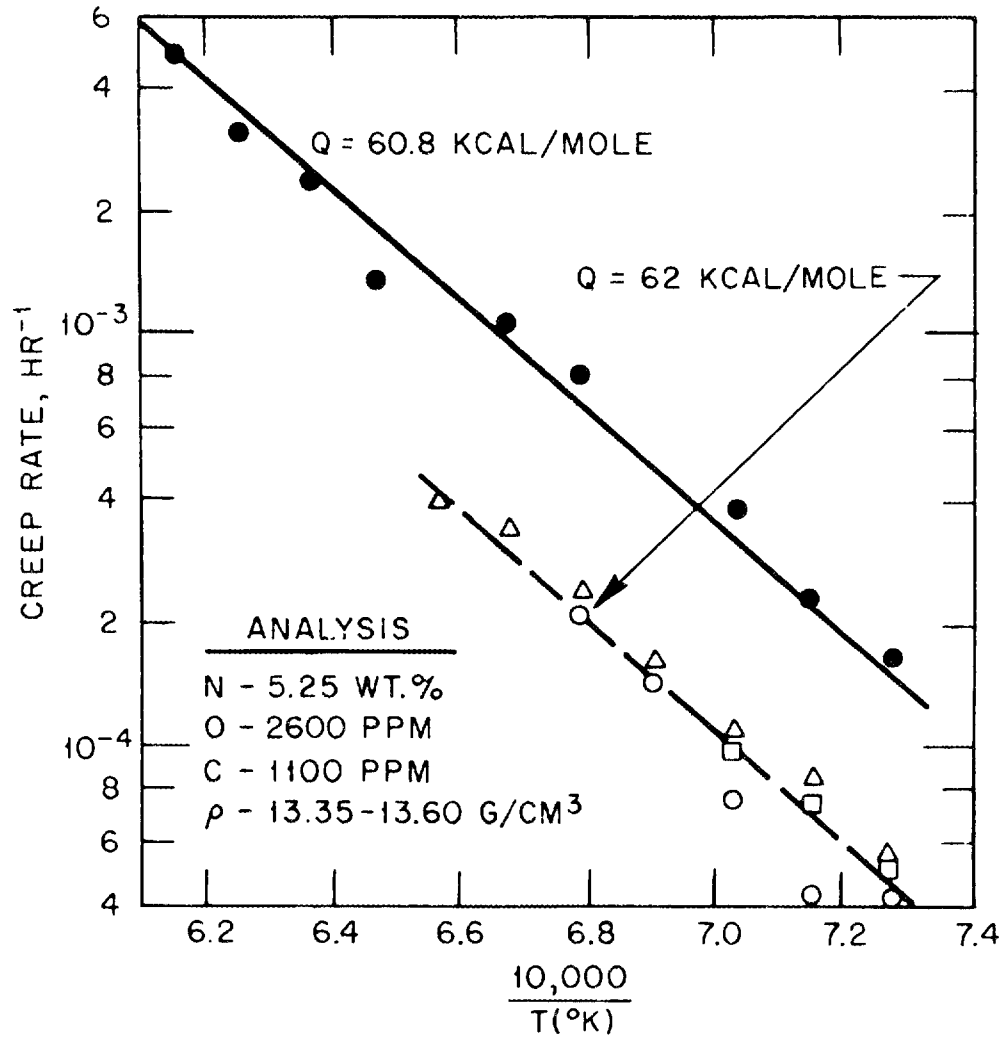


Figure 5. Compressive creep of uranium mononitride. Legend: \square, \circ, Δ 6000 pounds per square inch; \bullet 8000 pounds per square inch.*

*M. Fassler, F. J. Huegel, and M. A. DeCrescente, "Compressive Creep of UC and UN," Part I, PWAC-482, Middletown, Connecticut, Pratt and Whitney Aircraft-CANEL, Division of United Aircraft Corporation (October 1965).

The self-diffusion of nitrogen-15 in UN was studied by Sturiale and DeCrescente (13). The results are illustrated graphically in Figure 6. Over the temperature range 1500 to 1870°C., the diffusion coefficient is given by

$$D^N \text{ (square centimeters per second)} = 2.6 \times 10^{-4} \exp(-55,000/RT) .$$

The equilibrium vapor pressure of nitrogen over UN is plotted as a function of temperature in Figures 7 and 8. In the high-temperature region, shown in Figure 7, good agreement was found among different experimenters. However, a discrepancy existed in the lower temperature region which was subsequently studied by Inouye and Leitnaker, Figure 8. These curves were taken from a report (14) by Inouye and Leitnaker. Godfrey, Woolley, and Leitnaker also have made a critical evaluation of the thermodynamics of the UN system (15). The evaluation was done on the raw data collected by many experimenters at several laboratories.

II. GAS BUBBLE MIGRATION

Bubble migration occurs as the matrix atoms move from the leading to the trailing surface of a bubble. Three modes of bubble migration have been suggested: (1) surface diffusion, (2) evaporation-condensation, and (3) bulk diffusion. Bubble movement effectively occurs each time a vacancy enters or leaves a bubble. However, it is only when a driving force is present (e.g., a temperature gradient) that the motion of the gas bubbles becomes directionally oriented.

Experimental studies of gas bubble motion in a temperature gradient have been reported on three materials: Cu, UC, and UO₂. The

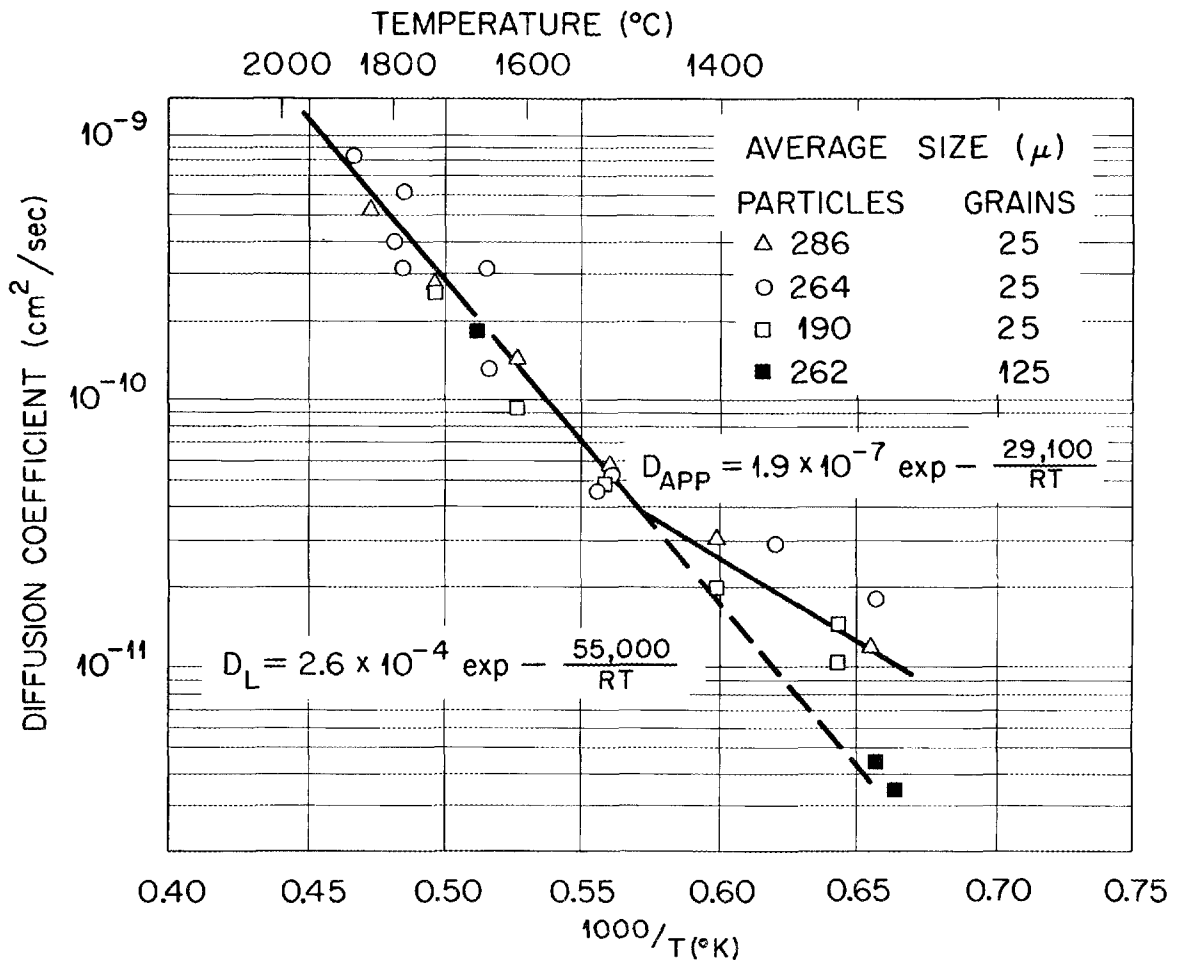


Figure 6. Diffusion coefficient of nitrogen in uranium nitride versus reciprocal absolute temperature.*

*T. J. Sturiale and M. A. DeCrescente, "Self-Diffusion of Nitrogen in Uranium Mononitride," FWAC-482, Middletown, Connecticut, Pratt and Whitney Aircraft-CANEL, Division of United Aircraft Corporation (October 1965).

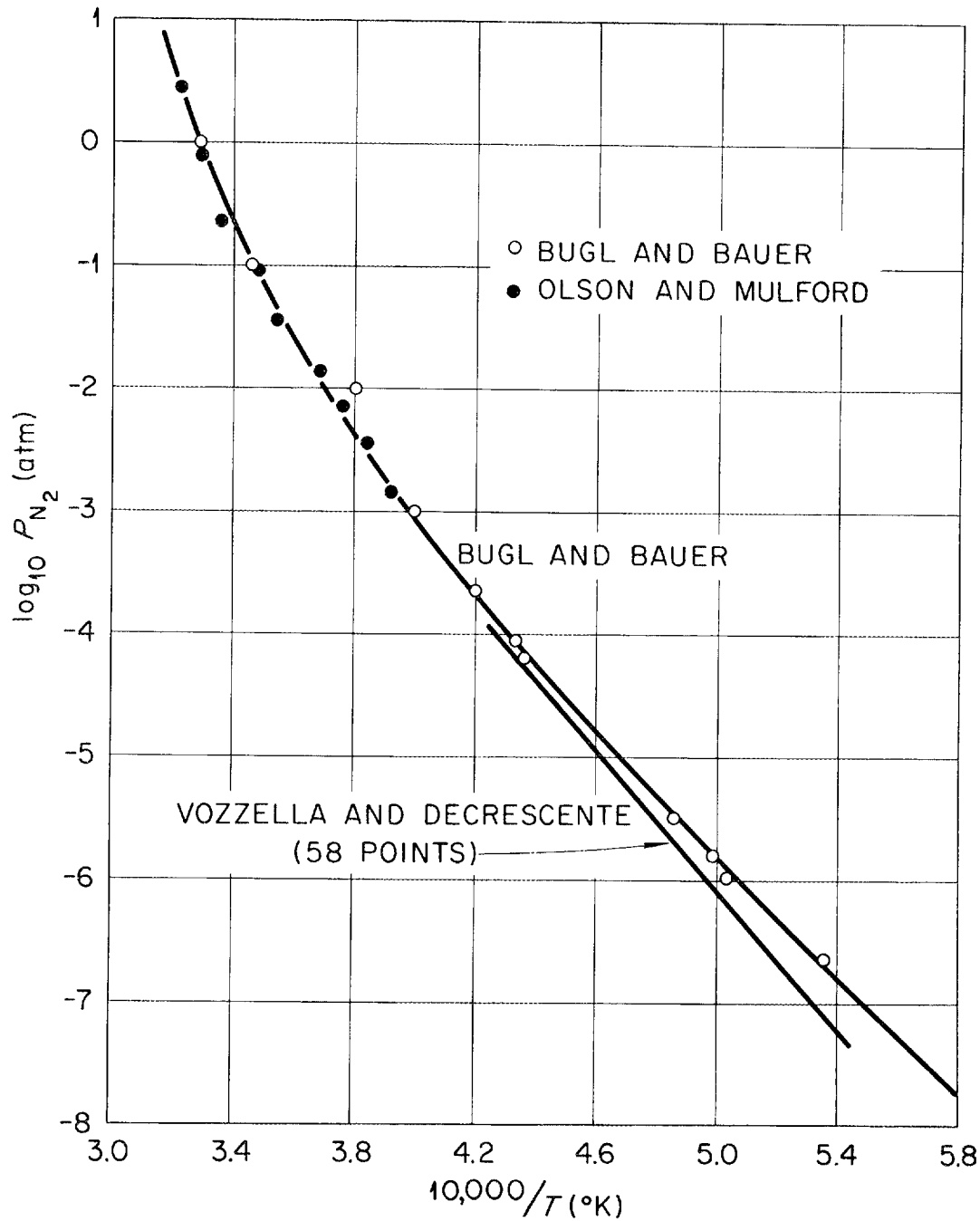


Figure 7. Pressure of nitrogen in equilibrium with uranium nitride plus uranium (*l*, sat. N_2) from 1450 to 2850°C.*

*H. Inouye and J. M. Leitnaker, "Equilibrium Nitrogen Pressures and Thermodynamic Properties of UN," accepted for publication in the "Journal of the American Ceramic Society."

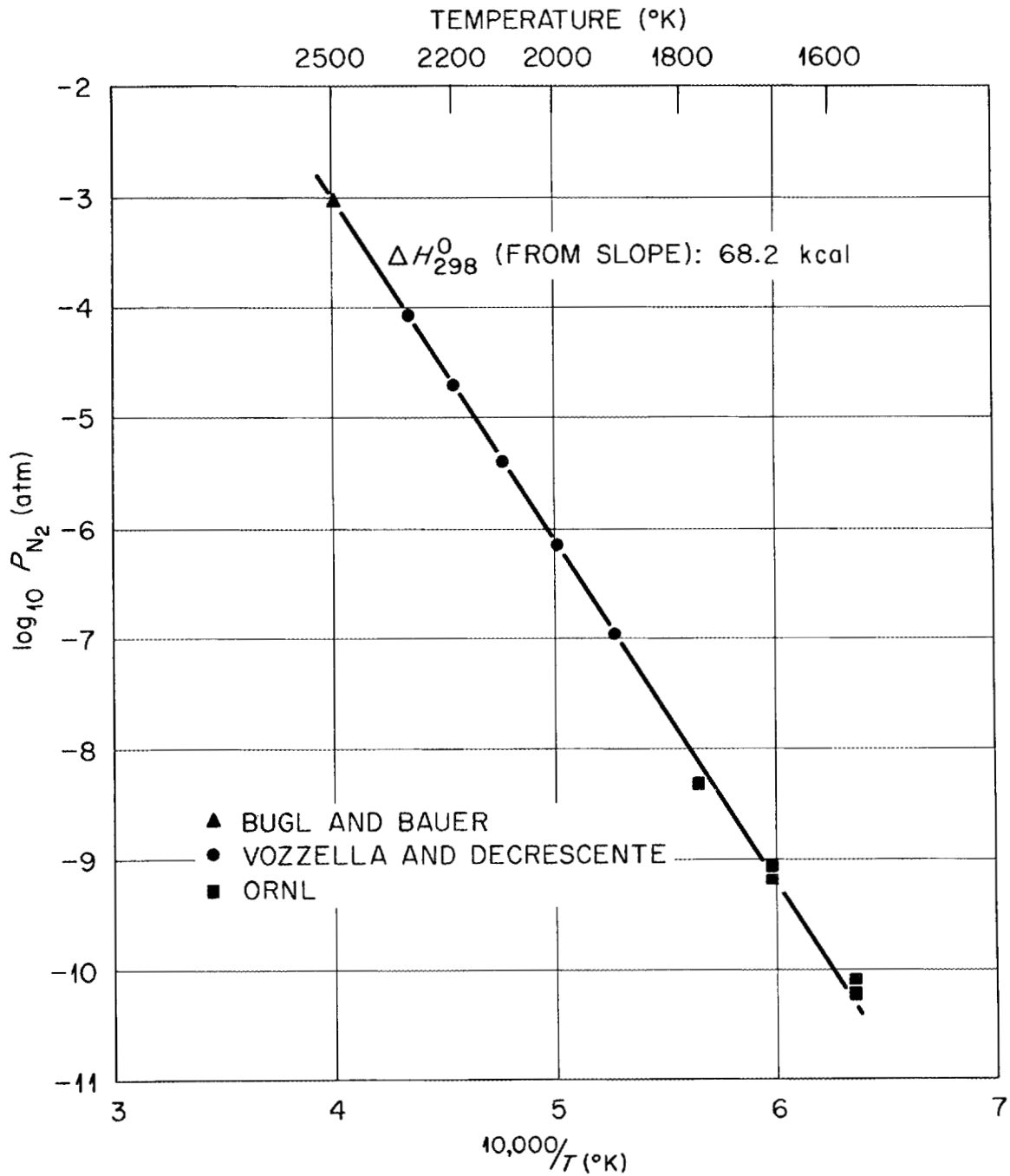


Figure 8. Pressure of nitrogen in equilibrium with uranium nitride plus uranium (*l*, sat. N_2) from 1300°C. to 2225°C.*

*H. Inouye and J. M. Leitnaker, "Equilibrium Nitrogen Pressures and Thermodynamic Properties of UN," accepted for publication in the "Journal of the American Ceramic Society."

evidence presented indicated that bubbles in copper (16) and UC (17) move by surface diffusion while bubbles in UO_2 (18) migrate by evaporation-condensation. Some work by Gulden (19) suggests that very small UO_2 bubbles may migrate by bulk diffusion.

The equation derived by Shewmon (20) for predicting the velocity of gas bubble movement by surface diffusion is

$$\frac{dx}{dt} = \frac{2D_s \delta Q}{kT^2} \cdot \frac{dT}{dx} \frac{1}{r}, \quad (1)$$

where

$\frac{dx}{dt}$ = velocity of bubble,

D_s = surface diffusion coefficient,

δ = thickness of high diffusivity layer around the bubble,

Q = heat of transport, the energy carried with an atom as it migrates down the temperature gradient,

k = Boltzmann's constant,

T = average temperature,

$\frac{dT}{dx}$ = temperature gradient,

r = radius of a bubble.

The thickness of the high diffusivity layer, δ , is assumed to be the same as the lattice parameter for face-centered cubic materials because only the surface atoms are diffusing. The quantity, Q , is not known from experiment for such systems, but from theoretical considerations Shewmon (20) has suggested that its value should be of the order of magnitude of the activation energy for surface diffusion. From the

above equation it is apparent that bubbles migrating by surface diffusion move at a velocity inversely proportional to the radius. Thus bubbles migrating from a single source would be expected to show a size distribution such that smaller bubbles would migrate further than large bubbles. Gruber (21) derived the same equation except that, instead of a constant term of 2, he showed this to be 1.78 for face-centered cubic materials.

For bubble migration by evaporation-condensation, Speight (22) derived

$$V_b \approx \frac{r}{(6\pi\gamma\sigma^2)} \left(\frac{8kT}{\pi m}\right)^{\frac{1}{2}} \left(\frac{\rho_g}{\rho_s}\right) \left(\frac{l}{T}\right) \frac{dT}{dx}, \quad (2)$$

where

V_b = velocity of bubble,

r = radius of bubble,

γ = surface tension,

σ = diameter of vapor atom,

m = mass of vapor atom,

$\frac{\rho_g}{\rho_s}$ = ratio of density of matrix atoms in vapor to their density
in the solid,

l = latent heat per atom.

Thus, bubbles migrating by an evaporation-condensation mechanism are expected to move at a velocity directly proportional to the bubble radius.

The third mechanism by which bubbles can move is volume diffusion. This mechanism requires that vacancies leave the bubble at the trailing surface, migrate through the bulk of the specimen to the leading surface,

and be reabsorbed into the bubble at the leading surface. The equation derived by Shewmon (20) for predicting the bubble velocity by this mechanism is given below:

$$\frac{dx}{dt} = \frac{2D_b Q}{fkT^2} \cdot \frac{dT}{dx} , \quad (3)$$

where

D_b = bulk diffusion coefficient,

Q = heat of transport,

f = correlation coefficient.

Thus, bubbles move by bulk diffusion at a velocity independent of the bubble size.

No work has ever conclusively proven or disproven Equations (1) through (3). While the surface diffusion equation is thought to hold for copper, the uncertainties in the experiment on copper by Barnes and Mazey (16) were such that the average temperature and the temperature gradient are only estimates, and no quantitative analysis was performed on UC and UO₂. In addition, a private communication with Shewmon (23) revealed that he has observed helium bubbles in gold which migrated at a rate six orders of magnitude slower than these equations predict. These experiments were performed by isothermally annealing thin films of gold with coalescence occurring from random walk.

The only driving force for bubble movement considered in Equations (1) and (2) is a temperature gradient. Three other possible driving forces (3, 16) are dislocation movement, grain boundary sweeping, and strain gradients. Dislocation movement is probably the

most important of these three as Barnes has shown that dislocations exhibit a large binding force with the bubbles. However, Barnes and Mazey's work (16) on thin films of copper bombarded with helium atoms shows that a temperature gradient is important if not the predominant driving force. Also, Gruber's (21) calculations show that bubble coalescence by random walk is of little significance.

Selleck and DeCrescente (17) showed that helium bubbles migrate by surface diffusion in UC. Right-circular cylinder samples of UC were bombarded with 100,000 electron volt alpha particles and then heat treated on a tungsten bar for one minute. This provided a temperature gradient of approximately 90°C. per millimeter with a temperature of about 750°C. at the bombarded end. A plot of the distance the bubbles moved as a function of average reciprocal bubble radius is shown in Figure 9. The resulting straight line was interpreted by Selleck and DeCrescente as indicative of a surface diffusion mechanism.

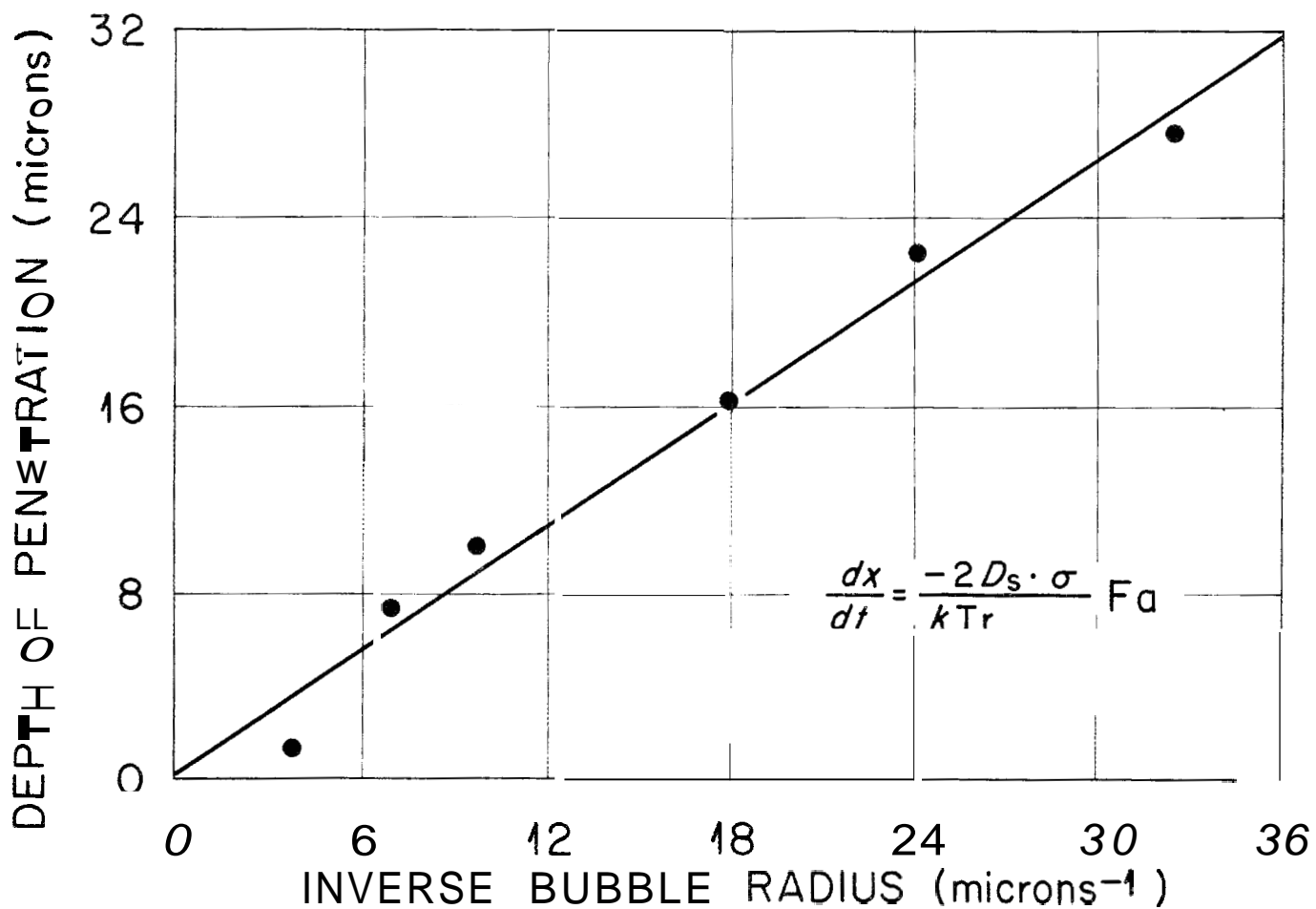


Figure 9. Helium bubble migration distance in uranium carbide as a function of average reciprocal bubble radius. The specimen was held at temperature for one minute.*

* E. G. Selleck and M. A. DeCrescente, "Fission-Gas Migration Studies in Uranium Carbide," *AWAC-476*, Middletown, Connecticut, Pratt and Whitney Aircraft-CANEL, Division of United Aircraft Corporation (October 1965).

CHAPTER III

MATERIALS AND EQUIPMENT

I. PREPARATION OF URANIUM NITRIDE SAMPLES

The UN samples used in this study were fabricated* by cold pressing and sintering UN powder. The synthesis, fabrication, and sintering steps are shown in Figures 10 through 12. A typical microstructure of an as-sintered UN specimen is shown in Figure 13. Some of the characteristics of the UN samples produced by this procedure are shown in Table I.

In addition to the cold-pressed-and-sintered pellets fabricated at ORNL, ten arc-melted samples were purchased from Battelle Memorial Institute, Columbus, Ohio. These samples were fabricated by melting uranium in 30 atmospheres of nitrogen and casting the resulting UN into 1-inch billets. The center of these castings contained quite large grains from which single-crystal, two-, or three-crystal pellets were cut. These crystals were used primarily to develop a thinning technique for UN.

*The pellets were fabricated by R. A. Potter of the Metals and Ceramics Division of the Oak Ridge National Laboratory.

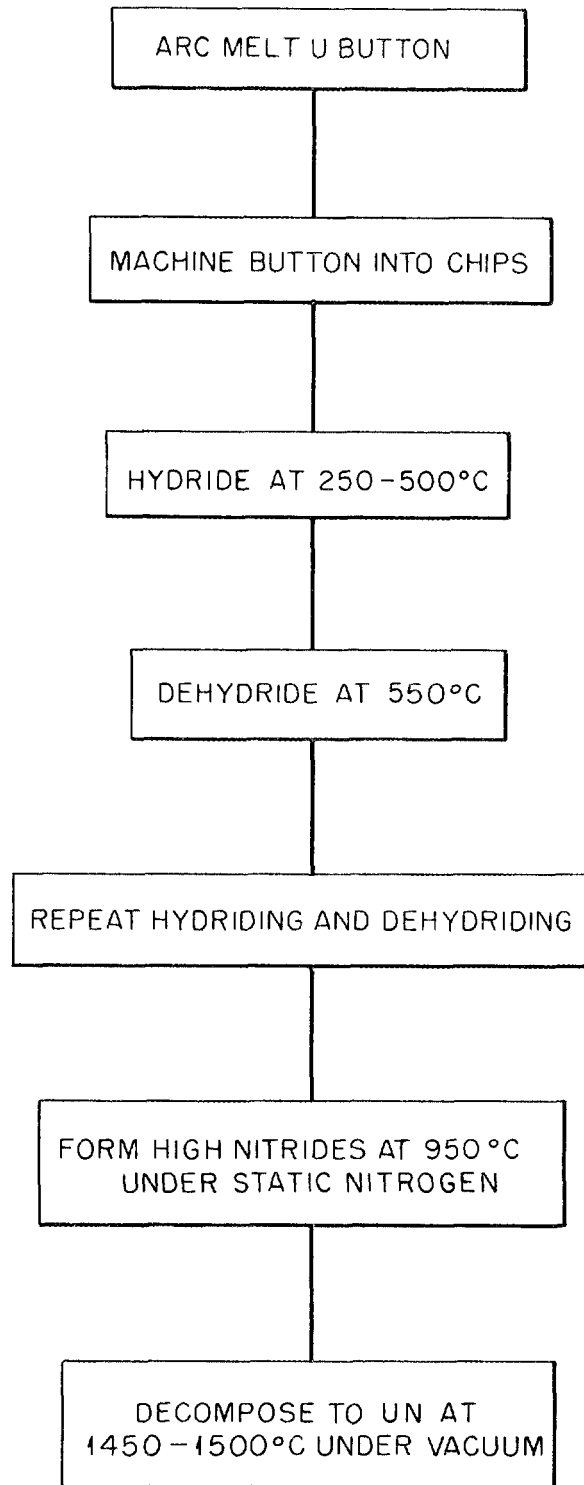


Figure 10. Synthesis of uranium nitride powder.

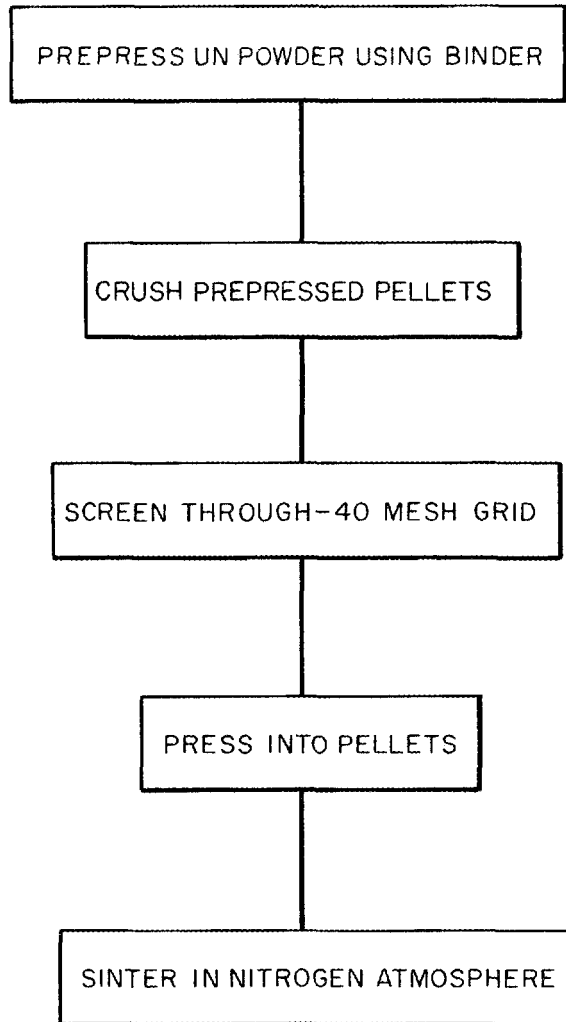


Figure 11. Fabrication of uranium nitride pellets.

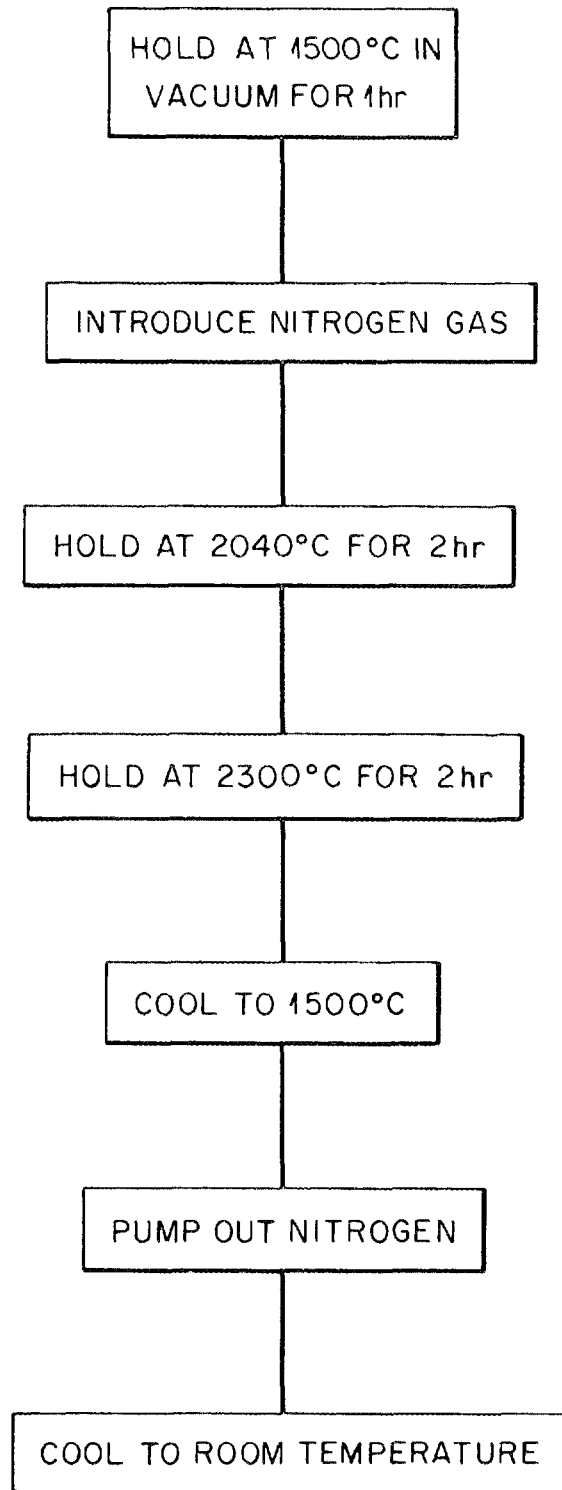


Figure 12. Sintering cycle for uranium nitride pellets.

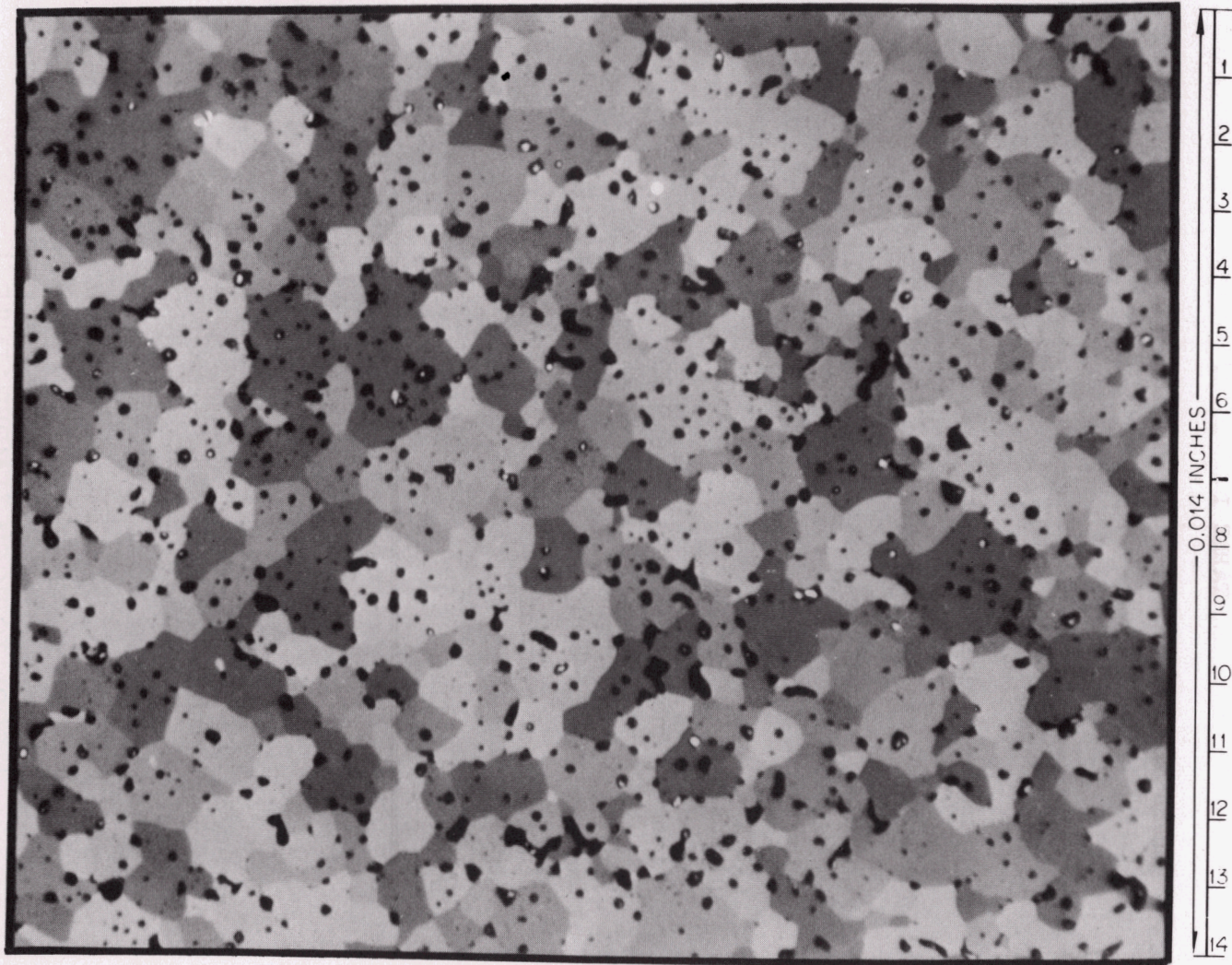


Figure 13. Typical microstructure of as-sintered uranium mononitride.

TABLE I
CHARACTERISTICS OF URANIUM NITRIDE SPECIMENS
USED FOR HELIUM INOCULATION

Chemical analysis	
Nitrogen, weight per cent	5.3 ± 0.2
Oxygen, weight per cent	0.1 ± 0.02
Carbon, weight per cent	0.01 ± 0.01
Uranium	Balance
Dimensions	
Length, inch	0.300
Diameter, inch	0.300
Density, per cent of theoretical	94
Number of pellets	40

II. SAMPLE HOLDER FOR COCKCROFT-WALTON ACCELERATOR

A schematic drawing of the specimen holder used in the Cockcroft-Walton accelerator is shown in Figure 14. The UN samples were placed into the holder that is made to fit on the end of the beam tube of the accelerator. The sample holder is constructed primarily of stainless steel, containing Teflon as an electrical insulator; and a tantalum shield placed in front of the specimen prevents the beam from hitting and affecting the Teflon. The shield was made from 0.010-inch-thick tantalum foil with a 2-millimeter aperture which allowed most of the beam to strike the UN specimen. Before the tantalum shield was used, the spread in the gas-ion beam allowed the helium ions to strike the Teflon, resulting in loss of vacuum and consequently a shutdown of the accelerator. Electrical current was read from the copper cooling lines and gave a measurement of the ion flux.

The bombardment of some uncooled stainless steel specimens showed the necessity of water cooling during bombardment. The bombarded surface of a stainless steel specimen was examined by replication after bombardment in our initial setup which did not provide water cooling. The replicated surface, Figure 15, showed a large number of impressions (1.98×10^8 per square centimeter), indicating that the helium gas atoms had agglomerated into bubbles and migrated back out the bombarded surface. Immediately after bombardment, the stainless steel specimens were observed to be quite hot, suggesting that the bubbles may have been sufficiently mobile to cause the observed effect. Since one would expect the

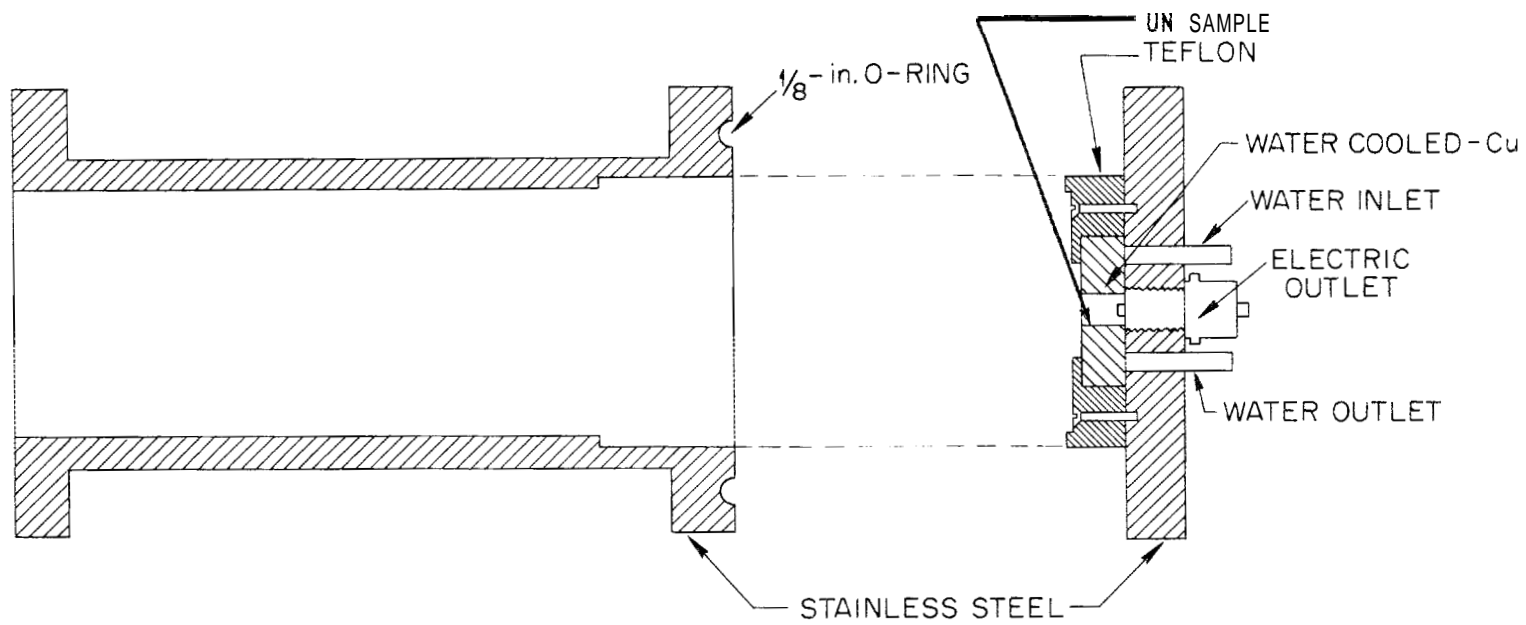


Figure 14. Schematic drawing of sample holder for Cockcroft-Walton accelerator.



Figure 15. As-bombarded surface of type 304 stainless steel sample showing impressions where helium bubbles have migrated out of the bombarded surface. 12,500X. Reduced 16.5 per cent of the original.

bombarded surface to be hotter than the remainder of the specimen, the resulting temperature gradient would be expected to cause bubble migration out of the bombarded surface as observed.

III. TEMPERATURE GRADIENT FURNACE

By far the most formidable task was the development of a high-temperature furnace capable of producing a desired temperature gradient across the sample. A schematic diagram of the final furnace design is shown in Figure 16. The heating unit for this furnace, shown in Figure 17, consists of 0.040-inch molybdenum wire wrapped around a cylindrical piece of tungsten-2 per cent ThO_2 . A coating of Al_2O_3 , flame sprayed on the tungsten-2 per cent ThO_2 element, provided electrical insulation between the molybdenum wire and the element. A second overcoat of Al_2O_3 was flame sprayed over the wrapped element. With this heating unit we were able to achieve 1500°C . on the cold end of specimens being heat treated. Details of the experimental procedure associated with this furnace are presented in Chapter IV.

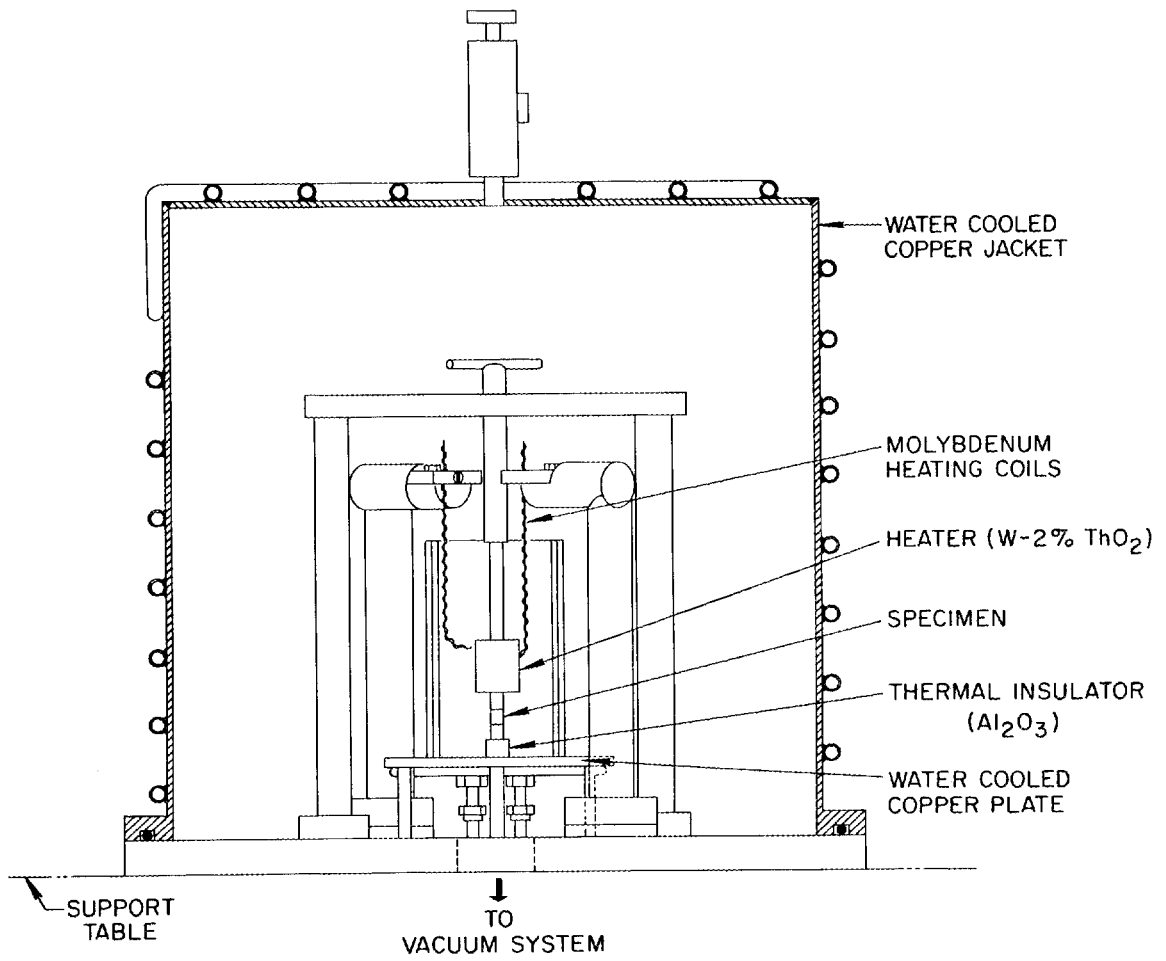


Figure 16. Temperature gradient furnace.

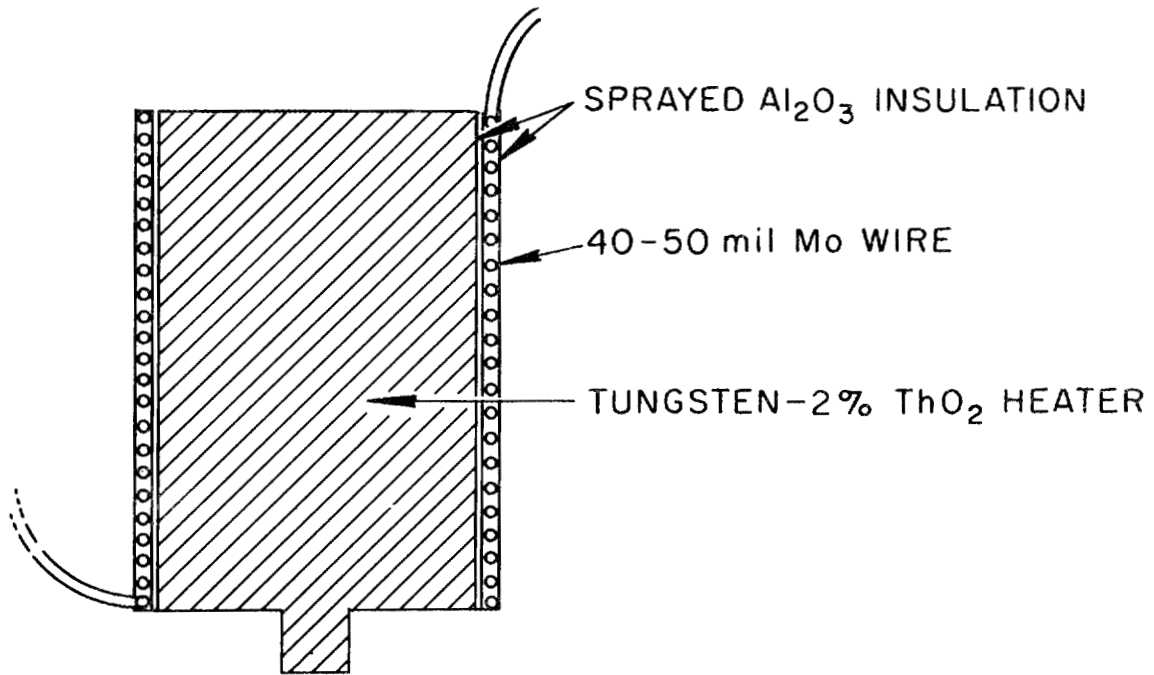


Figure 17. Heating unit for temperature gradient furnace.

CHAPTER IV

EXPERIMENTAL PROCEDURE

I. INJECTION OF HELIUM GAS

The UN specimens were bombarded on one end with helium ions from a Cockcroft-Walton accelerator. The helium ions were accelerated to a nominal energy of 250 kilo-electron volts. The calculations presented below show that the ions should have come to rest in a monolayer about 5400 angstroms below the surface of the specimens. The ion bombardment step is illustrated in Figure 18.

Because the alpha particle energies are low, the ratio of the alpha-particle stopping cross section to proton stopping cross section is less than 4.0. For 250 kilo-electron volt alpha particles this ratio is 2.20 (24). The range of 250 kilo-electron volt alpha particles in air, R_{air} , is 0.21 milligram per square centimeter. For other absorbers the range (25) is given by:

$$R_z = R_{\text{air}} [0.90 + 0.0275 Z + (0.06 - 0.0086 Z) \log E/M], \quad (4)$$

where

R_z = range of alpha particles in elemental material containing
z protons,

Z = number of protons in atoms of material being bombarded,

E = energy of bombarding alpha particles,

M = mass of alpha particles.

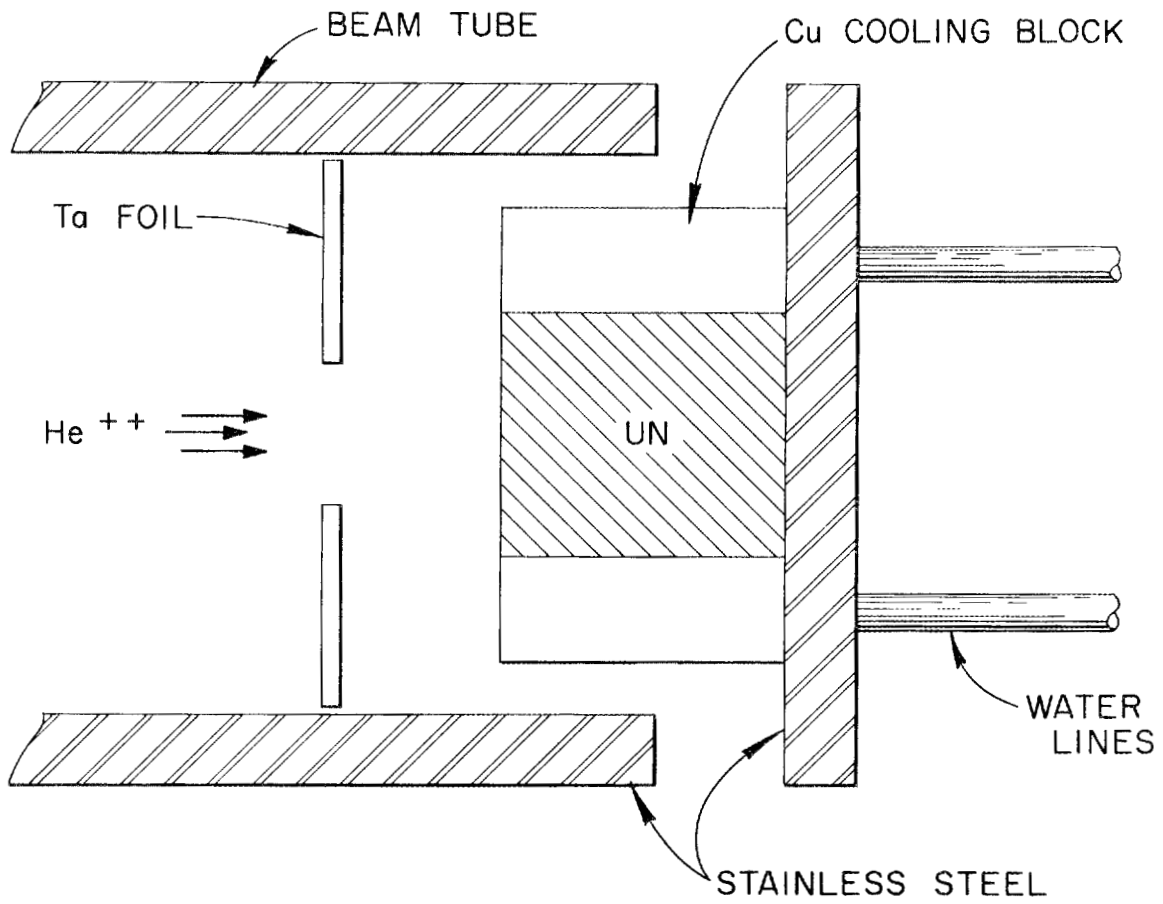


Figure 18. Illustration of ion bombardment step.

From this equation one can calculate

$$R_U = 0.896 \text{ milligram per square centimeter ,}$$

$$R_N = 0.229 \text{ milligram per square centimeter ,}$$

where

$$R_U = \text{range of alpha particles in uranium,}$$

$$R_N = \text{range of alpha particles in nitrogen.}$$

For homogeneous UN the effective range (25), R_{UN} , is given by

$$1/R_{UN} = W_U/R_U + W_N/R_N , \quad (5)$$

where

$$R_{UN} = \text{range of alpha particles in UN,}$$

$$W_U = \text{weight fraction of uranium,}$$

$$W_N = \text{weight fraction of nitrogen.}$$

Thus, the range of 250 kilo-electron volt alpha particles in UN is

$$R_{UN} = 0.775 \text{ milligram per square centimeter .}$$

Using a density of 14.32 grams per cubic centimeter, the penetration distance, d , is

$$d = R_{UN}/\rho_{UN} = 5400 \text{ angstroms ,} \quad (6)$$

where

$$d = \text{depth of penetration,}$$

$$\rho_{UN} = \text{density of UN.}$$

For bombardment conditions of 100 microamperes for 5 minutes, 9×10^{16} gas atoms will be deposited in a sample. This corresponds to

3.25 helium atoms per 10^6 uranium atoms. However, in the deposition zone, 2 millimeters in diameter by 5400 angstroms in length, the gas-atom concentration is approximately one-half helium atom per uranium atom.*

The actual number of helium ions deposited in a sample was difficult to measure. As the ions gave up their energy and came to rest in a sample, they acquired two electrons, resulting in a net flow of electrons into the UN sample and a current which could be measured. Because it was necessary to cool the sample, the copper cooling coil was in direct contact with the UN and provided a source of electrons. Both inlet and outlet copper water lines connected to the cooling coil provided an equal number of electrons, and the rest of the specimen holder was electrically insulated. Our current measurements were taken from one of the two water lines near the point where the lines came through the back of the stainless steel holder.

The number of ions sputtered from the surface during bombardment is not significant. At 1 to 2 kilo-electron volts, the number of sputtered ions should be less than 10 per cent of the impinging beam. Above 1 to 2 kilo-electron volts, the number of sputtered ions drops off rapidly (26).

*These concentrations are equivalent to burnups of 0.0013 and 195 atom per cent uranium, respectively, assuming one gas atom is produced every four fissions.

II. HEAT TREATMENT

After the helium ion bombardment the samples were heat treated in a high-temperature, temperature gradient. Temperatures were measured by using an optical pyrometer and sighting directly on the sample through a pyrex sight glass mounted in the water-cooled jacket of the furnace, Figure 16, page 31. Two corrections to the observed temperatures were required: first, for the pyrex sight glass, Table VI, Appendix A; and second, for the lack of blackbody conditions, Figure 35, Appendix B. The specimens were usually held at maximum temperature for about 2 hours, although in many cases it was less than this because of heating element failures. The bombarded ends were placed on the cooler end of the temperature gradient so that the bubbles would migrate into the bulk of the specimen.

A limitation of our experimental technique was the inability to heat the specimens to temperature rapidly. Heatup times were on the order of 30 minutes to 2 hours which represented an appreciable fraction of the total test time. The test times used in the calculations of the surface diffusion coefficients, D_s , were the times that the samples remained at the ultimate temperature plus 15 minutes to allow some correction for the diffusion occurring during the heatup period. In order to estimate the magnitude of the error introduced in the values of D_s by this approach, a detailed calculation of the bubble diffusion distance for the single crystal was made, taking into account diffusion during the 2-hour heatup period. This value of diffusion distance was about

25 per cent greater than obtained from the approximate treatment discussed above. Since the heatup time was long for this sample, this would represent approximately the maximum error introduced by the slow heatup rates.

The sample temperatures reported were those corresponding to the mean value of temperature over the region in which migration occurred in each sample.

III. SAMPLE PREPARATION AND EXAMINATION

After heat treatment the samples were sectioned longitudinally parallel to the temperature gradient. The samples were first examined by light microscopy and then by replication electron microscopy. A double-replication technique was used with parlodian for the primary replica. The parlodian was stripped from the sample, shadowed with platinum, and then coated with carbon, which served as the secondary replica. In the first replicas examined, there was no coordination of the replica orientation with respect to the sample even though the general region of the sample was known. Eventually a technique was developed to maintain the orientation with respect to the bombarded edge. Later samples were shadowed in the direction of bubble movement, which also provided a guide to the correct orientation.

Replication electron microscopy was used for the bulk of this research in preference to thin-film transmission for several reasons. First and most important, the effects observed by studying the migration in bulk specimens should more nearly simulate the effects one

would observe in an irradiation environment. Second, temperature and temperature gradient control will be much more accurate in bulk specimens heated in a furnace than in thin films heated on an electron microscope hot stage. Third, an acceptable technique of thinning sintered UN has not been worked out. Finally, since the hot stage in the electron microscope can only attain a maximum temperature of approximately 1000°C., preliminary calculations for surface diffusion and evaporation-condensation indicated that bubble coalescence and migration might not be effected. In bulk specimens, however, the temperature is only limited by the quality of the heating equipment, which can be improved if necessary.

Thin films of the single-crystal specimen and replicas of fractured surfaces were used to support the results obtained on the polished surfaces, but they could not be used for quantitative measurements. An electrolytic solution of orthophosphoric acid and alcohol proved the most successful for the thinning process.

CHAPTER V

RESULTS AND DISCUSSION

A total of 43 samples were bombarded in the Cockcroft-Walton accelerator, and 25 of these samples were successfully subjected to various heat treatments. The heat treatments spanned the range of 985 to 1585°C. and temperature gradients from 75 to 880°C. per centimeter. The heat treatments (with the qualifications discussed in Chapter IV, page 33) and conditions of helium ion injection for the specimens examined are summarized in Table II. A more detailed illustration of the individual heat treatments for some of the samples discussed herein is shown in Appendix C.

I. CONTROL SAMPLES

For purposes of comparison, some UN control samples were first examined in the unbombarded condition. Figure 19 shows replicas taken from unbombarded UN samples in both the polished and as-fractured conditions. The matrix in all cases appears to be very smooth with the exception of sintering porosity. The sintering porosity shows crystallographic surfaces indicating that some planes in UN have lower energies than others, but no attempt was made to determine the relative planar energies.

Samples of arc-cast and cold-pressed-and-sintered UN were also examined by thin-film electron microscopy. Thin films of cold-pressed-and-sintered UN were hard to produce since the etching solution

TABLE II

HEAT TREATMENTS AND CONDITIONS OF HELIUM ION
INJECTION^a FOR SPECIMENS EXAMINED

Specimen Number	Cumulative Helium Dose (Number of atoms)	Temperature (°C.)	Temperature Gradient ^b (°C./cm)	Time at Temperature (minutes)
	× 10 ¹⁶			
336-3	3.6	1700	0	120
336-4	3.6	1400	0	120
336-6	18.0	1070	400	65
336-8	4.32	1190	230	90
336-9	6.48	1135	230	70
336-10	6.48	1110	170	100
336-14	7.92	1225	80	70
336-15	14.4	1700	0	120
336-14	14.4	1400	0	120
336-19	3.24	1245	500	85
353-1	9.00	1100	75	85
353-7	23.40	1200	500	100
353-10	18.00	1190	430	30
353-12	18.00	1255	200	75
353-16	18.00	985	200	95
353-19	18.00	1490	160	60
353-A	18.00	1430	250	60
353-B	18.00	1435	880	90
353-C	18.00	1430	200	10
353-D	18.00	1430	800	10
353-E	18.00	1500	560	60
353-F		1330	640	60
353-G	18.00	1455	880	45
C-I-51	19.80	1300	235	3
C-I-50	1108.80	1010	175	30
Single crystal	18.00	1320	580	75

^aEnergy of alpha particles was 250 ± 10 kilo-electron volts.

^bTemperature given is that on the cooler end of the sample.



Figure 19. Representative photomicrographs from unbombarded control samples. (a) Replica of as-sintered uranium nitride showing a smooth matrix and associated sintering porosity. 25,000X. (b) Sintering porosity showing definite crystallographic surfaces. 58,000X. (c) Fracture surface of as-sintered uranium nitride showing sintering porosity in a grain boundary. 33,750X. (d) Fractured surface of as-sintered uranium nitride showing a three-grain intersection. 50,000X. Reduced 16 per cent of the original.



Figure 19 (continued).

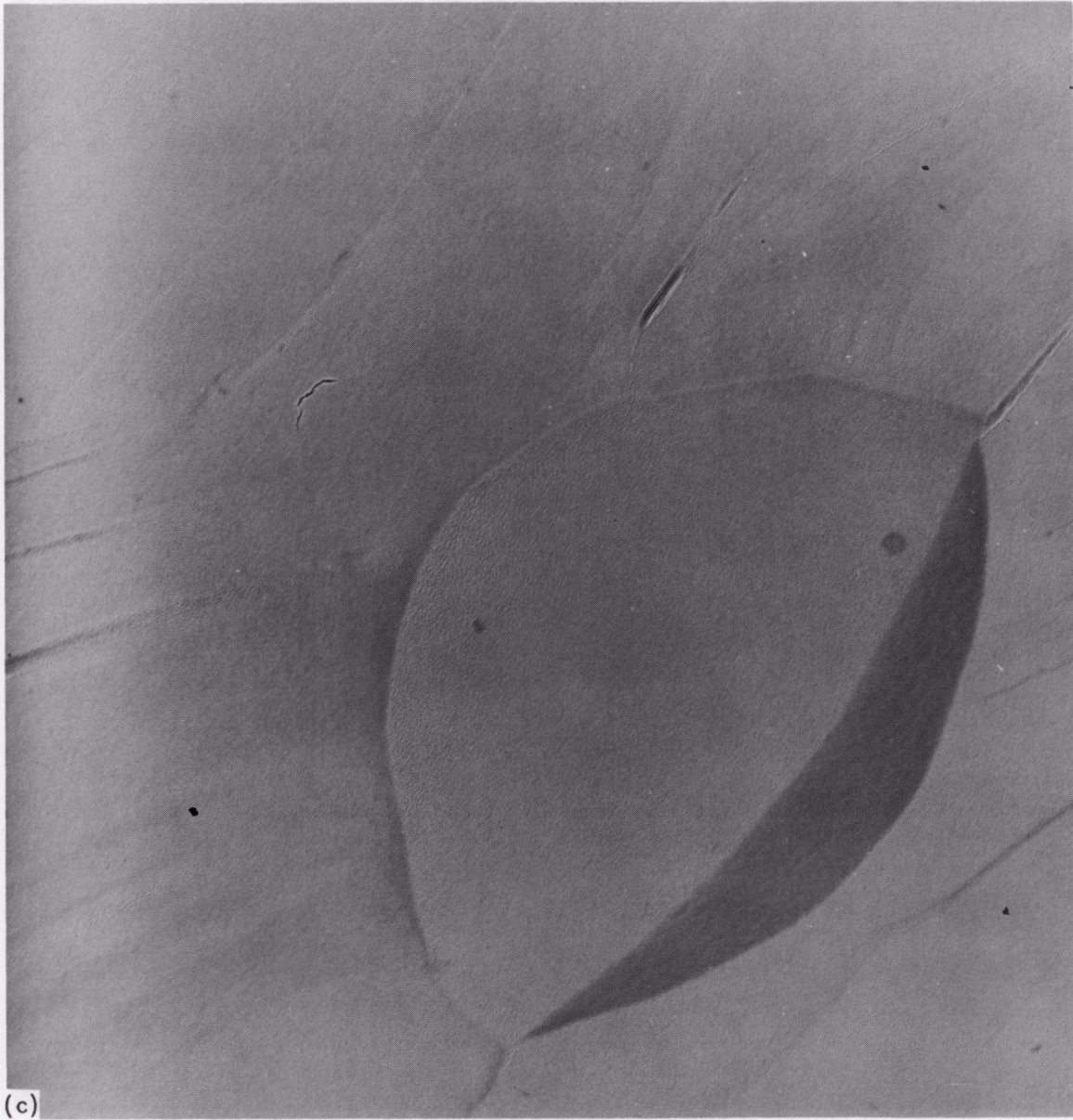
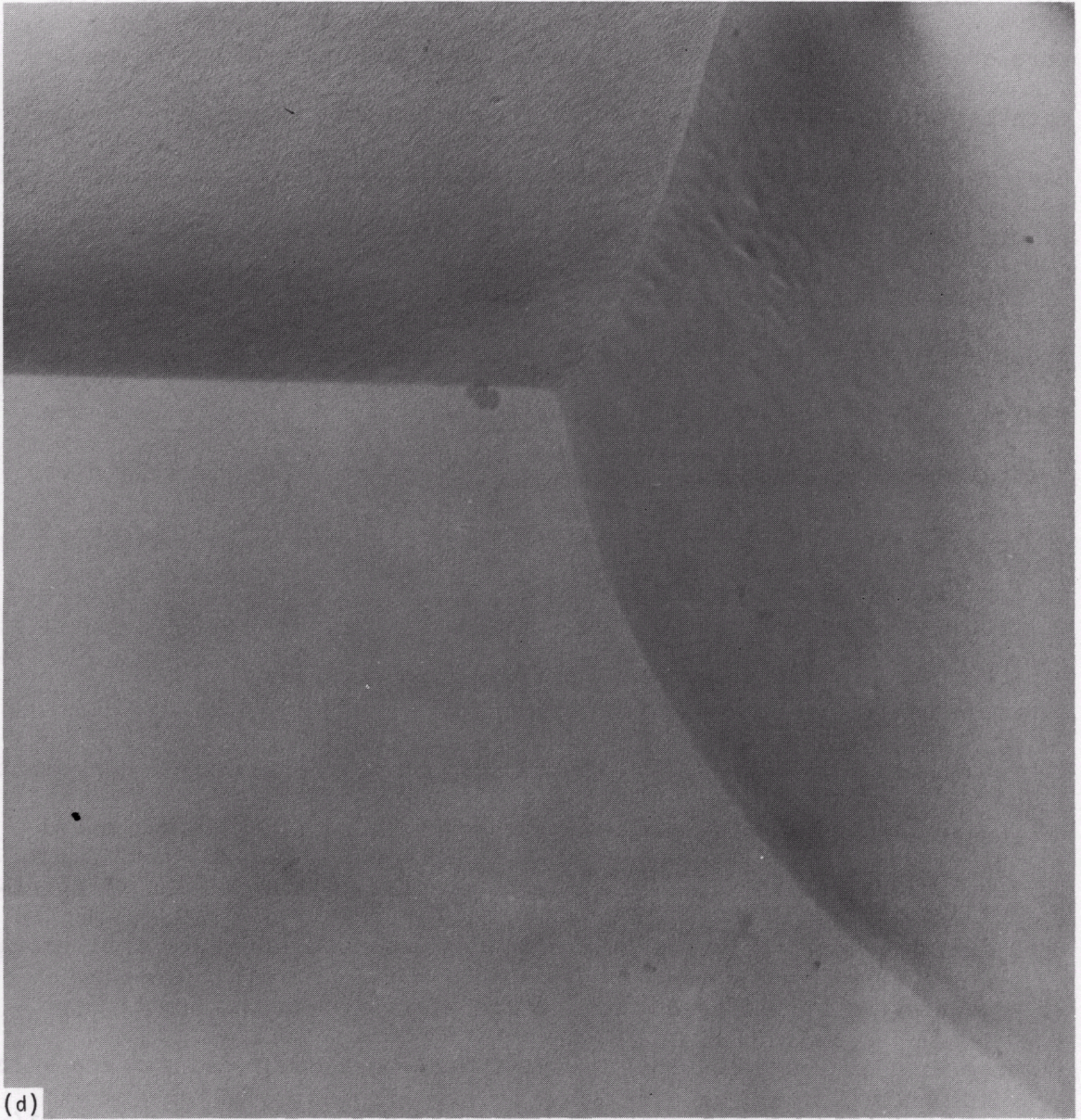


Figure 19 (continued).



(d)

Figure 19 (continued).

preferentially attacked the edges of the pores. However, a few areas were observed and photographed, Figure 20a. Arc-cast UN proved to be much better to work with, and large thin areas were observed. The arc-cast material, however, was hypostoichiometric and a dispersion of large precipitates (600 to 60,000 angstroms in diameter) was present as shown in Figure 20b. These precipitates were identified by an electron microprobe analysis to be free uranium. Selected area diffraction patterns indicated that a surface film, probably U_2N_3 , was present on both the arc-cast and the sintered thin films. The surface film probably gives the matrix its rough textured appearance as observed in the high magnification (50,000 times) photographs.

II. EFFECTS OF HELIUM ION BOMBARDMENT

In order to investigate the effects of the helium ion bombardment on the surface of the UN specimens, we examined replicas of bombarded surfaces. The results show that, despite water cooling of the UN specimens during bombardment, the heat absorbed was not dissipated fast enough to prevent some bubble agglomeration and migration during bombardment. Figures 21(a) through (c) show various areas on a bombarded surface which suggest that helium bubbles have burst through the surface. Figure 21(a) is a low-magnification photomicrograph showing a rather large portion of the surface. The region toward the bottom of this photograph appears to have a large number of defects on the surface. Figures 21(b) and (c) suggest that the bubbles may migrate more rapidly down grain boundaries and defects.



Figure 20. Transmission photomicrographs of unbombarded control sample. (a) As-sintered uranium nitride. 50,000X. No reduction. (b) Arc-cast uranium nitride containing precipitates of free uranium. 25,000X. Reduced 15 per cent of the original.

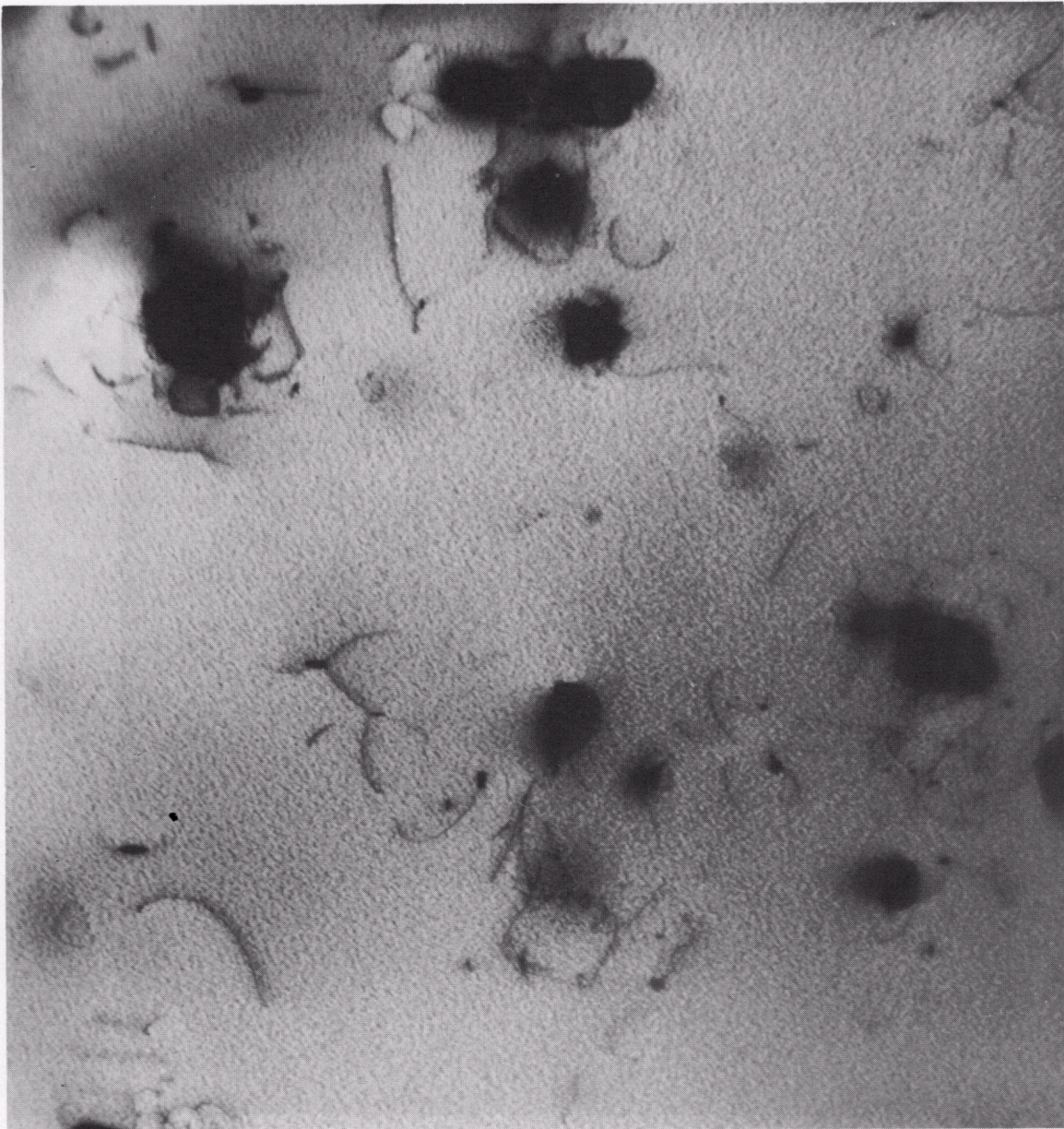
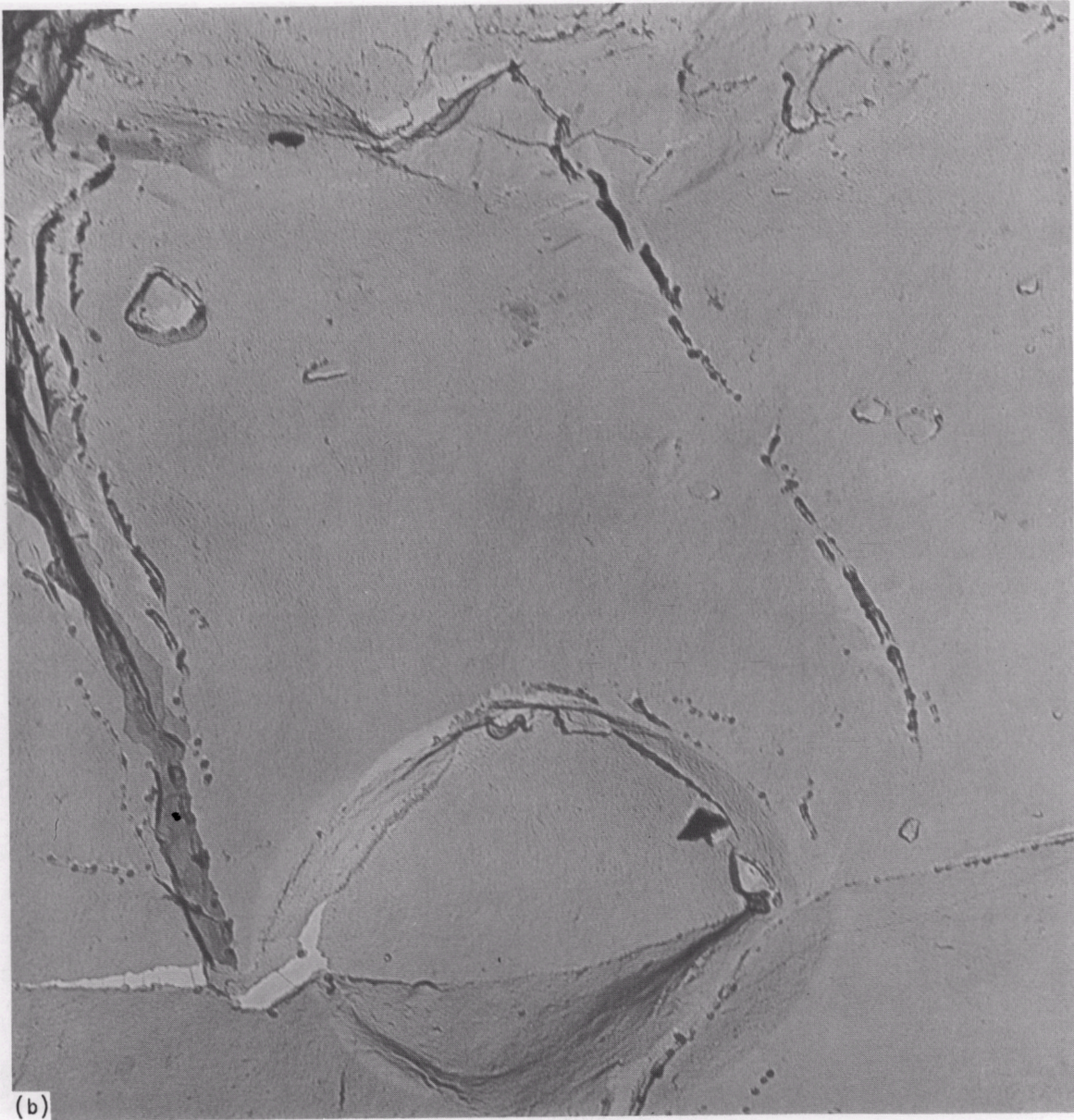


Figure 20 (continued).

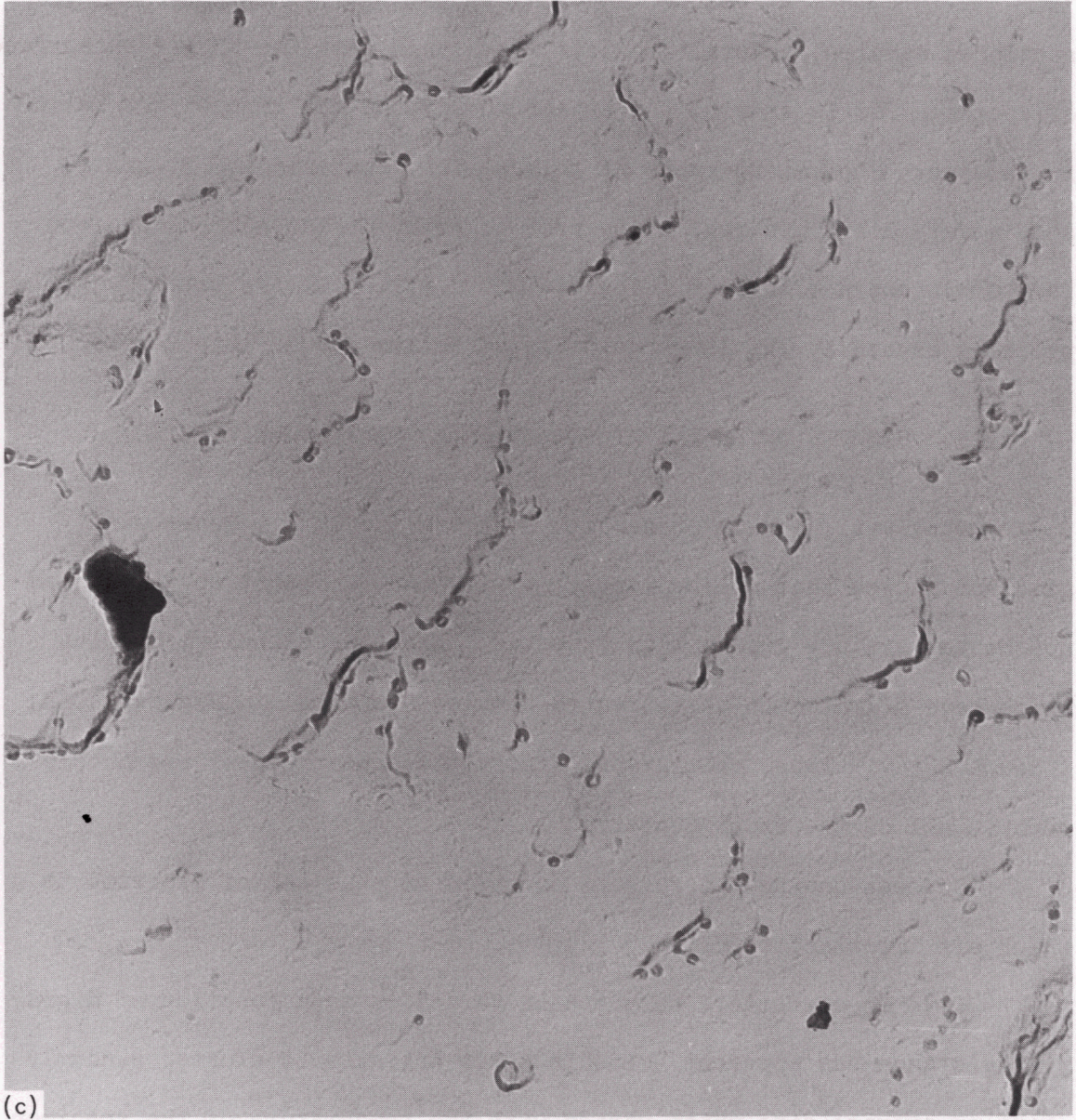


Figure 21. Replicas of as-bombarded surface prior to heat treatment. (a) A low-magnification photograph illustrating the general features of the surface. 5,500X. (b) A region in the bombarded surface in which bubbles appear to have migrated preferentially down grain boundaries back out of the surface during bombardment; the matrix appears relatively clean compared with the grain boundaries. 37,500X. Reduced 16 per cent of the original.



(b)

Figure 21 (continued).
The figure shows a large, roughly circular structure with a textured, layered appearance, possibly a biological or material specimen, surrounded by a network of fine, dark, branching lines. The structure has a central region with a different texture, possibly a core or a different layer. The overall appearance is that of a cross-section of a complex material or biological tissue.



(c)

Figure 21 (continued). as before (b) (S)

Turning our attention now to the heat treated and longitudinally sectioned samples, several replicas were taken near the bombarded surface of specimen 353-12 showing the appearance of the matrix near the helium ion source. Photomicrographs of this region, for example, Figure 22, show a very disturbed region observed to be about two microns in from from the bombarded surface. The disturbed effect on the matrix was probably caused by the large quantity of helium gas in this region.

III. RESULTS OF BUBBLE MIGRATION IN A TEMPERATURE GRADIENT

Observations made on samples heat treated in a temperature gradient showed that helium bubbles were found, and that they migrated up the temperature gradient as expected. Examples of helium bubbles which have migrated in heat-treated samples are shown in Figures 23(a) through 23(d). These photographs typify the appearance of the bubbles seen in all of the experiments.

Several unexpected results occurred in this set of experiments which are important to note:

(1) No systematic bubble size variation as a function of migration distance was apparent. Bubble sizes appeared to cluster randomly about an average size which varied with the temperature of the specimen.

(2) While bubbles were observed to be present at grain boundaries, they also were observed to pile up behind them or occur occasionally as "bands" of bubbles in the longitudinal sections of the specimens.

(3) Bubbles appeared as projections instead of holes.



Figure 22. Disturbed region of the matrix observed to be two microns from the bombarded surface of specimen 353-12 after heat treatment. 57,500X.

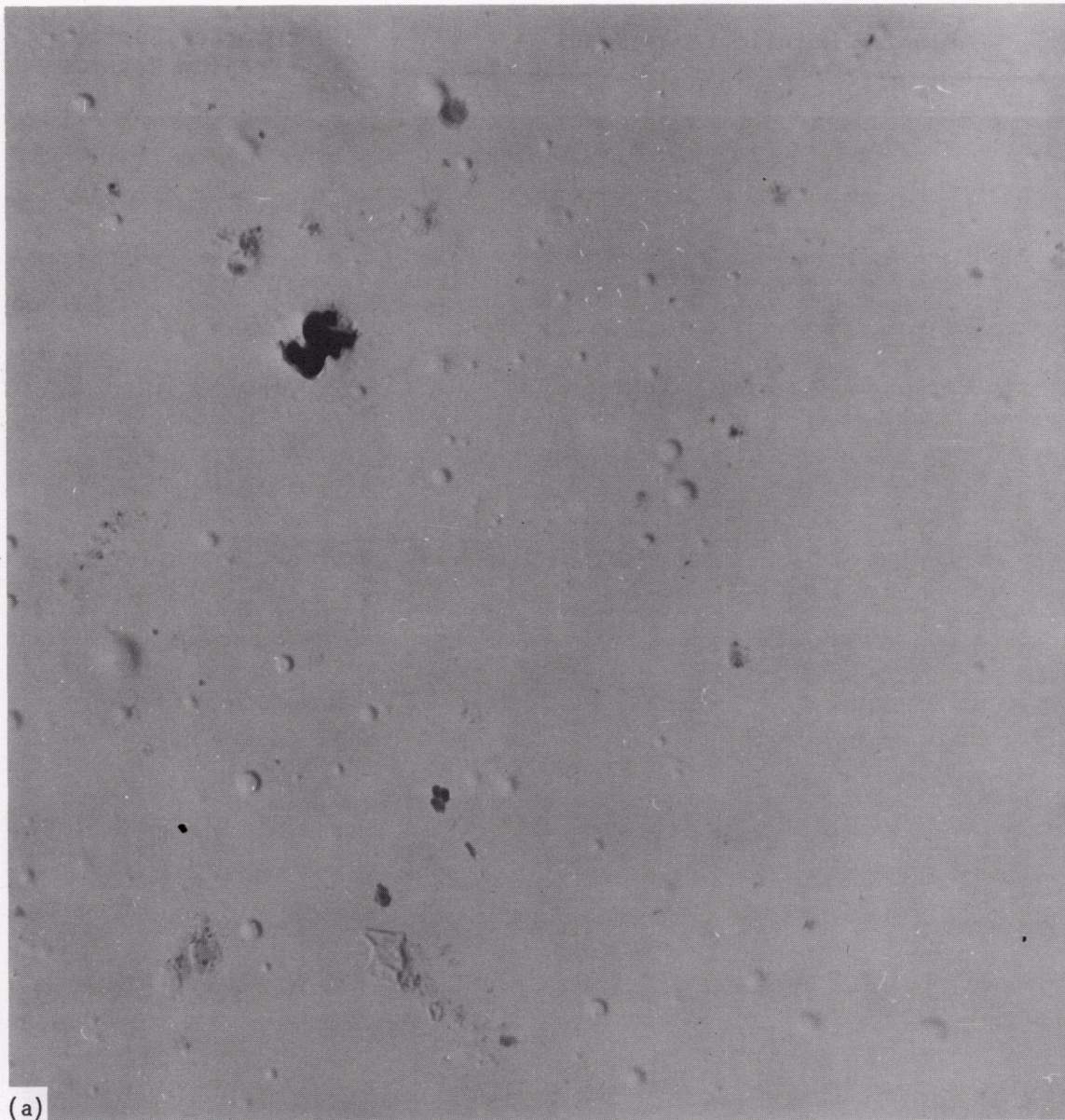


Figure 23. Examples of helium bubbles which have migrated into the uranium nitride samples. (a) Specimen 353-E heat treated at 1585°C . in a temperature gradient of 560°C . per centimeter. 16,250X. (b) Specimen 336-6 heat treated at 1075°C . in a temperature gradient of 400°C . per centimeter. 17,000X. (c) Fractured surface of specimen 353-10 heat treated at 1190°C . in a temperature gradient of 170°C . per centimeter. 60,000X. (d) Low-magnification photomicrograph of specimen 353-A heat treated at 1445°C . in a temperature gradient of 250°C . per centimeter. 5,000X. Reduced 16.5 per cent of the original.

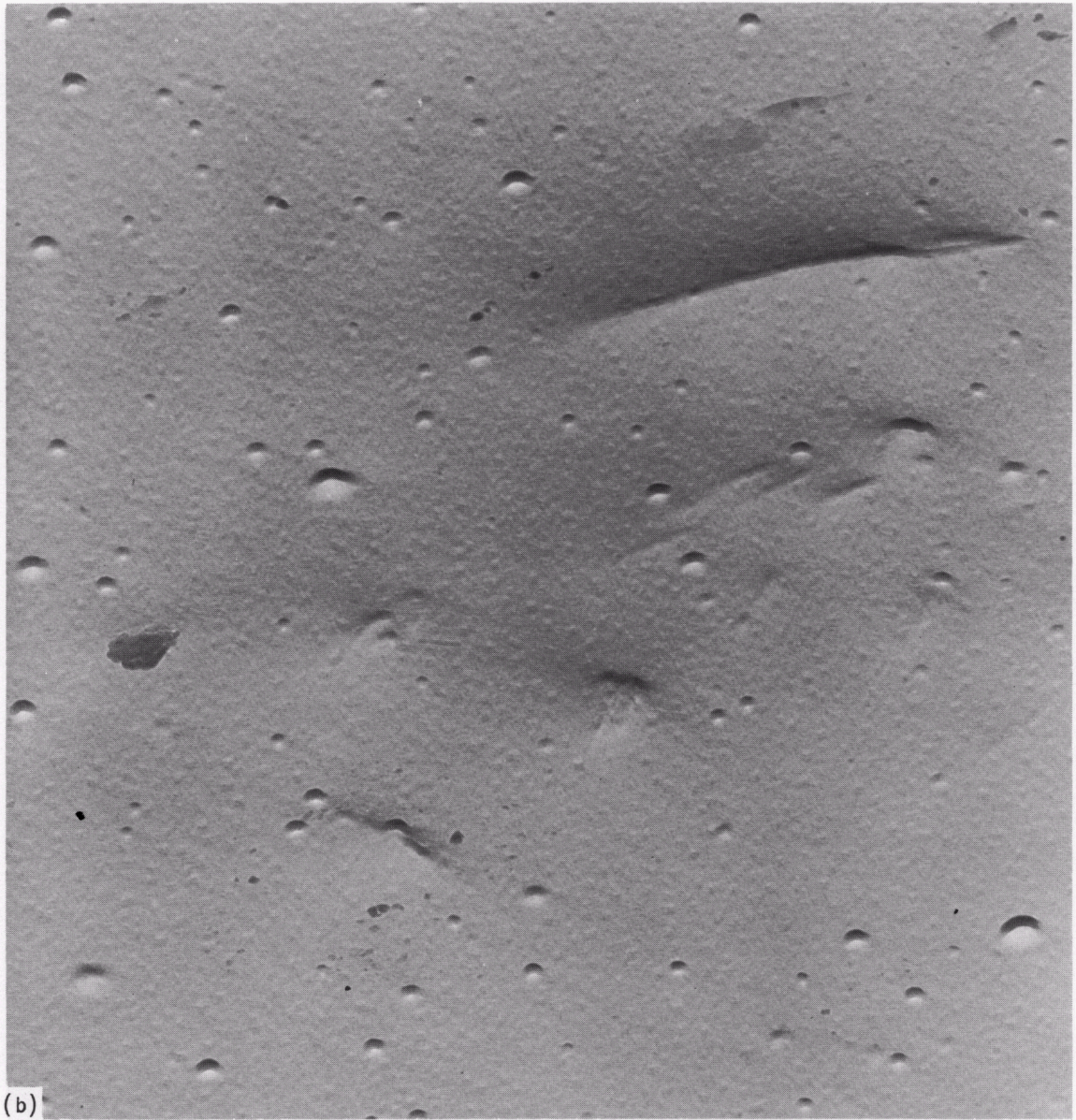
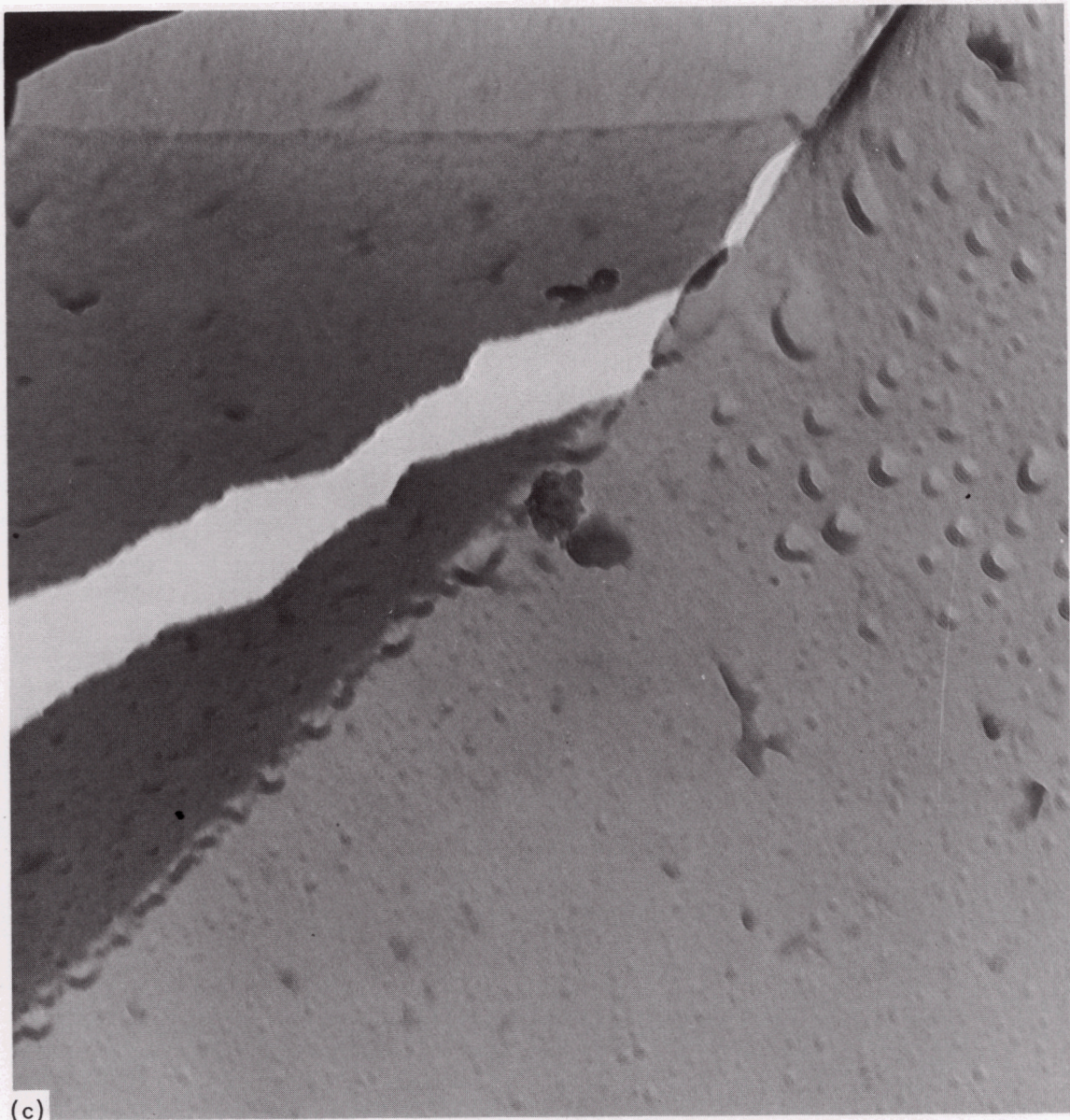


Figure 23 (continued).



(c)

Figure 23 (continued).

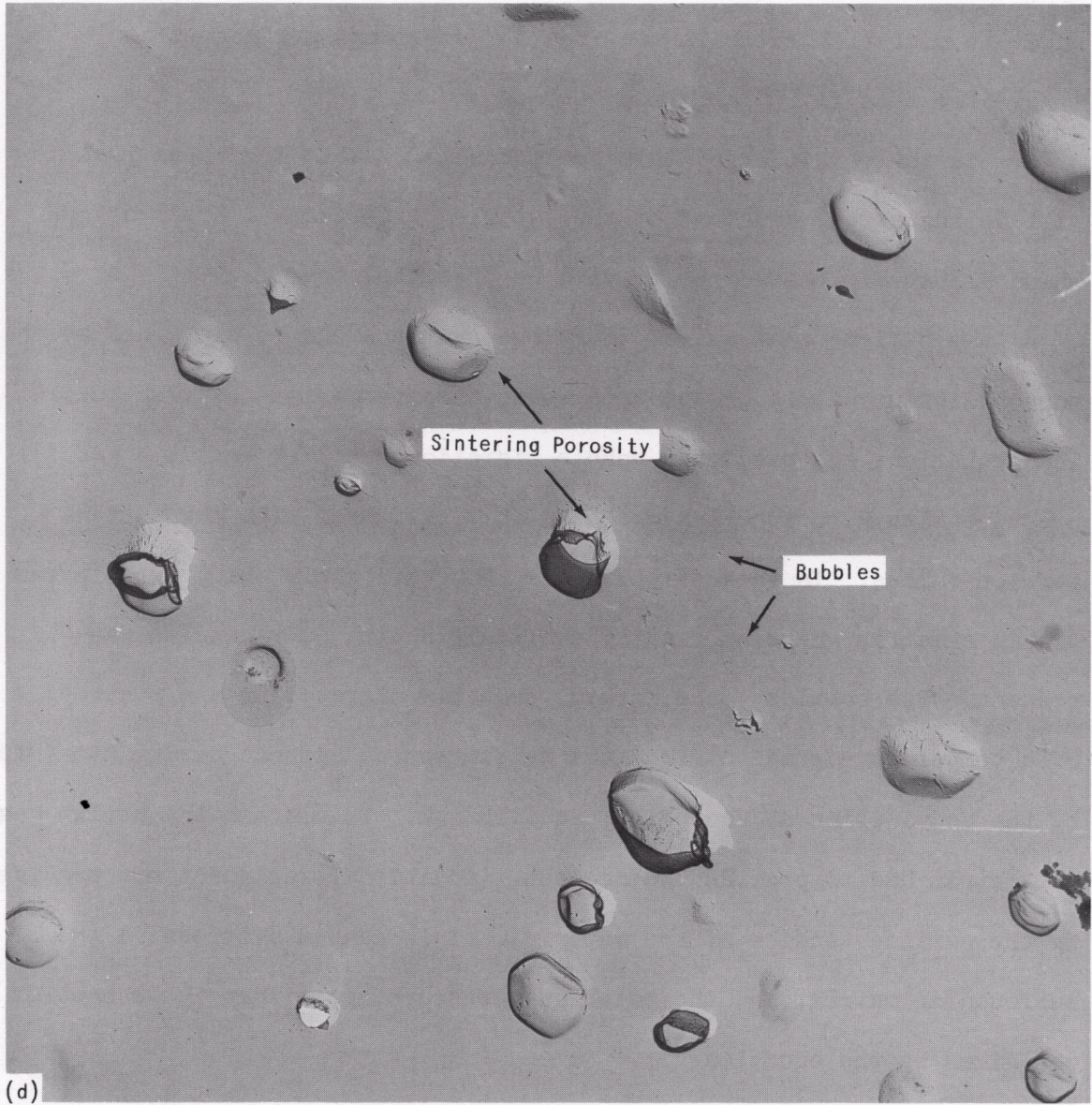


Figure 23 (continued).

(4) Bubble migration rates were much greater than expected. The apparent migration rates ranged from 300 angstroms per second at 985°C. to greater than 11,000 angstroms per second at 1585°C.

In the remainder of this section some reasons for these results will be suggested, and some of the detailed experimental observations which illustrate these results will be presented.

We believe that all of these observations can be explained by the nonequilibrium nature of the bubbles in these experiments. The theoretical equations and predicted bubble migration behavior assume a gas pressure within the bubbles which is in equilibrium with the surface tension forces. In these experiments, however, the bubbles were formed within a matrix where no readily available source of vacancies was present. The bubbles, once formed, probably migrated in the presence of a temperature gradient from the helium source without having attained, by the acquisition of vacancies, equilibrium. To contain the helium gas, the matrix had to provide the necessary additional restraint not provided by the surface tension of the material. This caused a stress in the surrounding matrix, and the total gas pressure, p , within these bubbles was given by the equation

$$p = -\sigma + \frac{2\gamma}{r}, \quad (7)$$

where

σ = stress in matrix.

The resultant stress in the matrix was composed of a radial compressive stress field and a circumferential tensile stress field with corresponding elastic strain fields. The stress field around the bubbles

probably caused the bubbles to repel each other, preventing coalescence and resulting in the unchanging size distribution as a function of the migration distance.

The stress, σ , on a point midway between two bubbles with equal stress fields can be described by the equation

$$\sigma = \frac{16\left(p - \frac{2\gamma}{r_o}\right)\left(r_o^3\right)}{d^3} \quad (8)$$

where

p = pressure within a bubble,

γ = surface tension of matrix UN,

r_o = equilibrium radius of the bubble,

d = distance between the bubble centers.

Thus, as two bubbles come together the stress at the midpoint is raised; hence the bubbles will tend to repel each other, preventing coalescence.

The existence of large strain fields in samples cooled to room temperature after heat treatment was established by observations of bubbles in thin films of the single crystal, Figure 24(a) and (b). The bubbles appear dark because the strain fields in the region around the bubbles cause the beam to be diffracted. These dark areas were observed to remain stationary and did not fade in and out as the sample was tilted and rotated in the electron beam, thus eliminating the possibility that the dark regions were dislocation loops. The white regions in the centers of the bubbles resulted from the beam passing through a region where the electrons were not diffracted by the strain field; in this sample, this



Figure 24. Transmission electron photomicrographs of the single crystal specimen. (a) Helium bubbles with peripheral dark areas indicating strain fields. 100,000X. (b) Very thin region of sample with large light areas which may have resulted from bubbles bursting through the surface of the film or from preferential etching of the region near the bubble. 100,000X. Reduced 18 per cent of the original.

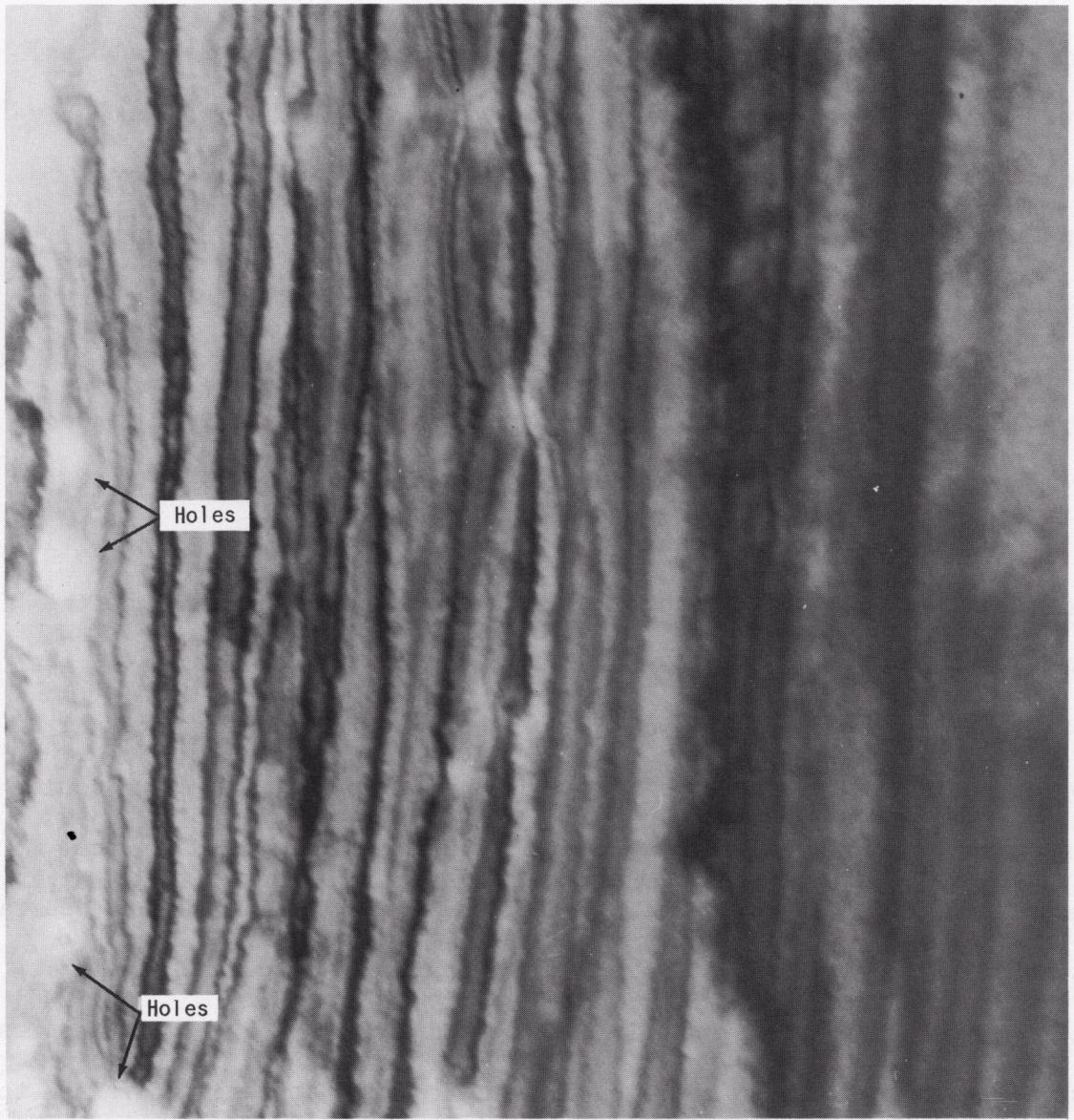


Figure 24 (continued).

represents the region where the displacements of the atoms are nearly at right angles and parallel to the beam. These dark areas (bubbles) were not observed in the thinner portions of the thin films, probably because the thicknesses of the very thin sections are nearly equal to the bubble diameters. In the thinner sections, however, holes which were slightly larger than the bubbles in the thicker sections were observed without the associated strain fields. These holes may have been caused by the bubbles bursting through the surfaces in these thinner regions, releasing the helium gas and thereby eliminating the matrix strain.

One should not conclude that a radial compressive stress field existed around the bubbles at the migration temperature based on the observation of strain fields at room temperature, because cooling the sample to room temperature would be expected to reduce the internal pressure in the bubbles by a factor of the order of 5. This reduction in pressure would result in a residual tensile stress field in the matrix if the pressure in the bubbles was in equilibrium with the surface tension forces at temperature. For reasons to be discussed later, it is believed that the stress fields observed in Figure 24(a) are compressive. Assuming this to be true, the stress field at temperature had to be even more compressive.

After the bubbles left the helium source or bombarded region, they migrated up the temperature gradient until they reached a grain boundary, where the first bubbles were probably trapped. The grain-boundary binding energy, B.E., presented to the bubbles is

$$\text{B.E.} = \pi r^2 \gamma_{\text{UN-UN}} , \quad (9)$$

where

r = bubble radius,

$\gamma_{\text{UN-UN}}$ = grain-boundary surface energy.

After several bubbles became trapped at a grain boundary, the stress field around each of these bubbles acting together presented a barrier to the bubbles coming behind. An example of the resulting pileup of bubbles is shown in Figure 25. This series of photomicrographs was taken from specimen 336-6 which was heat treated at 1075°C. (on the cooler or bombarded end) with a temperature gradient of 400°C. per centimeter. The bubbles are piled up at an interface (grain boundary) near the far left-hand side of Figure 25. The bubbles were migrating from right to left with the bombarded surface being some place to the right. No bubbles are present to the left of the grain boundary. A plot of the apparent bubble size as a function of distance from the interface is shown in Figure 26, indicating that the average diameter varied randomly about a value of 400 angstroms. This is further evidence that stress fields have prevented coalescence of the bubbles. A plot of bubble density as a function of distance from the interface, Figure 27, showed a definite indication that bubbles were piled up behind the interface. The second-phase material present in these replicas was not identified. There does not appear to be any significant coalescence of the bubbles in this region nor any trapping of bubbles at the second-phase interfaces. Bubbles were observed to have migrated to a depth of 350 microns from the bombarded end. Beyond this depth a clean matrix was observed.

Interface
| (Grain Boundary)

← Direction of Bubble Motion

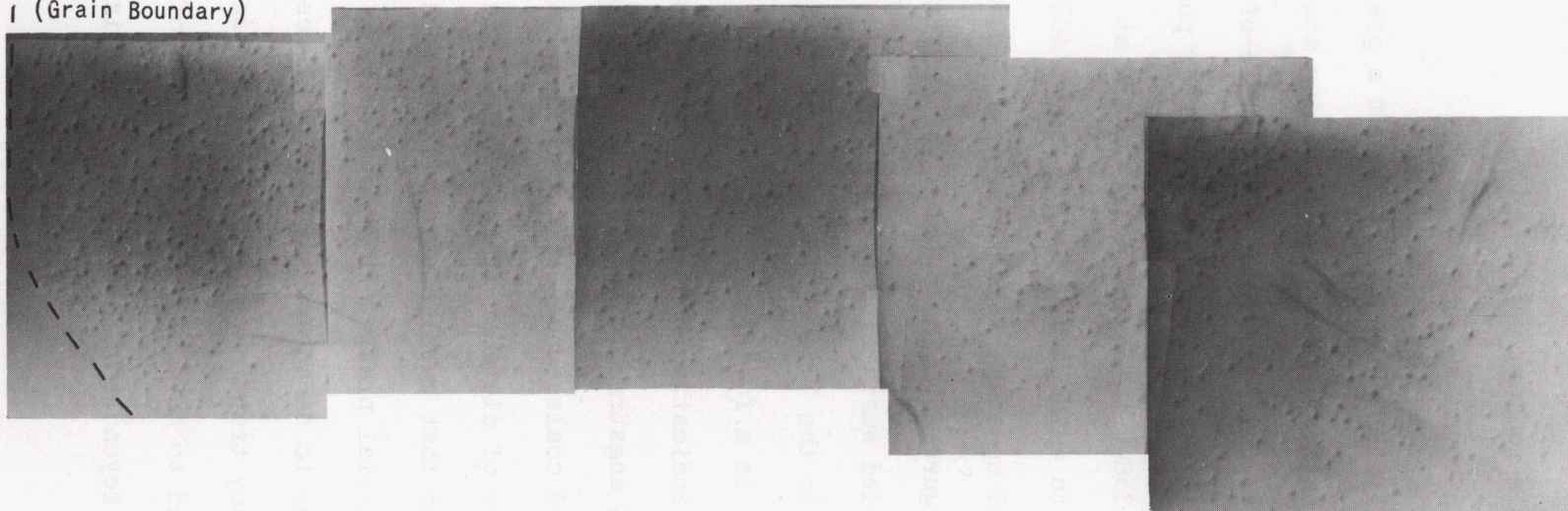


Figure 25. Bubble distribution in specimen 336-6 heat treated at 1075°C. for one hour with temperature gradient of 400°C. per centimeter. The bombarded surface was to the right of the photograph and the bubbles appear to pile up in the left hand region probably at a grain boundary.

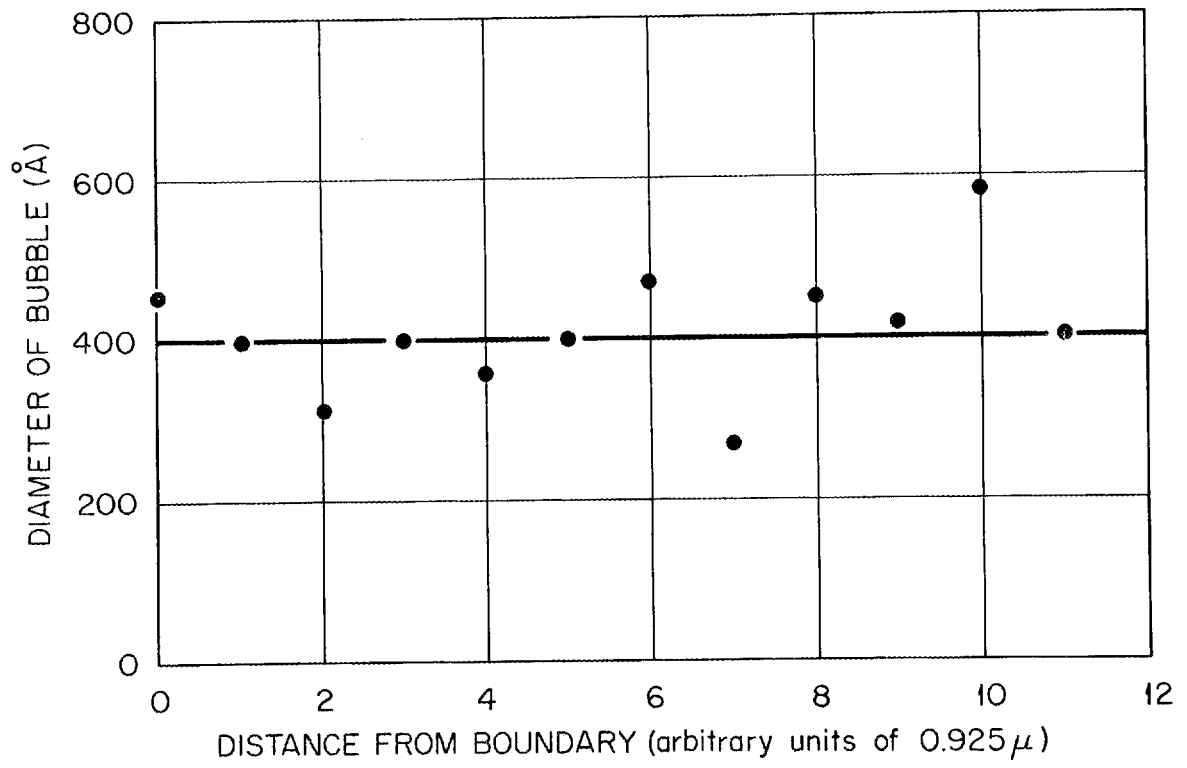


Figure 26. Bubble size as function of distance from boundary.

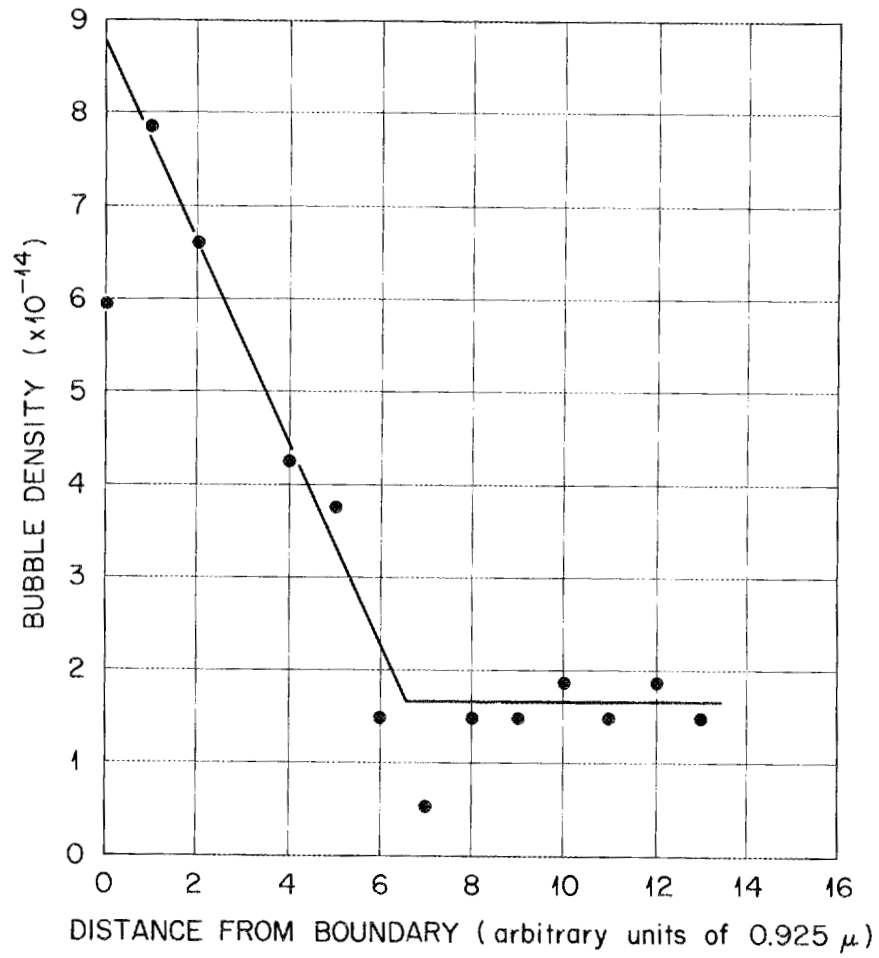


Figure 27. Bubble density as function of distance from boundary.

As bubbles continued to pile up behind the bubbles at grain boundaries, additional forces were probably exerted on the grain-boundary bubbles to overcome the grain-boundary binding energy. Since each bubble is subjected to a driving force (temperature gradient), the force on the grain-boundary bubbles will be the sum of the forces on each of the bubbles piled up at the grain boundary. When the sum of these forces becomes large enough, a bubble can break away from the grain boundary and migrate through the matrix until it reaches the next boundary. Some equilibrium number of bubbles should eventually be piled up at the grain boundaries, and a steady-state condition should be reached and maintained as long as the bubble source exists.

Additional evidence that gas bubbles are trapped at grain boundaries is seen in Figure 28 which shows the fractured surfaces of specimen 353-10 after heat treatment. The specimen was fractured in the transverse direction (perpendicular to the temperature gradient); thus, quantitative measurements of bubble migration distances were not possible.

As the temperature was increased, the number of piled-up bubbles near grain boundaries decreased. In specimen 336-6, where the temperature gradient was relatively large (400°C per centimeter) but the absolute temperature was only 1075°C ., the bubbles appeared very dense near the boundary. But in specimen 353-E, for example, which had an absolute temperature of 1585°C . and a temperature gradient of 560°C . per centimeter (Figure 29), fewer bubbles were piled up at a single grain boundary. However, the bubbles had penetrated further into the sample and the pileups at successive boundaries gave the appearance of bands.



Figure 28. Surface of specimen 353-10 intergranular fractured with associated helium bubbles. The line showing a preponderance of gas bubbles is a three-grain intersection which appears to be an unusually stable trapping site for the bubbles. 15,000X. Reduced 17 per cent of the original.

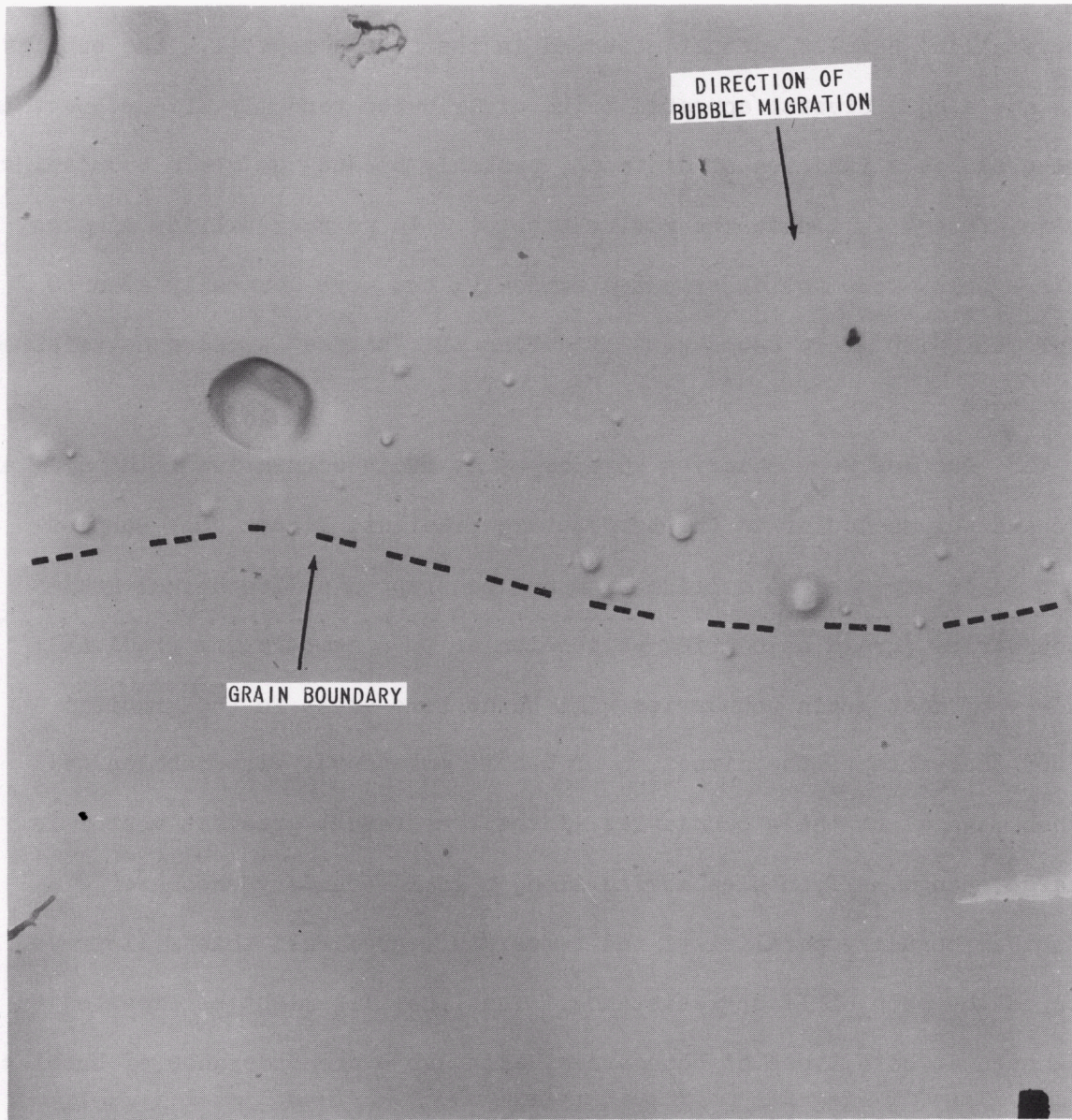


Figure 29. Bubbles in specimen 353-E which have apparently been trapped at a grain boundary. This specimen was heat treated at 1585°C. in a temperature gradient of 560°C. per centimeter. 35,000X. Reduced 17 per cent of the original.

The piling up of bubbles observed at the grain boundaries in polycrystalline samples was not observed in the single crystal. The bubbles in the single crystal appeared to be distributed randomly with respect to size and as a function of distance, probably because no grain boundaries were present to impede the moving bubbles. In polycrystalline samples the bubbles were not distributed randomly, but were generally seen to interact with grain boundaries producing the "banded" appearance referred to above.

Bubbles were observed to line up at grain boundaries both parallel to and perpendicular to the temperature gradient, Figure 30. Bubbles should be expected to collide with and be trapped at isothermal grain boundaries (grain boundaries perpendicular to a temperature gradient); however, most grain boundaries will be at some angle to the gradient (and therefore to the direction of bubble movement). The bubbles will then move along these boundaries if the temperature gradient vector is large enough. If bubbles moving along a grain boundary encounter another boundary parallel to the temperature gradient, this will prove to be the path of least resistance. Thus, bubbles might be expected to be seen at both types of boundaries, although a preponderance of bubbles should exist at isothermal boundaries and pileups should be observed only behind nearly isothermal boundaries.

A very interesting feature of this work was the appearance of the bubbles as projections instead of holes. The bubbles were always shadowed opposite the sintering porosity. Two possible explanations for this are:

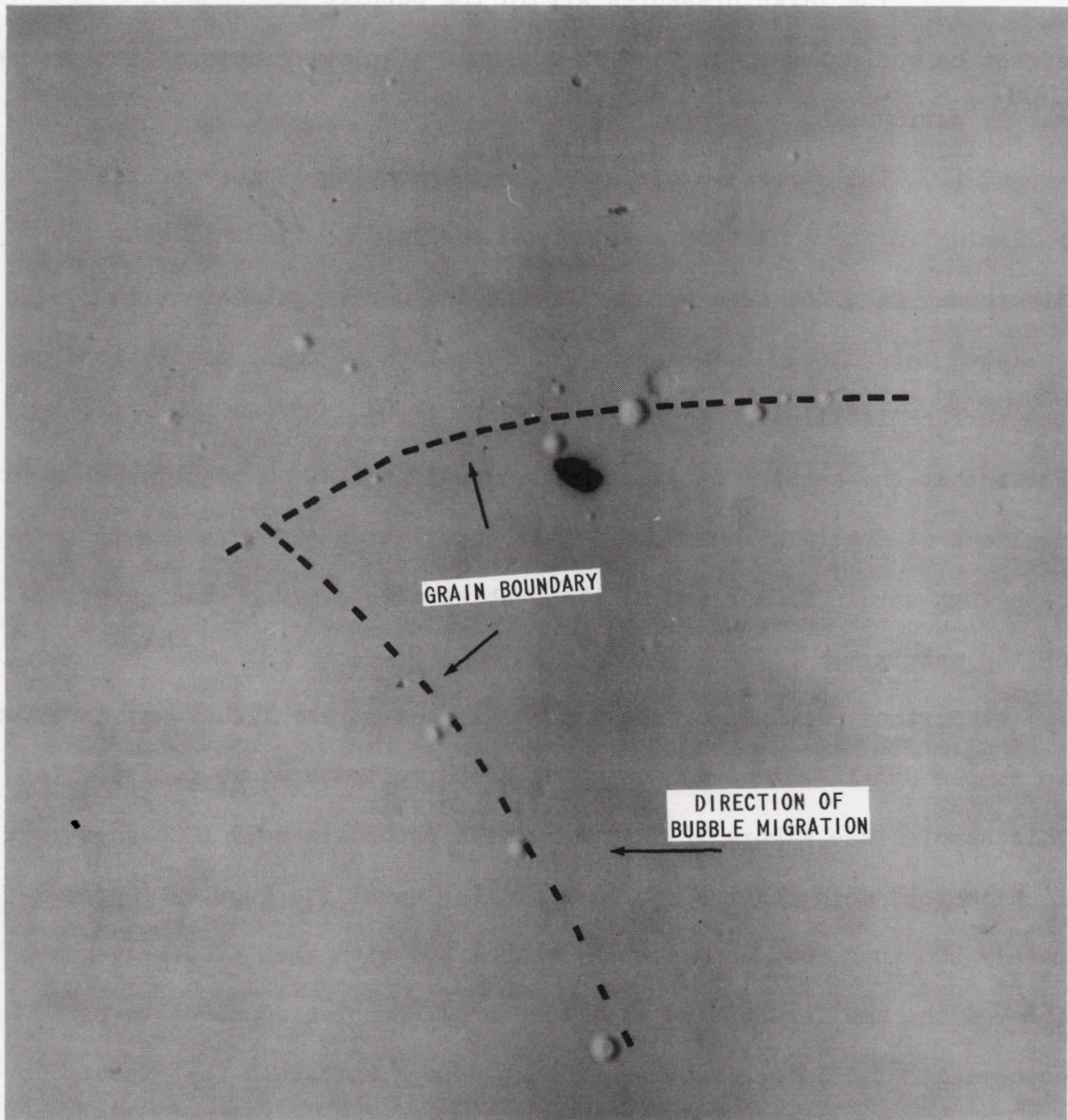


Figure 30. Bubbles lined up at grain boundaries both parallel and perpendicular to the temperature gradient. The bubbles were shadowed in the direction parallel to the temperature gradient. 42,000X. Reduced 17 per cent of the original.

(1) The large pressures within the bubbles may cause a blistering effect on the polished surface as a result of plastic deformation of the matrix surrounding a bubble.

(2) The stress in the matrix may change the nature of the polishing in the localized area around the bubble. In this case the stress may make the area around the bubbles harder so that it is polished more slowly. The method of formation of these projections on the surface is illustrated in Figure 31. Figure 28, page 68, clearly shows that the bubbles appeared as projections instead of holes even in replicas of fractured surfaces. This observation also appears to indicate that strain fields around the bubbles have a strengthening effect on the matrix.

Further evidence of the interaction of stress fields was observed in sample 353-12 which was subjected to three temperature cycles. In this sample (see Figure 32) large bubbles (approximately 1000 angstroms in diameter) were observed to have smaller satellite bubbles (approximately 200 angstroms in diameter) associated with them. Coalescence of some of the smaller bubbles with the larger bubbles appeared to be occurring. The larger bubbles had grown to a size such that faceted or planar surfaces could be observed, while the smaller bubbles appeared spherical, presumably because of the higher pressures. The satellite bubbles indicate that an attractive force existed between the larger and smaller bubbles; this is contrasted to the results in the rest of the experiments.

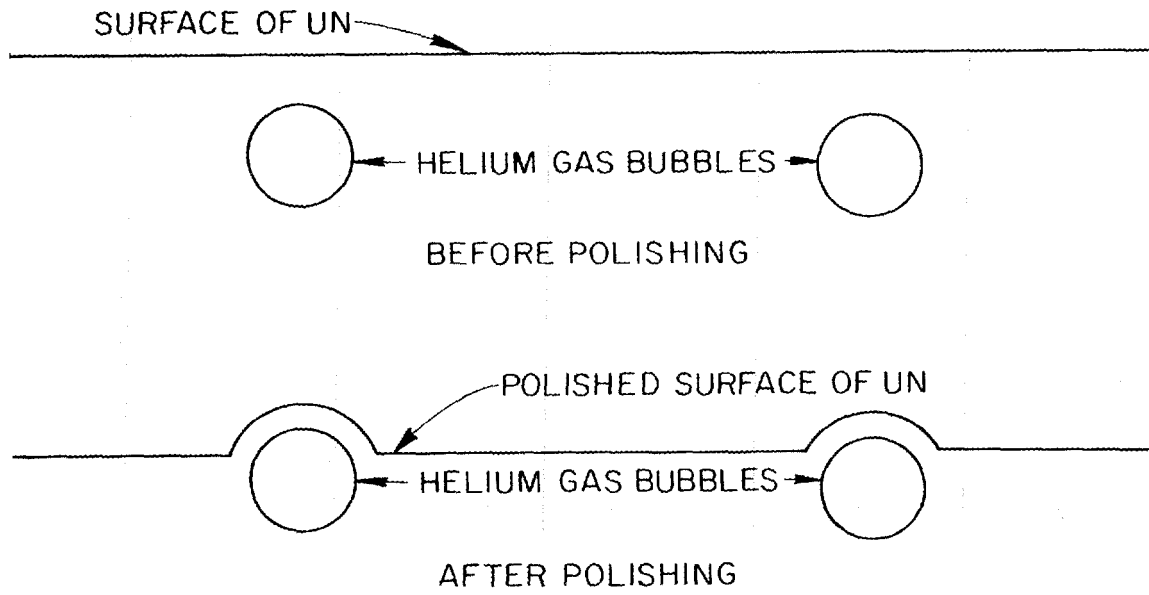


Figure 31. Illustration of how bubbles may form projections on the surface after polishing.

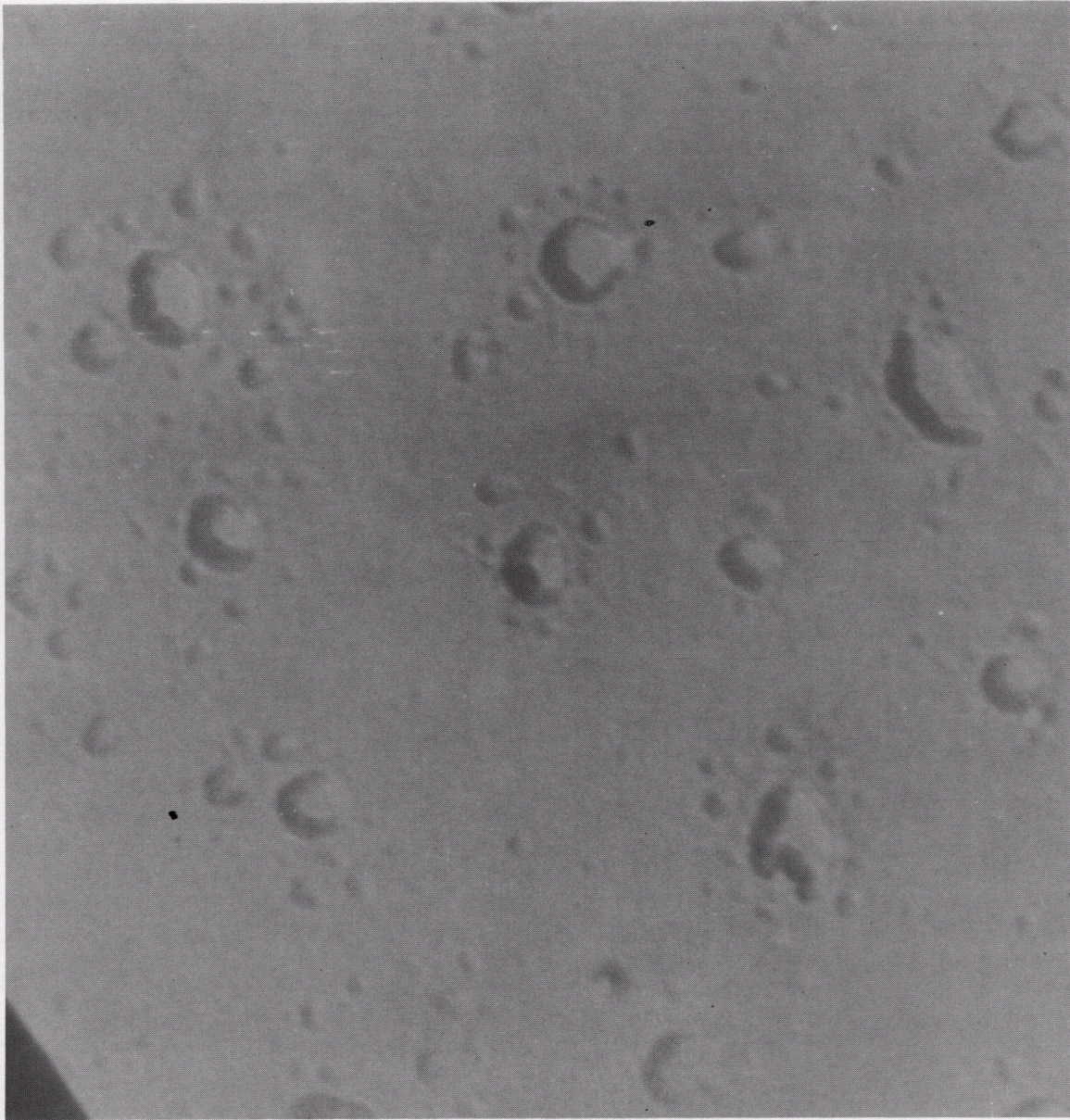


Figure 32. Photomicrographs of specimen 353-12 after multiple heat treatments. Large bubbles (1000 angstroms in diameter) which exhibit planar interfaces are surrounded by smaller satellite bubbles (200 angstroms in diameter) which are nearly spherical. 115,000X. Reduced 16 per cent of the original.

The anomalous results discussed above might be attributed to the multiple heat treatments (Figure 33) given this specimen. The presence of the crystallographic planar surfaces of the larger bubbles suggests that they may have been close to equilibrium at temperature. No clear explanation is apparent, however, to explain why the gas pressure within the large bubbles in this specimen reached equilibrium with the surface tension of the bubble but did not do so in other specimens, some of which were taken to higher temperatures. Nevertheless, in this sample (and only in this sample) the bubbles were observed to be shadowed in the same direction as the sintering porosity - a fact which indicated that we were observing holes. Since samples which were believed to have compressive stress fields in the matrix around the bubbles were shadowed as projections, we attribute the appearance of the bubbles as holes to the absence of these compressive stress fields. Further, if the bubbles were nearly at equilibrium at the heat treatment temperature, residual radial tensile stresses would be expected after cooling to room temperature.

The single crystal which showed the room temperature stress field in transmission electron microscopy showed projections instead of holes in the replicas of the polished surface. If the above explanation for the observation of holes is correct, the stress fields around the bubbles in the transmission samples must be compressive. These stress fields must also have been compressive at temperature, since an increase in temperature would always be expected to increase the gas pressure in the bubbles.

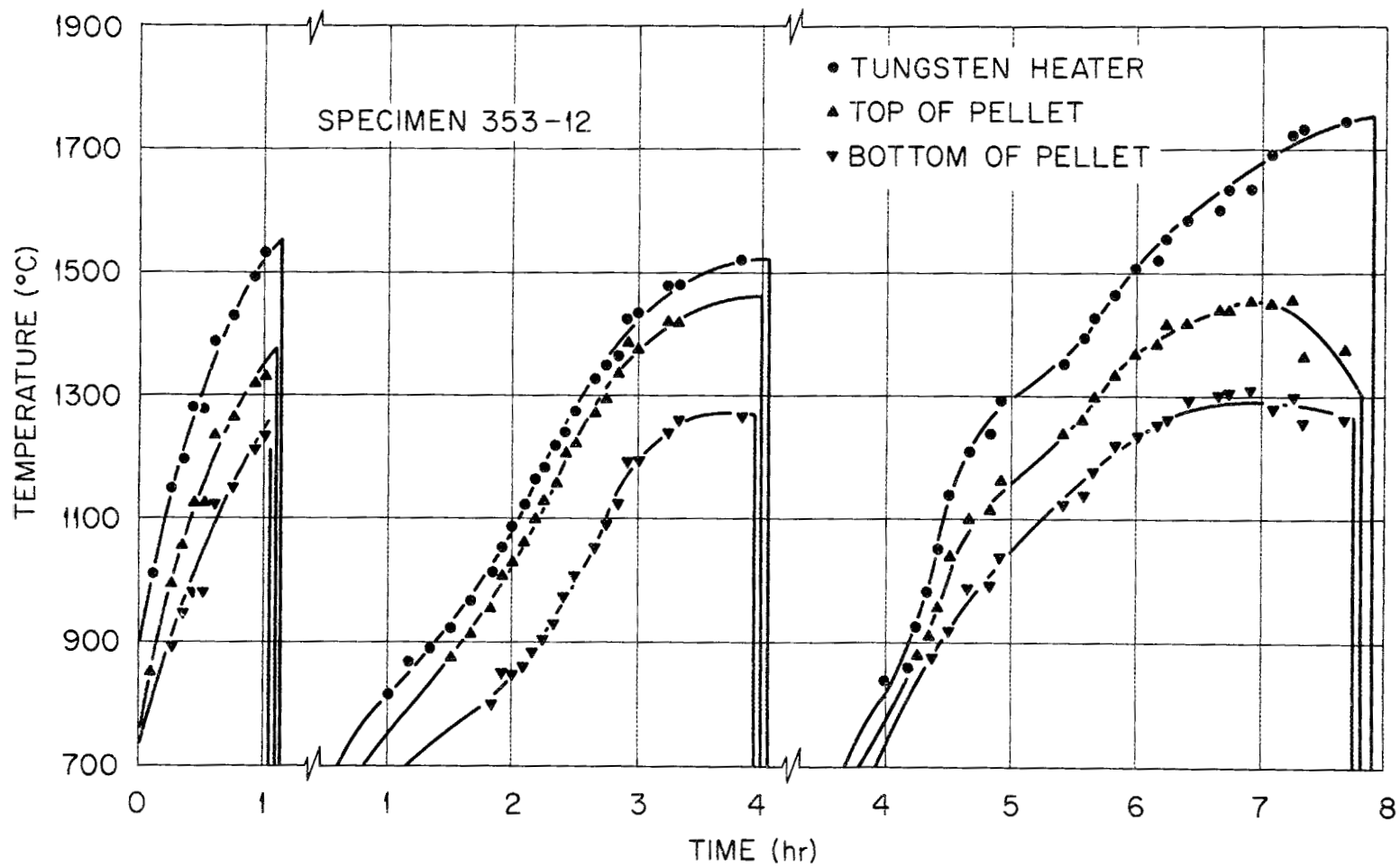


Figure 33. Illustration of multiple heat treatments of specimen 353-12

As mentioned previously, the migration rates of the helium bubbles were much greater than expected. A calculation of the migration rates predicted by an evaporation-condensation mechanism shows that the bubbles observed in specimen 336-6 would move at a rate of 2×10^{-8} angstroms per second. They were experimentally observed to migrate at a rate of approximately 900 angstroms per second. This example is typical, showing that the evaporation-condensation model predicts migration rates a factor of 10^{10} too slow. We expect, intuitively, that bulk diffusion should be even slower than evaporation-condensation since it requires that vacancies be removed from the bubbles at the leading surface and migrate through the matrix to be reabsorbed on the trailing surface. In the only experiments to date which proposed bulk diffusion as a model of migration, Gulden (19) calculated an activation energy of 130,000 calories per mole. The existence of a shortage of vacancies in the bubbles in UN makes volume diffusion even less likely. Thus we concluded that the mechanism by which the bubbles move is surface diffusion.

From the observed migration distances, an approximate surface diffusion coefficient was calculated for some of the samples by using the equation derived by Gruber (21). The calculations were made on the bubbles which had migrated furthest into the specimens assuming that these bubbles were the first to form. The following equation was used to make the calculation:

$$D_s = \frac{rkT^2}{1.78 \delta Q} \cdot \frac{\Delta x}{\Delta t} \cdot \frac{1}{\left(\frac{dT}{dx}\right)} \quad (10)$$

Equation (10) is a slightly modified form of Gruber's equation. The equation was modified by breaking the velocity down into the experimentally measured components of migration distance, Δx , and the heat treating time, Δt . A value of $Q = 10,000$ calories per mole and $\delta = 4.89 \times 10^{-8}$ centimeter was assumed for these calculations. The rest of the variables were measured in the experiments. The results of these calculations are shown in Table III and are plotted in Figure 34. The value of D_0 computed from the curve is 1.92×10^3 square centimeters per second. The activation energy for surface diffusion, Q_s , was calculated to be 42,200 calories per mole.

The results of these calculations are only approximate because of five principal sources of error:

(1) The observed bubble radii are artificially large because we were looking at the matrix projections caused by the stress fields instead of the actual bubbles. The thin-film transmission photomicrographs of the single crystal suggest that the radii measured on replicas are about a factor of 2 too large. This error produces an apparent diffusion coefficient about a factor of 2 too large.

(2) The heat of transport for UN surface diffusion in a temperature gradient is not known. We assumed 10,000 calories per mole to obtain order of magnitude calculations of the surface diffusion coefficient. This is the value assumed by Gruber (27) in his calculations for the migration of helium bubbles in copper. Shewmon (20) states that the heat of transport should be equal to or less than the activation

TABLE III
RESULTS OF CALCULATIONS OF DIFFUSION COEFFICIENTS

Specimen Number	Migration Distance (microns)	Temperature Gradient (°C./cm)	Maximum Temperature (°C.)	Time at Maximum Temperature (min)	Average Bubble Radius (angstroms)	Calculated Surface Diffusion Coefficient (cm ² /sec)
353-1	1650	75	1105	85	500	9.6×10^{-3}
353-16	175	200	985	95	200	1.2×10^{-4}
353-19	> 3000	160	1515	60	1000	$> 3.8 \times 10^{-2}$
353-A	> 1300	250	1445	60	1250	$> 1.3 \times 10^{-2}$
353-E	> 3000	560	1585	60	1400	$> 8.2 \times 10^{-2}$
353-G	> 3000	880	1585	45	1000	$> 1.0 \times 10^{-2}$
Single crystal	5000	580	1465	75	730	9.8×10^{-3}
336-6	350	400	1075	65	200	1.9×10^{-4}

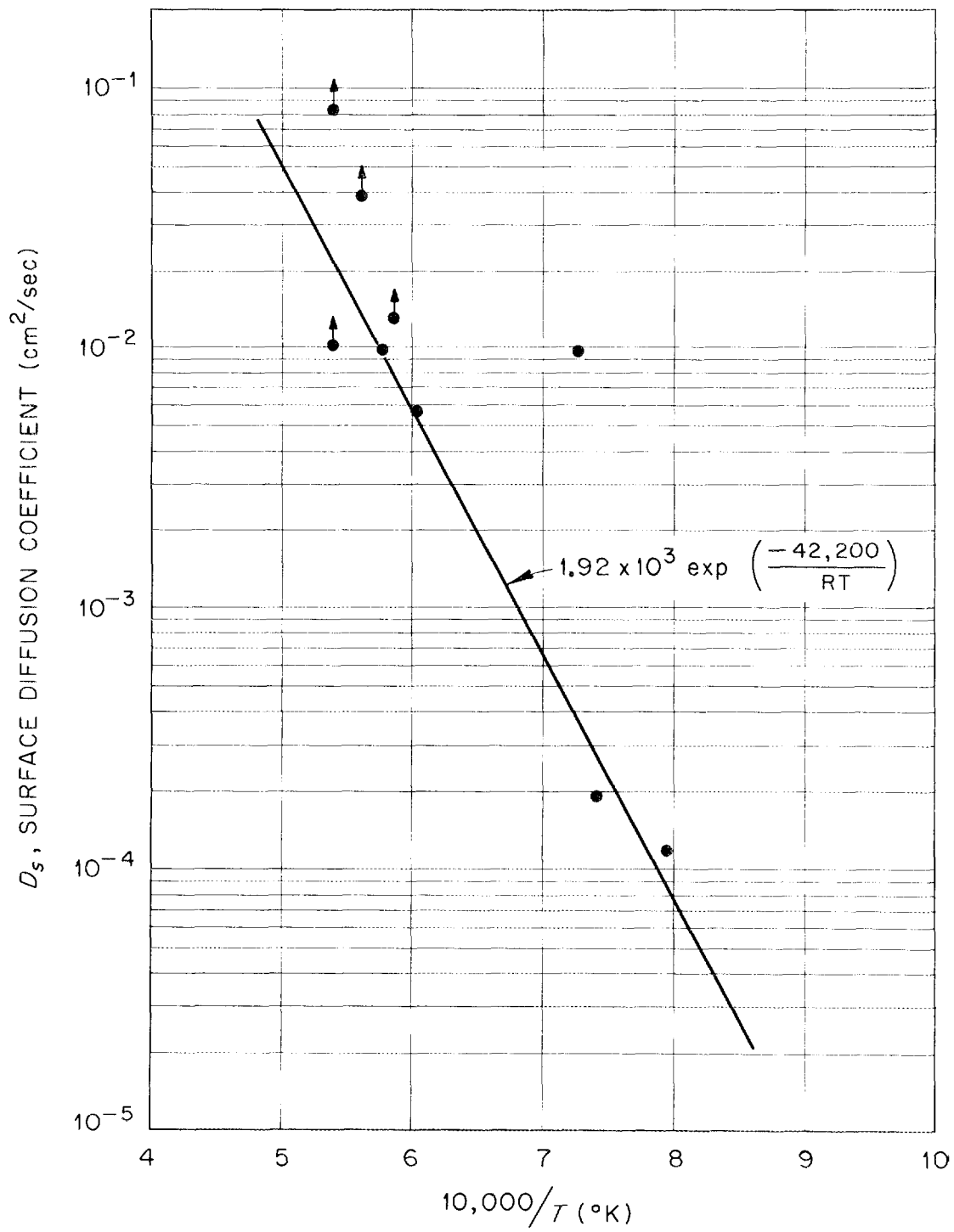


Figure 34. Surface diffusion coefficient as a function of reciprocal temperature.

energy. If we used the activation energy calculated from the curve in Figure 34, the diffusion coefficients would be raised by a factor of 4.22.

(3) The slow heatup to temperature discussed earlier causes the diffusion coefficients to be in error by as much as 25 per cent.

(4) Some error was introduced by using the mean temperature in the region of migration as the temperature to be substituted into Equation (10).

(5) All of the observed migration rates should be artificially small except in the single crystal because of the interactions of the bubbles with grain boundaries. The effect of the interactions of bubbles and grain boundaries is probably more important at low temperatures; this is illustrated by the large pileups at grain boundaries in samples heat treated at low temperatures.

IV. FURTHER DISCUSSION AND COMPARISON OF THE RESULTS WITH THOSE FOR PREVIOUS INVESTIGATIONS

The experimental results on UN are compared in Tables IV and V with helium bubble migration rates computed for UC and copper from the results of previous investigators. The bubbles are thought to migrate in all three materials by the surface diffusion mechanism. For purposes of calculation the "heat of transport" was assumed to be 10,000 calories per mole in all three materials. Table IV is a general comparison of the bubble velocities observed experimentally under the various experimental conditions plus a specific comparison at 750°C. for bubbles of 350 angstroms radius. The temperatures in the experiments on copper

TABLE IV

COMPARISON OF MIGRATION RATES OF HELIUM BUBBLES SUBJECTED
TO A TEMPERATURE GRADIENT IN UN, UC, AND COPPER

Material	Temperature (°C.)	Bubble Radius (angstroms)	Temperature Gradient (°C./cm)	Velocity of Bubbles (angstroms/sec)
<u>Experimental Results</u>				
UN	985	200	200	300
	1585	1000	560	> 11,000
UC	750	2500	900	200
		300	900	5,800
Copper	800(?)	350	2×10^5 (?)	1,000
<u>Comparison of 350 angstroms bubbles at 750°C.</u>				
UN	750	350	900	19 ^a
UC	750	350	900	5,200
Copper	800(?)	350	2×10^5 (?)	1,000

^aCalculated.

TABLE V
 COMPARISON OF SURFACE DIFFUSION COEFFICIENTS
 OF UN, UC, AND COPPER

Material	Temperature (°C.)	D_s (cm ² /sec)
<u>At 750°C.</u>		
UN	750	1.8×10^{-6}
UC	750	4.4×10^{-4}
Copper	750 ^a	7.5×10^{-7}
<u>At $T/T_m = 0.376^b$</u>		
UN	900	2.5×10^{-5}
UC	750	4.4×10^{-4}
Copper	237	1.6×10^{-21}

^aDetermined from grain-boundary grooving experiments. J. Choi and P. Shewmon, "Effect of Orientation on the Surface Self-Diffusion of Copper," Trans. Met. Soc. AIME 224, 589 (1962).

^bAssuming melting points: 2450°C. for UC, 2850°C. for UN, and 1083°C. for copper.

are only guesses so the validity of the comparison is unknown. Table V is a comparison of the surface diffusion coefficients at 750°C. and at temperatures which correspond to 0.376 of the melting point. The value listed for copper was determined from grain-boundary grooving experiments. These tabulated values show that the surface diffusion coefficient in UN is lower than in UC or copper at any given temperature. The surface diffusion coefficient in UN is lower than in UC by a factor of 17 at a fraction of the melting temperature, T_m , equal to 0.376. The surface diffusion coefficient at $0.376 T_m$ in copper is significantly less than either UN or UC.

The temperature gradient for the bubble migration experiments in copper was estimated by Gruber by substituting the surface diffusion coefficient determined from the grain-boundary grooving experiments into Equation (10). However, the temperature was not accurately known. Since the surface diffusion coefficient is an exponential function of temperature, an inaccurate estimate of the temperature would result in an erroneous choice of surface diffusion coefficient and substantial inaccuracies in the calculated temperature gradient.

A second explanation for the large differences of bubble migration rates in UN and copper (at a given fraction of the melting point) might be that the stress field around the bubbles in UN and UC enhanced the migration rates. Barnes and Mazey showed that their bubbles in copper reached equilibrium rapidly, thus eliminating any matrix stress field. In heating thin films of copper, a vacancy source (the surface) is available to the bubbles which is probably less than 500 angstroms away

and which allows the bubbles to come to equilibrium rather quickly at temperature. In the bulk UN samples, on the other hand, no source of vacancies was available to the bubbles except thermal vacancies.

CHAPTER VI

CONCLUSIONS AND RECOMMENDATIONS

The conclusions derived from the experimental results are summarized below:

(1) Helium bubbles in UN move up a temperature gradient by surface diffusion.

(2) From the observed migration distances a surface diffusion coefficient was calculated to be $1.92 \times 10^3 \exp(-42,200/RT)$.

(3) Large stress fields probably existed around the bubbles preventing their coalescence.

(4) Helium bubbles became trapped at grain boundaries during the heat treatment of the samples, and subsequent pileups of bubbles at grain boundaries were observed due to the interaction of the stress fields around the bubbles.

(5) Bubbles appeared as projections instead of holes on polished or fractured UN surfaces. It was suggested that this phenomenon resulted from an effect of the room temperature stress fields on the polishing and fracture characteristics.

(6) The presence of stress fields around the bubbles may affect the migration rates. If this is the case, the results would not be directly applicable to irradiation behavior because the excess vacancies from fission spikes would probably allow the bubbles to come to equilibrium quite rapidly.

The results from these experiments provided many ideas which would be of interest to pursue in subsequent investigations. Some of these ideas are listed below:

(1) The stress fields associated with the bubbles apparently hardened and strengthened the matrix in the immediate vicinity of the bubbles. This effect was quite unexpected and no satisfactory explanation is apparent.

(2) The interaction of the bubbles with grain boundaries undoubtedly influenced the observed migration distances and the subsequent calculation of surface diffusion coefficients. More single-crystal experiments should be run to determine a more accurate diffusion coefficient.

(3) Since grain boundaries and other microstructural details were more readily observed in replicas of fractured surfaces than in replicas of polished surfaces, more definitive results might be obtained by developing a technique to longitudinally section the samples by fracturing.

(4) Additional short-time experiments should be run using equipment capable of attaining test temperatures rapidly.

(5) An attempt should be made to determine the effect of the stress fields on the diffusion coefficient. This might be done by annealing the sample, after an initial heat treatment in a temperature gradient, to allow the bubbles to come to equilibrium with the matrix.

(6) The interaction of helium atoms with precipitates should be studied to determine the effectiveness of precipitates as pinning sites for bubbles.

REFERENCES

REFERENCES

1. Johnson, G. W., and R. Shuttleworth, "The Solubility of Krypton in Liquid Lead, Tin, and Silver," *Phil. Mag.* 4, 957-963 (1959).
2. Rufeh, F., "Solubility of Helium in Uranium Dioxide," UCRL-11043, Livermore, California, University of California Radiation Laboratory (March 19, 1964).
3. Barnes, R. S., and R. S. Nelson, "Theories of Swelling and Gas Retention in Reactor Materials," AERE-R-4952, Harwell, England, Atomic Energy Research Establishment (June 1965).
4. Greenwood, G. W., A.J.E. Foreman, and D. E. Rimmer, "The Role of Vacancies and Dislocations in the Nucleation and Growth of Gas Bubbles in Irradiated Fissile Material," *J. Nucl. Mater.* 4, 305-324 (1959).
5. Churchman, A. T., "Swelling and Fission-Gas Agglomeration in Metal Fuels," *Nuclear Metallurgy*, Vol. 6, New York, American Institute of Mining, Metallurgical and Petroleum Engineers (1959).
6. Kramer, D., W. V. Johnston, and C. G. Rhodes, "Reduction of Fission-Product Swelling in Uranium Alloys by Means of Finely Dispersed Phases," *J. Inst. Metals* 93, 145-152 (1965).
7. Inouye, H., Metals and Ceramics Division, Oak Ridge National Laboratory, Oak Ridge, Tennessee, Personal Communication, June 20, 1967.
8. Bugl, J., and D. L. Keller, "Uranium Mononitride - A New Reactor Fuel," *Nucleonics* 22(9), 66 (September 1964).
9. Hayes, B. A., and M. A. DeCrescente, "Thermal Conductivity and Electrical Resistivity of Uranium Mononitride," PWAC-481, Middletown, Connecticut, Pratt and Whitney Aircraft-CANEL, Division of United Aircraft Corporation (October 1965).
10. Leitnaker, J. M., Metals and Ceramics Division, Oak Ridge National Laboratory, Oak Ridge, Tennessee, Personal Communication, June 15, 1967.
11. Evans, P. E., and T. J. Davies, "Uranium Nitrides," *J. Nucl. Mater.* 10(1), 43-55 (1963).

12. Fassler, M., F. J. Huegel, and M. A. DeCrescente, "Compressive Creep of UC and UN," Part I, PWAC-482, Middletown, Connecticut, Pratt and Whitney Aircraft-CANEL, Division of United Aircraft Corporation (October 1965).
13. Sturiale, T. J., and M. A. DeCrescente, "Self-Diffusion of Nitrogen in Uranium Mononitride," PWAC-482, Middletown, Connecticut, Pratt and Whitney Aircraft-CANEL, Division of United Aircraft Corporation (October 1965).
14. Inouye, H., and J. M. Leitnaker, "Equilibrium Nitrogen Pressures and Thermodynamic Properties of UN," accepted for publication in the "Journal of the American Ceramic Society."
15. Godfrey, T. G., J. A. Woolley, and J. M. Leitnaker, "Thermodynamic Functions of Nuclear Materials: UC, UC₂, UO₂, ThO₂, and UN," ORNL-TM-1596, Revised, Oak Ridge, Tennessee, Oak Ridge National Laboratory (December 1966).
16. Barnes, R. S., and D. J. Mazey, "The Migration and Coalescence of Inert-Gas Bubbles in Metals," AERE-R-4223, Harwell, England, Atomic Energy Research Establishment (January 1963).
17. Selleck, E. G., and M. A. DeCrescente, "Fission-Gas Migration Studies in Uranium Carbide," PWAC-476, Middletown, Connecticut, Pratt and Whitney Aircraft-CANEL, Division of United Aircraft Corporation (October 1965).
18. Barnes, R. S., and D. J. Mazey, "The Movement of Helium Bubbles in Uranium Dioxide," AERE-R-4570, Harwell, England, Atomic Energy Research Establishment (1964).
19. Gulden, M. E., "Migration of Gas Bubbles in Irradiated Uranium Dioxide," J. Nucl. Mater. 23, 30-33 (1967).
20. Shewmon, P. G., "The Movement of Small Inclusions in Solids by a Temperature Gradient," Trans. Met. Soc. AIME 230, 1134-1137 (August 1964).
21. Gruber, E. E., "Migration of Pores in Solids," ANL-6868, Argonne, Illinois, Argonne National Laboratory (1963).
22. Speight, M. W., "The Migration of Gas Bubbles in Material Subject to a Temperature Gradient," J. Nucl. Mater. 13(2), 207-209 (1964).
23. Shewmon, P. G., Argonne National Laboratory, Argonne, Illinois, Personal Communication, October 1, 1966.

24. Marion, J. B., "1960 Nuclear Data Tables, Part 3, Nuclear Reaction Graphs," p. 19, College Park, Maryland, University of Maryland (August 1960).
25. Friedlander, G., and J. W. Kennedy, "Nuclear and Radiochemistry," New York, Wiley (1955).
26. Southern, A., Solid State Division, Oak Ridge National Laboratory, Oak Ridge, Tennessee, Personal Communication, October 2, 1967.
27. Gruber, E. E., "Calculated Size Distributions for Gas Bubble Migration and Coalescence in Solids," J. Appl. Phys. 38(1), 243-250 (1967).
28. Choi, J., and P. Shewmon, "Effect of Orientation on the Surface Self-Diffusion of Copper," Trans. Met. Soc. AIME 224, 589 (1962).

APPENDIXES

APPENDIX A

TABLE VI

SIGHT GLASS CALIBRATION FOR TEMPERATURE GRADIENT FURNACE

Temperature, °C.		2 1/8- by 5/32-in. Window Correction to be Added, °C.
True	Observed	
900	894	6
1000	992	8
1200	1190	10
1500	1485	15
1700	1681	19
1900	1878	22
2100	2074	26

APPENDIX B

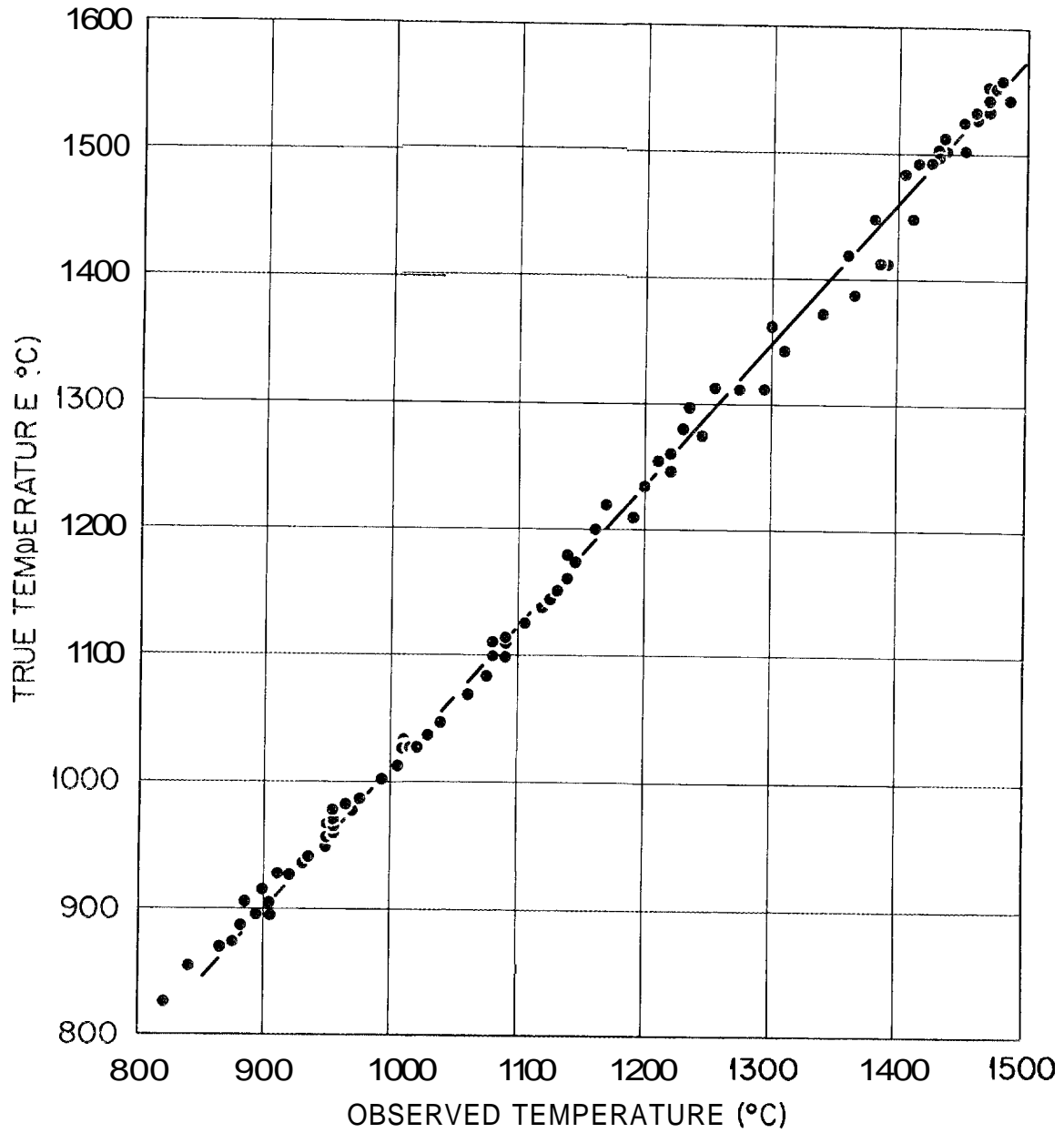


Figure 35. A graph of true temperature versus observed temperature to correct for the lack of blackbody conditions.

APPENDIX C

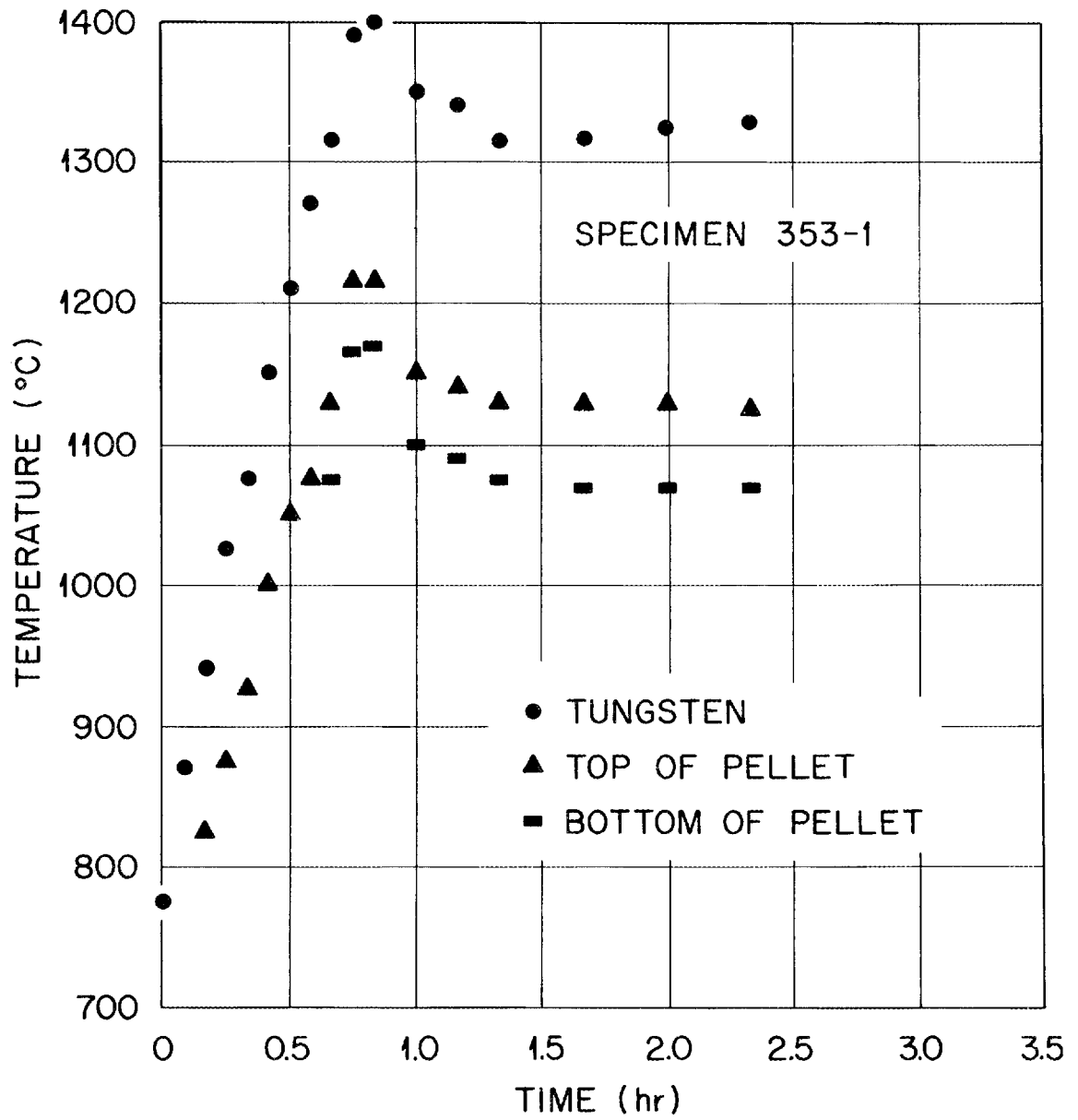


Figure 36. Temperatures recorded during heat treatment of specimen 353-1 as a function of time.

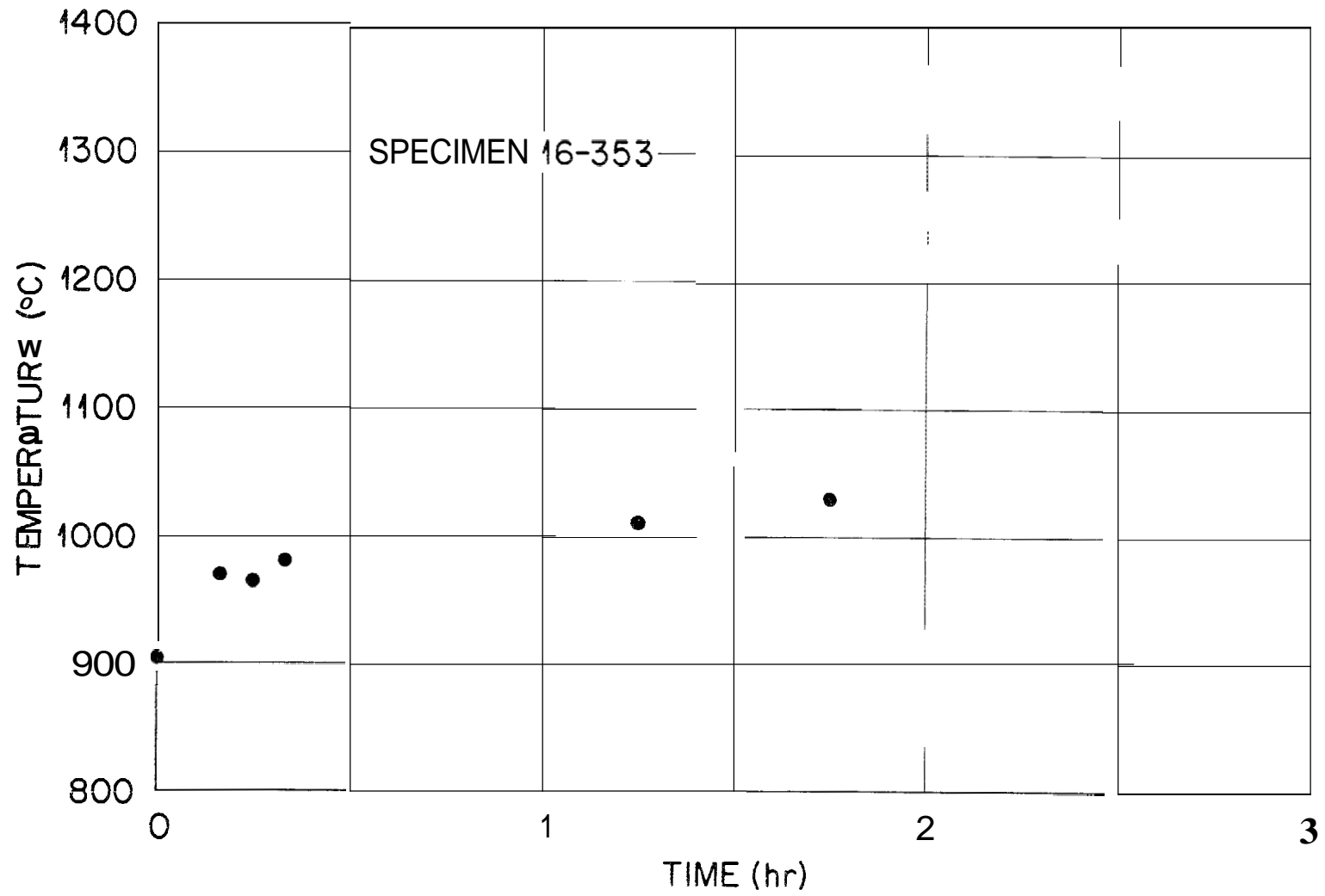


Figure 37. Temperature of bombarded end of specimen 16-353 as a function of time.

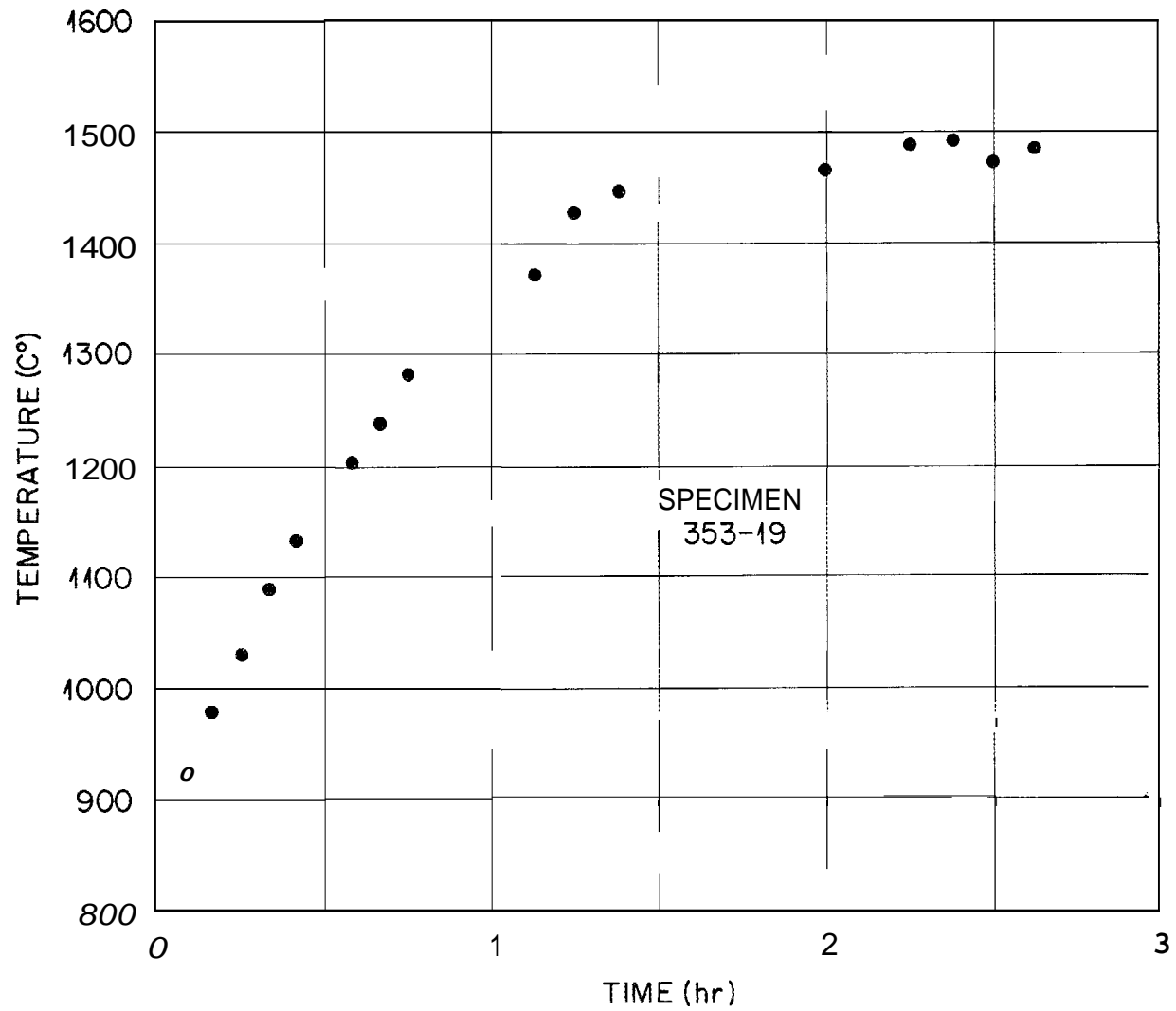


Figure 38. Temperature of bombarded end of specimen 353-19 as a function of time.

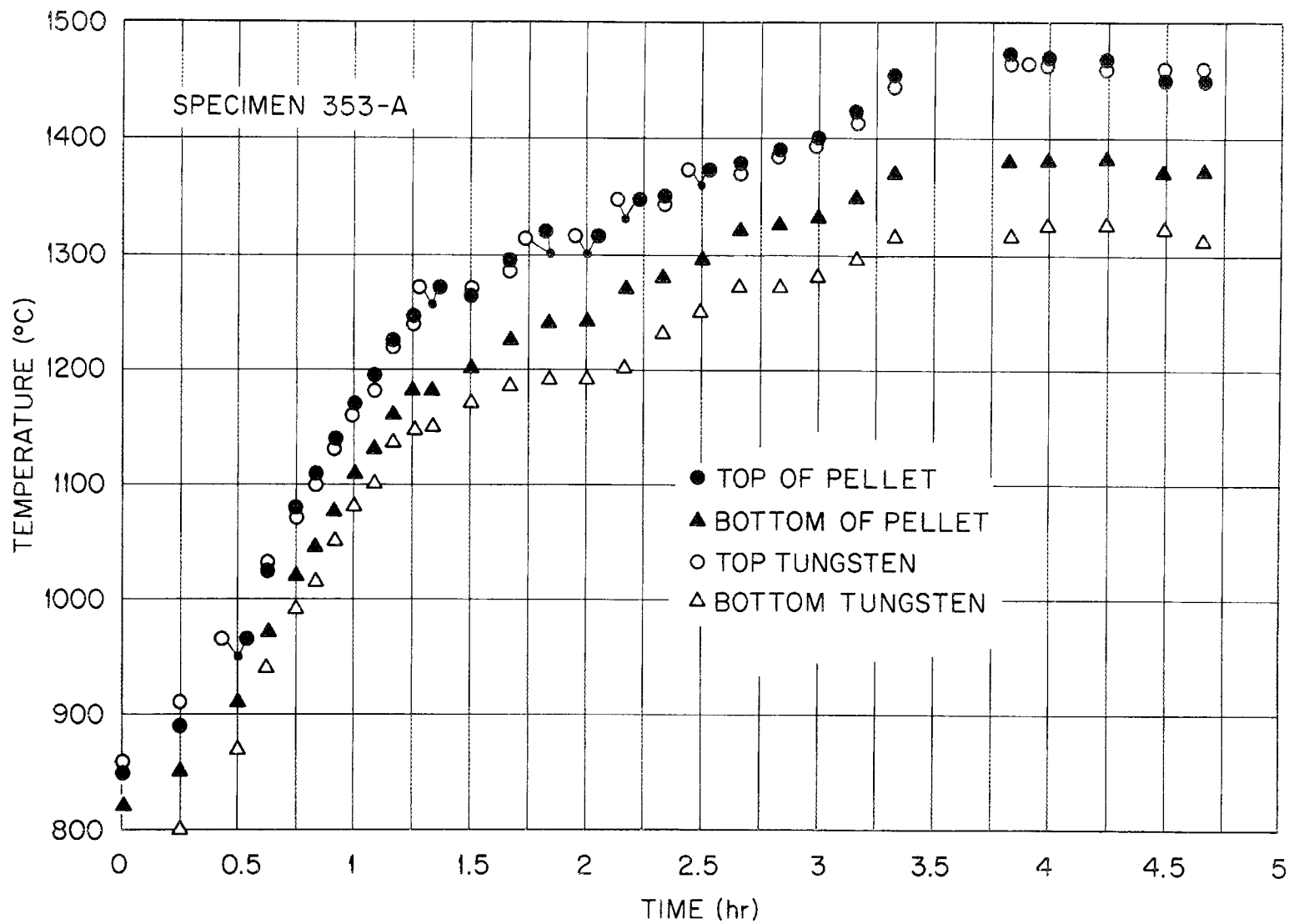


Figure 39. Temperature recorded during heat treatment of specimen 353-A as a function of time.

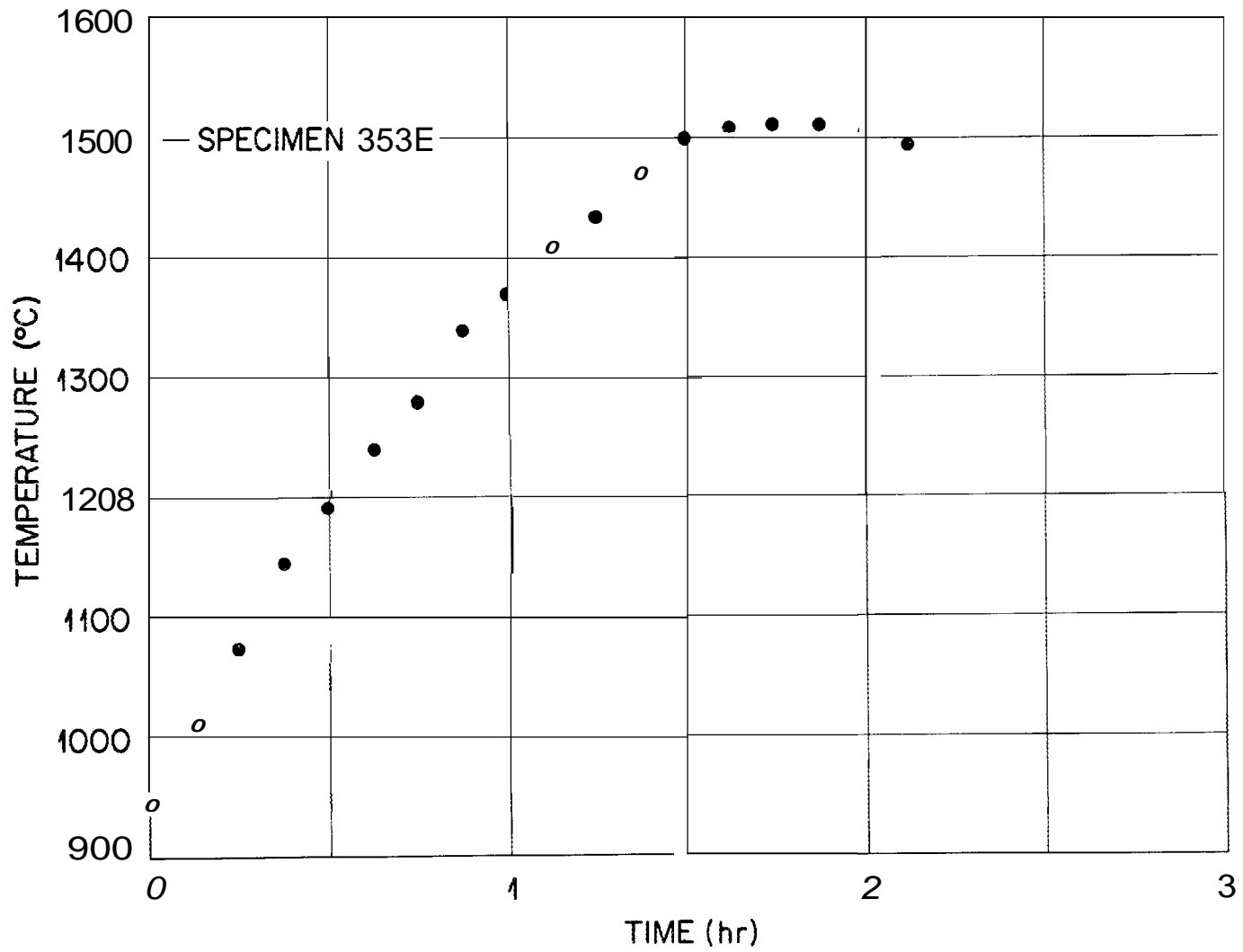


Figure 40. Temperature of bombarded end of specimen 3533 as a function of time.

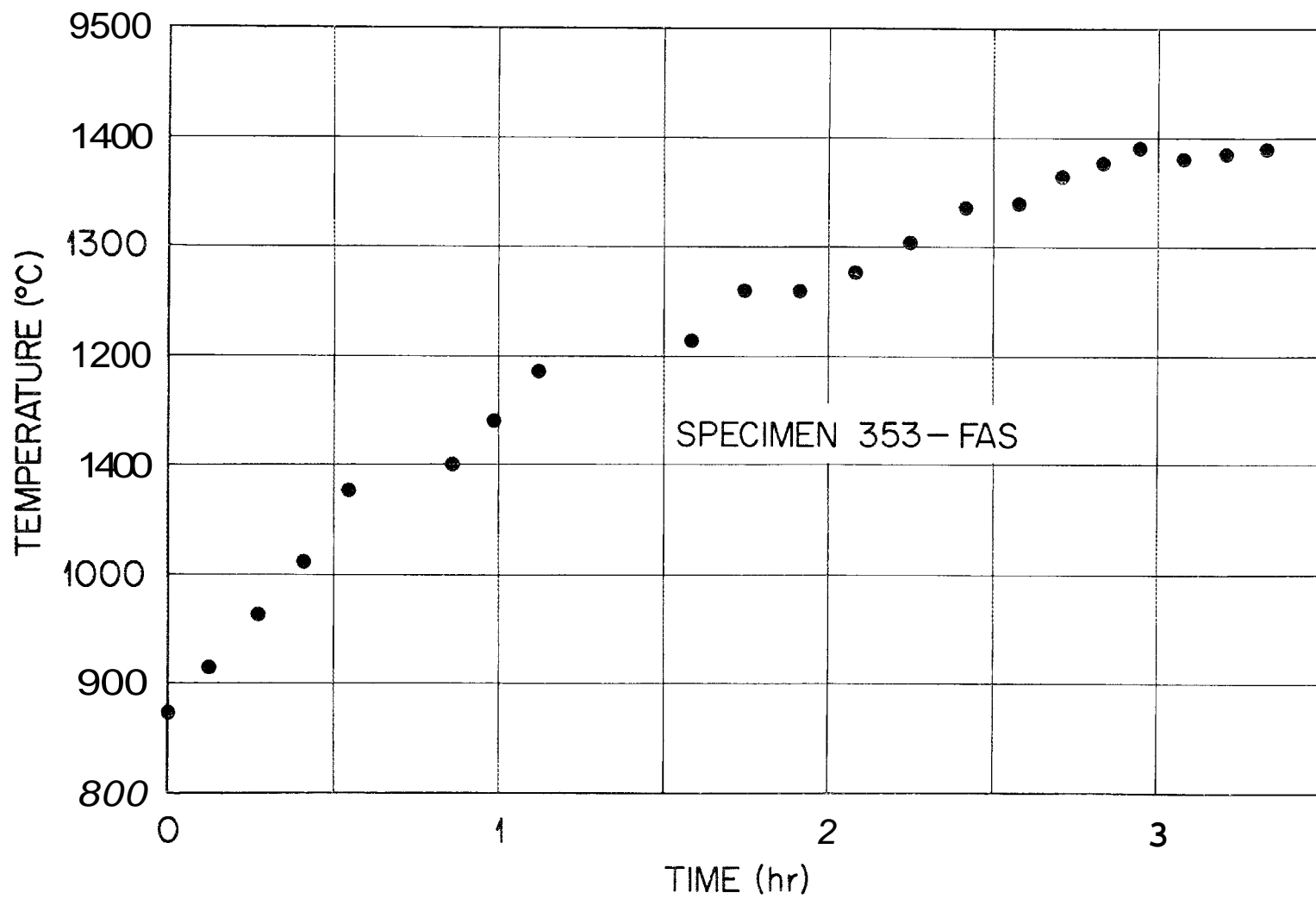
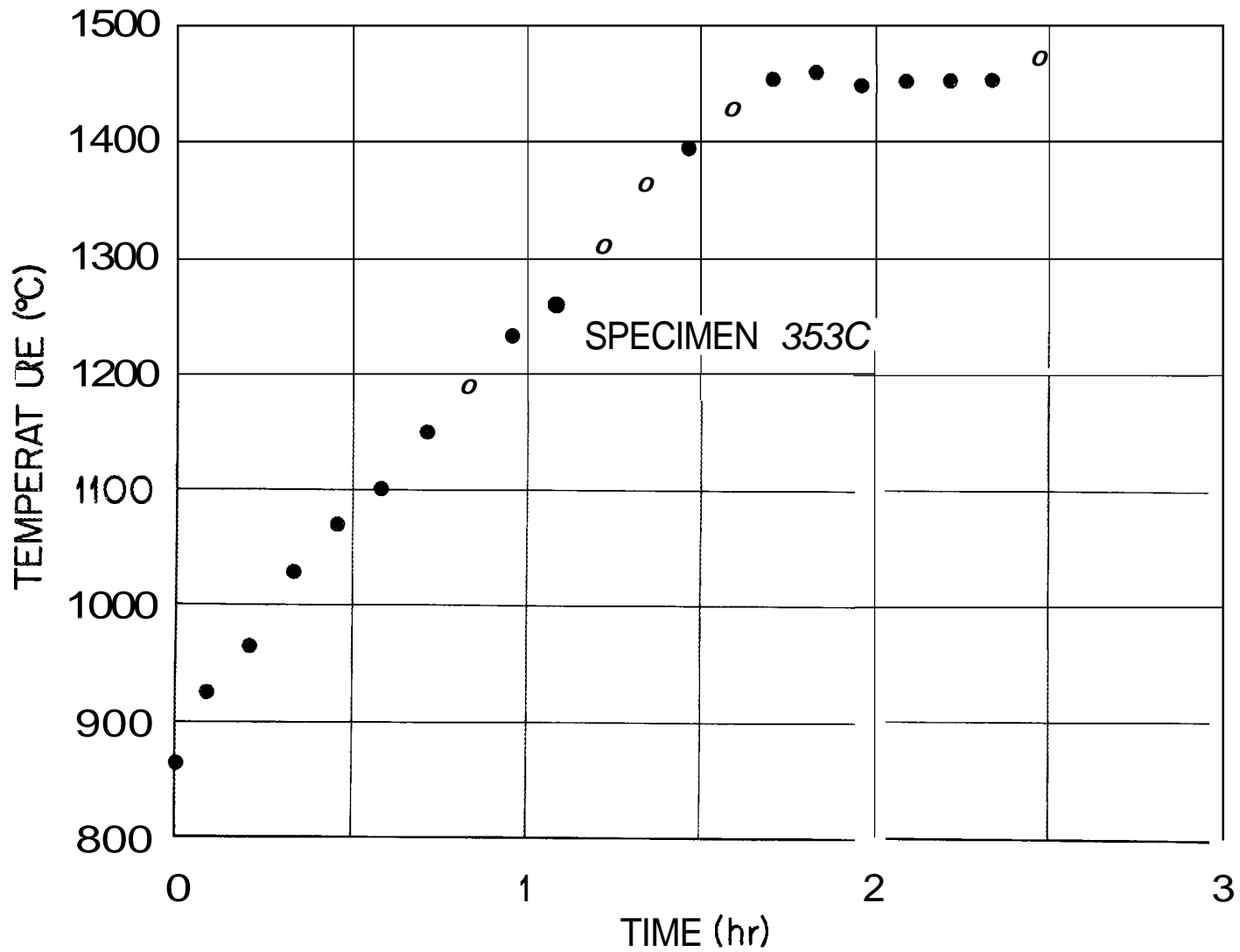


Figure 41. Temperature of bombed end of specimen 353-FAS as a function of time.



101

Figure 42. Temperature of bombarded end of specimen 353G as a function of time.

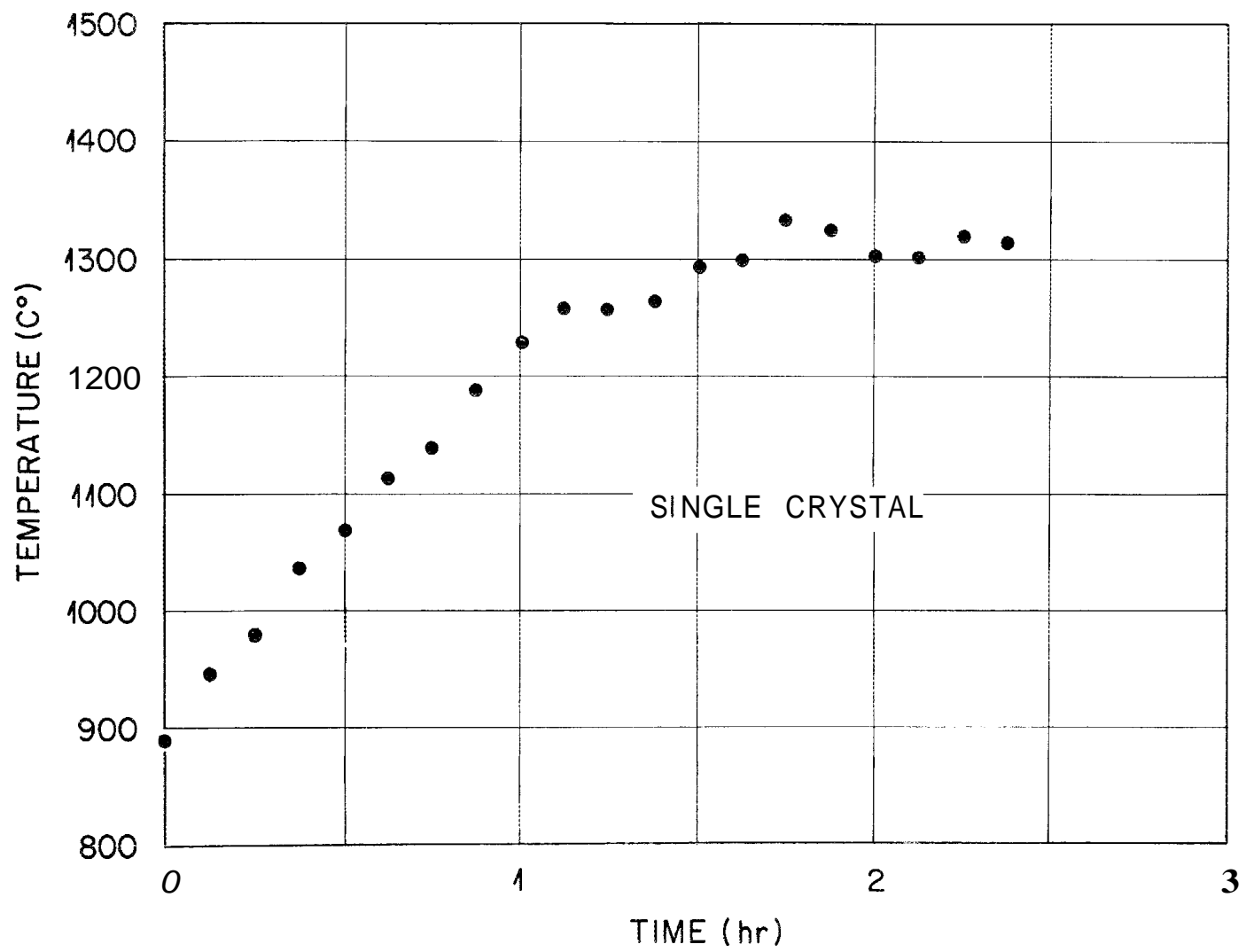


Figure 43. Temperature of bombarded end of single-crystal specimen as a function of time.

INTERNAL DISTRIBUTION

- | | | | |
|--------|---|--------|---------------------|
| 1-3. | Central Research Library | 44. | R. T. King |
| 4-5. | ORNL - Y-12 Technical Library
Document Reference Section | 45. | C. E. Larson (K-25) |
| 6-15. | Laboratory Records | 46. | J. M. Leitnaker |
| 16. | Laboratory Records, ORNL R.C. | 47. | A. P. Litman |
| 17. | ORNL Patent Office | 48. | T. S. Lundy |
| 18. | G. M. Adamson, Jr. | 49. | R. N. Lyon |
| 19. | S. E. Beall | 50. | H. G. MacPherson |
| 20. | E. S. Bomar, Jr. | 51. | R. E. MacPherson |
| 21. | G. E. Boyd | 52. | R. W. McClung |
| 22. | E. J. Breeding | 53. | D. L. McElroy |
| 23. | J. E. Cunningham | 54. | C. J. McHargue |
| 24. | F. L. Culler | 55. | F. R. McQuilkin |
| 25. | V. A. DeCarlo | 56. | A. J. Miller |
| 26. | J. H. DeVan | 57. | C. S. Morgan, Jr. |
| 27. | W. S. Ernst, Jr. | 58. | A. R. Olsen |
| 28. | R. B. Fitts | 59. | R. A. Potter |
| 29. | A. P. Fraas | 60. | P. Patriarca |
| 30. | J. H. Frye, Jr. | 61. | D. K. Reimann |
| 31. | W. Fulkerson | 62. | J. E. Savolainen |
| 32. | R. E. Gehlbach | 63. | J. L. Scott |
| 33. | T. G. Godfrey | 64. | R. L. Senn |
| 34. | J. M. Googin (Y-12) | 65. | G. M. Slaughter |
| 35. | W. R. Grimes | 66. | S. H. Smiley (K-25) |
| 36. | A. G. Grindell | 67. | K. E. Spear II |
| 37. | W. O. Harms | 68. | K. R. Thoms |
| 38-40. | M. R. Hill | 69. | A. M. Weinberg |
| 41. | H. W. Hoffman | 70-89. | S. C. Weaver |
| 42. | H. Inouye | 90. | J. R. Weir |
| 43. | W. H. Jordan | 91. | C. S. Yust |

EXTERNAL DISTRIBUTION

92. Dan Albreds, University of California, Berkeley, Calif.
93. G. M. Anderson, AEC, Washington
94. C. H. Armbruster, Wright-Patterson AFB
95. Hans Beutler, Freistrasse 13, 8406 Winterthein, Switzerland
- 96-98. V. P. Calkins, General Electric, NMPO
99. S. S. Christopher, AEC, Washington
100. D. F. Cope, RDT, SSR, AEC, Oak Ridge Operations
101. J.W.R. Creagh, NASA, Lewis Research Center
102. J. Davis, Jet Propulsion Laboratory
103. R. W. Dayton, Battelle Memorial Institute
104. G. K. Dicker, AEC, Washington
105. E. M. Douthett, AEC, Washington

- 106. D. DeHalas, Pacific Northwest Laboratory, Richland
- 107. J. K. Elbaum, Code MAMP, Wright-Patterson AFB
- 108. D. C. Goldberg, Westinghouse Astronuclear Laboratory
- 109-110. D. H. Gurinsky, Brookhaven National Laboratory
- 111. R. Hall, NASA, Lewis Research Center
- 112. R. C. Hamilton, Institute for Defense Analyses,
1666 Connecticut Avenue, N.W., Washington, D. C.
- 113. E. E. Hoffman, General Electric, Cincinnati
- 114. W. R. Holman, Lawrence Radiation Laboratory
- 115. F. J. Huegel, University of California, Berkeley, Calif.
- 116. C. Johnson, Space Nuclear Systems Division, Space Electric
Power Office, AEC, Washington, D. C., 20545
- 117. J. S. Kane, University of California, Berkeley, Calif.
- 118. Don Keller, Battelle Memorial Institute, Columbus, Ohio
- 119. W. J. Larkin, AEC, Oak Ridge Operations
- 120. P. J. Levine, Westinghouse Advanced Reactors Division,
Waltz Mill Site, Box 158, Madison, Pa., 15663
- 121. J. J. Lombardo, NASA, Lewis Research Center
- 122. J. J. Lynch, NASA, Washington
- 123. T. P. Moffitt, NASA, Lewis Research Center
- 124-125. T. A. Moss, NASA, Lewis Research Center
- 126. R. A. Noland, Argonne National Laboratory
- 127. J. W. Prados, the University of Tennessee
- 128. W. E. Ray, Westinghouse Advanced Reactors Division,
Waltz Mill Site, Box 158, Madison, Pa., 15663
- 129. Louis Rosenblum, NASA, Lewis Research Center
- 130. A. J. Rothman, Lawrence Radiation Laboratory
- 131. A. L. Rothman, University of California, Berkeley, Calif.
- 132. B. Rubin, Lawrence Radiation Laboratory
- 133. N. D. Sanders, NASA, Lewis Research Center
- 134. H. Schwartz, NASA, Lewis Research Center
- 135. F. C. Schwenk, AEC, Washington
- 136. P. G. Shewmon, Argonne National Laboratory
- 137-141. J. M. Simmons, AEC, Washington
- 142. J. E. Spruiell, the University of Tennessee
- 143. E. E. Stansbury, the University of Tennessee
- 144. D. K. Stevens, AEC, Washington
- 145. G. W. Wensch, AEC, Washington
- 146. G. A. Whitlow, Westinghouse Advanced Reactors Division,
Waltz Mill Site, Box 158, Madison, Pa., 15663
- 147. M. J. Whitman, AEC, Washington
- 148. Laboratory and University Division, AEC, ORO
- 149-163. Division of Technical Information Extension